

**The Impact of Internal Climate Variability on Marine
Phytoplankton in a Warming Climate**

by

Geneviève Wheeler Elsworth

B.S., Pennsylvania State University, 2012

M.S., McGill University, 2014

A thesis submitted to the
Faculty of the Graduate School of the
University of Colorado in partial fulfillment
of the requirements for the degree of
Doctor of Philosophy
Department of Geological Sciences

2022

Committee Members:

Nicole Lovenduski, Chair

Thomas Marchitto

Irina Overeem

Kristopher Karnauskas

Julia Moriarty

Elsworth, Geneviève Wheeler (Ph.D., Geological Sciences)

The Impact of Internal Climate Variability on Marine Phytoplankton in a Warming Climate

Thesis directed by Prof. Nicole Lovenduski

ABSTRACT OF THE DISSERTATION

Marine phytoplankton (algae) play a key role in the Earth system by influencing ocean biogeochemical cycling, the flux of carbon dioxide from the atmosphere to the ocean, and the productivity of fisheries. The growth of these microscopic, unicellular primary producers is strongly affected by the oceanic physical and biogeochemical environment. As such, the variable and changing climate system has a large influence on phytoplankton abundance, its spatial distribution, and its temporal variability. Internal variability naturally arises from interactions between components of the coupled climate system, for example, between the ocean and the atmosphere. Whereas, anthropogenic changes to the climate system are considered to be externally forced, as they arise from greenhouse gas emissions. Phytoplankton experience both internal climate variability and externally forced anthropogenic changes, and it can be difficult to discern the influence of internal and external processes in the marine biosphere. Recent research suggests that it may be possible to separate internal and external influences on the coupled Earth system using large ensembles of Earth system models (ESMs). However, ESMs may not skillfully predict observed spatial patterns and temporal dynamics in real-world marine phytoplankton. In this dissertation, I use observational records and ESM ensembles to investigate the role of internal climate variability in marine phytoplankton in a warming climate. I first use a novel statistical emulation technique to place the remotely sensed record of surface ocean chlorophyll concentrations into the large ensemble framework. Much like a large initial condition ensemble generated with an ESM, the resulting observationally constrained synthetic ensemble represents multiple possible spatiotemporal evolutions of observed ocean chlorophyll, each with a different phasing of internal climate variability. I use the observationally constrained synthetic ensemble to contextualize the interpretation of long-

term trends in the presence of internal variability and identify a wider range of possible trends in chlorophyll due to the sampling of internal variability in subpolar regions than in subtropical regions. Next, I evaluate the statistical methodology of the observationally constrained synthetic ensemble in the context of a large ensemble of an ESM. When applying the statistical approach to the Community Earth System Model Large Ensemble (CESM1-LE) over the historical period, simulated variability in surface ocean chlorophyll concentration is able to be reproduced using the statistical method. Finally, I quantify the influence of anthropogenic climate change on variability in phytoplankton biomass using the CESM1-LE. I find a significant decrease in the interannual variance of phytoplankton biomass under a business-as-usual (RCP8.5) emission scenario, with heterogeneous regional trends. Statistical analysis of regional trends reveal zooplankton grazing (top-down control) as an important contributor to changes in phytoplankton variance. The results of this dissertation highlight the influence of internal climate variability on marine phytoplankton in a warming climate.

Dedication

To my husband, Kevi.

Acknowledgements

Chapters 2, and 3 are versions of the following articles, respectively, and should be cited as follows:

Elsworth, G. W., N. S. Lovenduski, K. A. McKinnon, K. M. Krumhardt, and R. X. Brady, 2020: Finding the fingerprint of anthropogenic climate change in marine phytoplankton. *Current Climate Change Reports*, 6(2), 37-46, doi:10.1007/s40641-020-00156-w.

Elsworth, G. W., N. S. Lovenduski, and K. A. McKinnon, 2021: Alternate history: A synthetic ensemble of ocean chlorophyll concentrations. *Global Biogeochemical Cycles*, 35(9), 1-13, doi:10.1029/2020GB006924.

Copyright of Elsworth et al. [2020] is retained by Springer Heidelberg; permission from Springer Heidelberg has been granted for reprint in this dissertation via publication-specific licenses. Copyright of Elsworth et al. [2021] is retained by the American Geophysical Union (AGU), licensed under the Creative Commons Attribution 4.0 License, freely allowing reprint in this dissertation. Reuse and distribution is subject to licensing permissions of the above identified copyright holders.

This research was supported by grants from the National Science Foundation (OCE-1558225 and OCE-1752724).

Many people have been crucial to my success while at University of Colorado Boulder. I would like to give a sincere thanks to:

- Professors Nicole Lovenduski and Thomas Marchitto, for their guidance and encouragement throughout which helped me become a more knowledgeable and confident scientist.

- My research mentors, committee members, and collaborators who have challenged me intellectually: Irina Overeem, Kris Karneckas, Julia Moriarty, Karen McKinnon, Kristen Krumhardt, Matt Long, and Sarah Schlunegger.
- My research groupmates in the Ocean Biogeochemistry Research Group (Riley Brady, Holly Olivarez, Sam Mogen, and, Genevieve Clow) for their stimulating discussion and technical support.
- My family from back home and in Colorado for their caring support and encouragement.

Contents

Chapter	
1	1
1.1	1
1.1.1	3
1.1.2	5
1.2	7
1.3	9
2	11
2.1	11
2.2	11
2.2.1	13
2.2.2	16
2.3	16
2.4	20
2.5	23
2.6	27
3	29
3.1	29
3.2	30

3.3	Data and Model Output	33
3.3.1	Observations	33
3.3.2	Community Earth System Model Large Ensemble	34
3.4	Creating a synthetic ensemble of the observational record	35
3.4.1	HOT	36
3.4.2	MODIS	39
3.5	Evaluating the synthetic ensemble methodology using CESM1-LE	41
3.6	Implications for the interpretation of observational records	44
3.7	Conclusions	48
4	Anthropogenic climate change drives non-stationary phytoplankton variance	49
4.1	Abstract	49
4.2	Introduction	50
4.3	Methods	52
4.3.1	Community Earth System Model 1 Large Ensemble	52
4.3.2	Model Evaluation	55
4.4	Results	56
4.5	Conclusions and Discussion	63
5	Summary and Conclusions	67
	Bibliography	71
	Appendix	
A	Supplementary Material for Chapter 3	86
B	Supplementary Material for Chapter 4	87

Tables

Table

4.1	Changes in phytoplankton biomass and its variability in the CESM1-LE	60
-----	--	----

Figures

Figure

1.1	Schematic of phytoplankton growth as a function of light, nutrient concentration, and temperature	3
1.2	Comparison between observed and modeled chlorophyll concentrations	4
1.3	Schematic of simple to complex biogeochemical ecosystem models	6
1.4	Simulated changes in net primary productivity (NPP) over the MODIS observational period (2002 to 2020) in the CESM1-LE	8
2.1	Mean chlorophyll concentration, standard deviation in chlorophyll concentration, and n^* over the MODIS remote sensing record	15
2.2	Schematic of the construction of a synthetic ensemble of regional ocean chlorophyll concentration in the Eastern Equatorial Pacific	25
2.3	Annual trends in global chlorophyll concentration of two synthetic ensemble members and the MODIS remote sensing record	27
3.1	Schematic illustrating the creation of a synthetic ensemble using the HOT dataset of chlorophyll concentration	37
3.2	Temporal evolution of chlorophyll a concentration in mg m^{-3} averaged over the upper 10 m at the Hawaii Ocean Time-Series (HOT)	39
3.3	Anomalous, monthly mean chlorophyll concentration in December 2015 (mg m^{-3}) of two synthetic ensemble members and the MODIS remote sensing record	40

3.4	Comparison of the evolution of global-mean surface ocean chlorophyll concentration in mg m^{-3} in the CESM1-LE and a synthetic ensemble generated from model large ensemble member 14 over the historical period from 1920 to 2005.	42
3.5	Fractional error of the interannual standard deviation in the synthetic ensemble generated from ensemble member 10 as compared to the original CESM1-LE	44
3.6	Comparison between the temporal evolution of chlorophyll a concentration in mg m^{-3} between the HOT record and synthetic ensemble members created from the original dataset	45
3.7	Annual trends in global chlorophyll concentration of two synthetic ensemble members compared to the original MODIS remote sensing record	46
3.8	Probability density functions of linear trends of 1,000 synthetic ensemble members derived from the MODIS remote sensing record	47
4.1	Comparison between observed and modeled phytoplankton biomass interannual variability	55
4.2	Change in annual mean total phytoplankton carbon concentration and the coefficient of variance in annual mean total phytoplankton carbon concentration simulated by the CESM1-LE	57
4.3	Percentage change in annual total phytoplankton carbon concentration and annual total phytoplankton variability over the RCP8.5 forcing scenario (2006 to 2100) simulated by the CESM1-LE	59
4.4	Distribution of the dominant phytoplankton functional type in biomass carbon simulated by the CESM1-LE	61
4.5	Reconstructed changes in the contribution of each driver variable to phytoplankton variance across the RCP8.5 forcing scenario in the CESM1-LE	64
A.1	The sensitivity of chlorophyll concentration derived from the MODIS ocean color record to ENSO and PDO	86

B.1	Holling Type III (sigmoidal) functional parameterization of zooplankton grazing rate in the biogeochemical ecosystem model of the CESM1-LE across a range of temperatures	88
B.2	Coefficient of variance (internal standard deviation divided by ensemble mean) in annual mean global surface ocean chlorophyll concentration from 2006 to 2100 across a suite of CMIP5 model ensembles	89
B.3	Total phytoplankton carbon concentration and the standard deviation in total phytoplankton carbon concentration simulated by the CESM1-LE averaged across the RCP8.5 forcing scenario	90

Chapter 1

Introduction

1.1 Importance of Phytoplankton in the Earth System

Marine phytoplankton are photosynthetic algae that inhabit the surface of the global ocean. These organisms are an important component of the global carbon cycle, strongly influencing air-sea CO₂ flux and marine carbon export. Although phytoplankton constitute a relatively small reservoir of carbon, their ability to photosynthetically fix carbon from the atmosphere enhances the ocean's role as a carbon sink [Friedlingstein et al., 2019]. The efficiency and strength of carbon sequestration by the marine biological pump strongly influences atmospheric CO₂ concentrations, with important feedbacks on the climate system [McKinley et al., 2017, Bindoff et al., 2019]. In addition to influencing the distribution of carbon in the ocean, phytoplankton also serve as the base of the marine food web, supporting diverse marine ecosystems by providing sustenance for higher trophic levels [Falkowski, 2012].

Phytoplankton growth is controlled by temperature and the availability of light and nutrients [Sigman and Hain, 2012]. Phytoplankton harvest light to convert inorganic carbon to organic carbon through the process of photosynthesis. The rate of photosynthesis increases linearly with increasing light levels, however, at high light levels, photosynthesis declines due to photoinhibition (Figure 1.1a). The global distribution of phytoplankton is tightly coupled to light availability which decreases from the equator to the poles. In nutrient-replete subpolar and polar regions, phytoplankton growth is restricted in the winter when light is limited and enhanced in the spring, summer, and autumn when light is more abundant, creating a strong seasonal cycle in chlorophyll.

In contrast, subtropical oceanic regions with ample light tend to be instead limited by the supply of nutrients due to a permanent thermocline, showing only moderate seasonality [Lalli and Parsons, 1997, Giovannoni and Vergin, 2012].

Phytoplankton require a variety of nutrients to support photosynthesis. The rate of nutrient uptake by phytoplankton increases with nutrient concentration to a half-saturation constant (K_n), at which growth rate is half its maximum value (Figure 1.1b). Due to a relatively larger surface area-to-volume ratio, smaller phytoplankton more efficiently assimilate nutrients than larger phytoplankton. At higher nutrient concentrations, the rate of phytoplankton nutrient uptake declines to a maximum growth rate (Figure 1.1b). Nutrients such as nitrate, phosphate, and silicate are considered macronutrients, which are required by phytoplankton in large amounts to support cellular growth and metabolism [Sarmiento and Gruber, 2006]. In contrast, micronutrients such as iron, zinc, and cobalt are required in small amounts for the activity of enzymes and other intracellular functions [Sarmiento and Gruber, 2006]. In the global ocean, phytoplankton can be limited by either macronutrients or micronutrients. In polar regions, particularly the Southern Ocean, phytoplankton are limited by micronutrients, such as iron, and there is an abundance of macronutrients [Moore et al., 2002]. In contrast, in regions of the subtropical gyres, phytoplankton are limited by low concentrations of macronutrients such as nitrate and phosphate.

Temperature influences the rate at which photosynthetic processes occur, with phytoplankton growth rate increasing exponentially with increasing temperature (Figure 1.1c). Surface temperatures in the global ocean vary with latitude, with cooler temperatures towards the poles and warmer temperatures towards the equator. Daily variability in surface temperatures is relatively small while annual variability varies regionally between 2 and 20 °C [Lalli and Parsons, 1997]. Temperature also varies with depth in the water column, with higher temperatures in the mixed layer (0 to 200 m) and lower temperatures with depth.

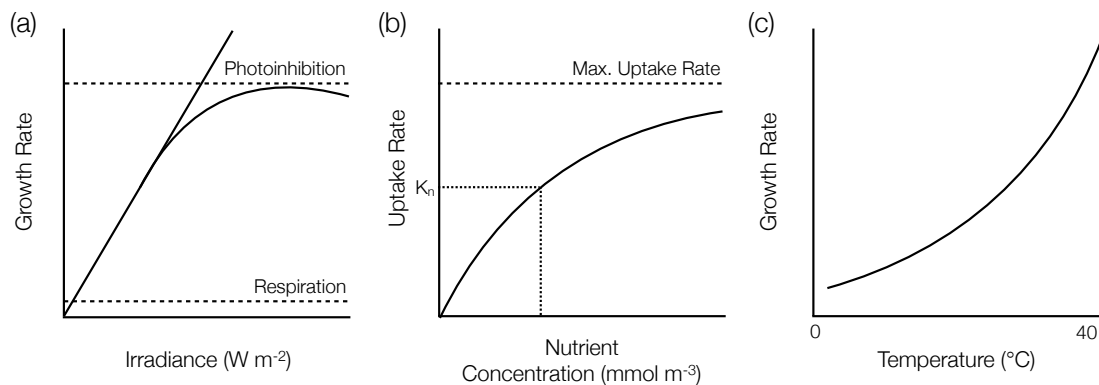


Figure 1.1: Schematic of phytoplankton growth as a function of light, nutrient concentration, and temperature. (a) Growth rate as a function of irradiance. Growth rate declines at high irradiance due to photoinhibition. (b) Nutrient uptake rate as a function of nutrient concentration. The half saturation constant, K_n , represents the growth rate at half the maximum value. (c) Growth rate as a function of temperature.

1.1.1 Observing Marine Phytoplankton

The spatial distribution of phytoplankton across the global ocean can be quantified by the remote measurement of ocean color, specifically the reflectance of the photosynthetic pigment chlorophyll a . Particles in the ocean, such as the photosynthetic pigment chlorophyll a , can absorb and scatter sunlight, altering the ocean's color. This color can be remotely observed by satellite imaging radiometers which measure the wavelength and intensity of any reflected electromagnetic radiation [Neville and Gower, 1977]. Chlorophyll reflects identifiable wavelengths and intensities, which can be used to infer certain phytoplankton properties and activities [Meister et al., 2012, Siegel et al., 2013]. Fluctuations in the relative intensity of the blue and green bands are driven by both changes in phytoplankton abundance in the surface water column and physiological responses to light and nutrient levels, allowing changes in the ocean biosphere to be observed on a variety of spatial and temporal scales [Behrenfeld et al., 2016]. Although the reflected signal may provide incomplete spatial coverage due to obscuring clouds and sun glint, 8-day and longer composites constructed from daily datasets which incorporate an atmospheric correction provide a near-complete image [Feng and Hu, 2016].

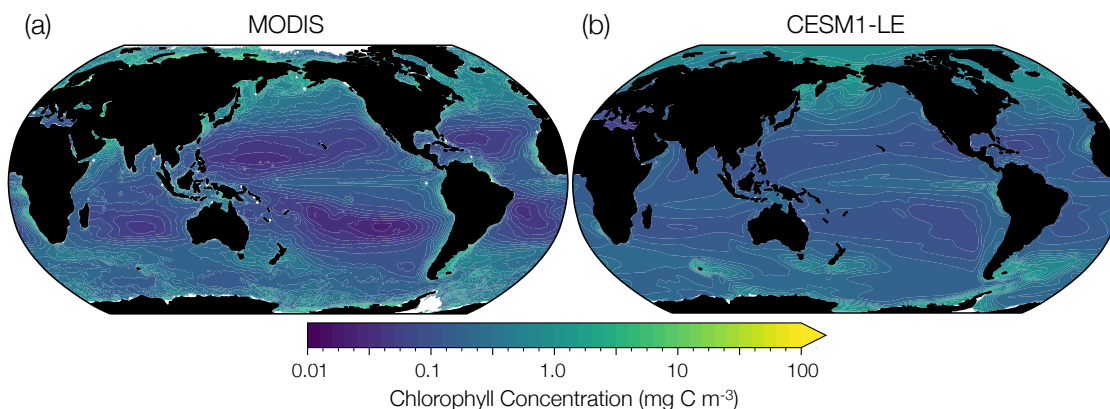


Figure 1.2: Comparison between observed and modeled chlorophyll concentrations. (a) Annual mean phytoplankton chlorophyll concentrations measured remotely by MODIS (2002 to 2020) (b) Annual mean phytoplankton chlorophyll concentration simulated by CESM1-LE over the historical period (1920 to 2005).

Algorithms which convert ocean color to phytoplankton chlorophyll a concentration (mg m^{-3}) have evolved from simple empirical regressions [Gordon and Morel, 1983] to complex radiative transfer equation inversions [Maritorena et al., 2002]. While each approach can be applied to a specific range of conditions, historically an algorithm based on the spectral ratio of remote sensing reflectance has been used to produce global chlorophyll a products from measurements made remotely by satellites. A commonly used algorithm to generate chlorophyll a products is the ocean color index (OCI), which measures the difference between reflectance measured in the green wavelengths and a linear reference between the blue and red wavelengths [Hu et al., 2012]. The OCI is particularly effective in the measurement of chlorophyll concentration below 0.25 mg m^{-3} which constitutes approximately three quarters of the global ocean [Hu et al., 2012]. These areas of relatively low chlorophyll concentration are concentrated in regions of the oligotrophic open ocean. Satellite-derived chlorophyll measurements can also be used in combination with other ocean variables (e.g., mixed layer depth, sea surface temperature) to estimate depth integrated net primary production (NPP) and biomass carbon of ocean phytoplankton [Saba et al., 2011, Bellacicco et al., 2020].

Over the past several decades, geospatial datasets of chlorophyll concentration have been

generated by multiple satellite instruments with varying spatial and temporal coverage. These include the Coastal Zone Color Scanner (CZCS), the Ocean Color and Temperature Sensor (OCTS), the Sea-viewing Wide Field-of-view Sensor (SeaWiFS), the Moderate Resolution Imaging Spectroradiometer (MODIS), the Medium Resolution Imaging Spectrometer (MERIS), and the Visible Infrared Imaging Radiometer Suite (VIIRS). Chlorophyll concentration varies spatially and temporally by orders of magnitude across the global ocean (Figure 1.2a). Variations in chlorophyll concentration may be attributed to changes in the physical environment, as well as phytoplankton physiology [Behrenfeld et al., 2016]. Annual-mean chlorophyll concentration is elevated in the subpolar, polar, equatorial, and eastern boundary upwelling regions; high concentrations in these regions result from the upwelling of deep, nutrient-rich waters to the surface ocean. In contrast, regions such as the subtropical gyres display relatively lower chlorophyll concentrations due to restrictions in nutrient supply (Figure 1.2a).

Marine phytoplankton can also be observed in situ using a variety of techniques which range in sampling scale. Phytoplankton can be sampled over large areas using continuous plankton recorders (CPRs). CPRs are devices which are towed behind ships which filter phytoplankton from the surface water column into discrete distance intervals. At smaller scales, phytoplankton can be observed at discrete locations using Conductivity, Temperature, Density (CTD) instruments which are lowered through the water column. These instruments simultaneously measure chlorophyll concentrations in the water column using fluorescence sensors. Water samples can also be sampled at discrete depth intervals in the water column using the CTD and analyzed using High Performance Liquid Chromatography (HPLC) to determine the concentration and type of photosynthetic pigments present. Qualitative assessments of phytoplankton concentration in the surface water column can be made using secchi disks which are lowered through the water column to determine water turbidity.

1.1.2 Modeling Marine Phytoplankton

Earth system models (ESMs) are coupled atmosphere-ocean-land general circulation models with explicit and interactive representation of terrestrial and marine carbon cycles and other

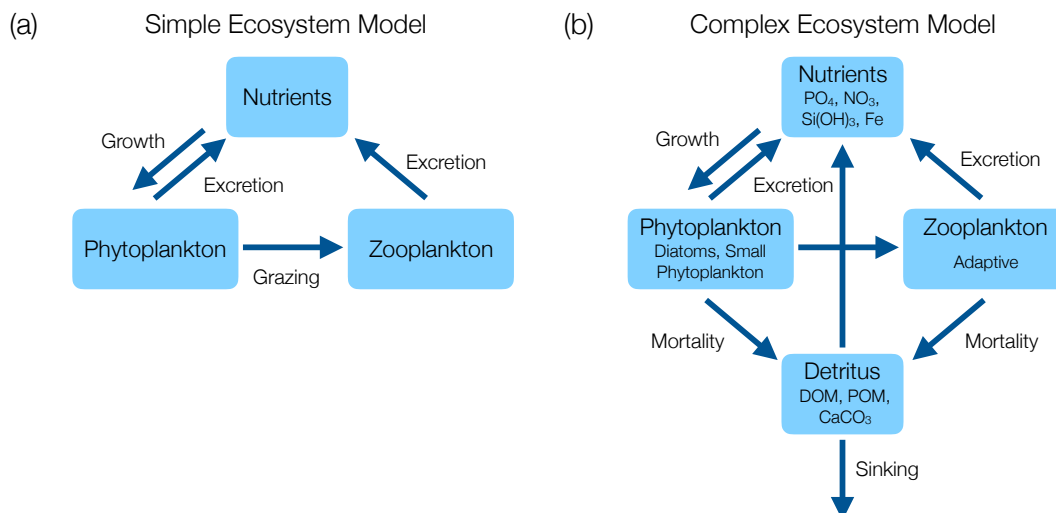


Figure 1.3: Biogeochemical ecosystem models range from simple to complex. (a) Simple NPZ models capture the relationships between nutrient, phytoplankton, and zooplankton reservoirs. (b) Complex NPZD models consider relationships between nutrients, phytoplankton, zooplankton, and a sinking detrital pool.

biogeochemical processes relevant to the climate system. The parameterization of biogeochemical/ecosystem models in ESMs can range from simple to complex. The most basic representation of a marine ecosystem can be modeled using a NPZ (Nutrient, Phytoplankton, Zooplankton) modeling framework (Figure 1.3a). NPZ models simulate relationships between nutrient, phytoplankton, and zooplankton over time. Simple NPZ models provide representation of a single phytoplankton functional type (PFT), a single zooplankton functional type (ZFT), and a single nutrient. In contrast, more complex NPZD (Nutrient, Phytoplankton, Zooplankton, Detritus) models consider relationships between nutrients, phytoplankton, zooplankton, and a sinking detrital pool (Figure 1.3b). Complex NPZD models often parameterize multiple nutrient co-limitation (e.g., ammonium, nitrate, phosphate, iron), multiple PFTs (e.g., diatoms, diazotrophs, small phytoplankton), and adaptive ZFTs. Additionally, the simulation of a sinking detrital pool allows for more realistic representation of nutrient recycling and export.

ESMs can be used as a predictive tool to identify long-term changes in phytoplankton abundance and productivity under different emission scenarios (Figure 1.2b). In simulations under

twenty-first century global warming conditions, phytoplankton abundance is predicted to decrease globally [Bopp et al., 2013, Steinacher et al., 2010, Henson et al., 2013]. Most models included in the Coupled Model Intercomparison Project Phase 5 (CMIP5) show consistent declines in phytoplankton abundance by 2100, though the magnitude of the decrease varies substantially between models [Bopp et al., 2013, Cabre et al., 2014] and across regions [Marinov et al., 2013, Laufkötter et al., 2015]. In addition to changes in phytoplankton abundance, phytoplankton community structure is also projected to shift, as nutrient reductions are predicted to favor the success of small phytoplankton relative to large phytoplankton [Marinov et al., 2010, Moore et al., 2013].

1.2 Climate Variability and Change

Understanding the impact of climate change on marine phytoplankton is challenged by our ability to disentangle fluctuations due to internal climate variability from those imposed by externally forced anthropogenic trends. Internal variability refers to variability in the climate system which occurs in the absence of external forcing, and includes processes related to the coupled ocean-atmosphere system (e.g., El Niño Southern Oscillation (ENSO), Pacific Decadal Oscillation (PDO)) [Santer et al., 2011, Deser et al., 2012, Meehl et al., 2013]. External forcing, in contrast, refers to the signal imposed by processes external to the climate system, such as solar variability, volcanic eruptions, and rising greenhouse gas concentrations from fossil fuel combustion [Deser et al., 2012, 2010, Schneider and Deser, 2018]. While not all external forcing is anthropogenic, the long-term rise in global temperature that leads to stratification and possible declines in chlorophyll concentration is anthropogenic, rather than natural [Rhein et al., 2013].

Phytoplankton can be influenced by internal climate variability through the propagation of physical climate variability to biologically relevant environmental variables. For example, a positive phasing of ENSO may display decreased phytoplankton biomass in the Eastern Equatorial Pacific due to relatively warmer sea surface temperatures which increase stratification and decrease upwelling nutrient flux [Chavez et al., 1998]. In contrast, a negative phasing of ENSO may display increased phytoplankton biomass in the Eastern Equatorial Pacific due to relatively cooler sea

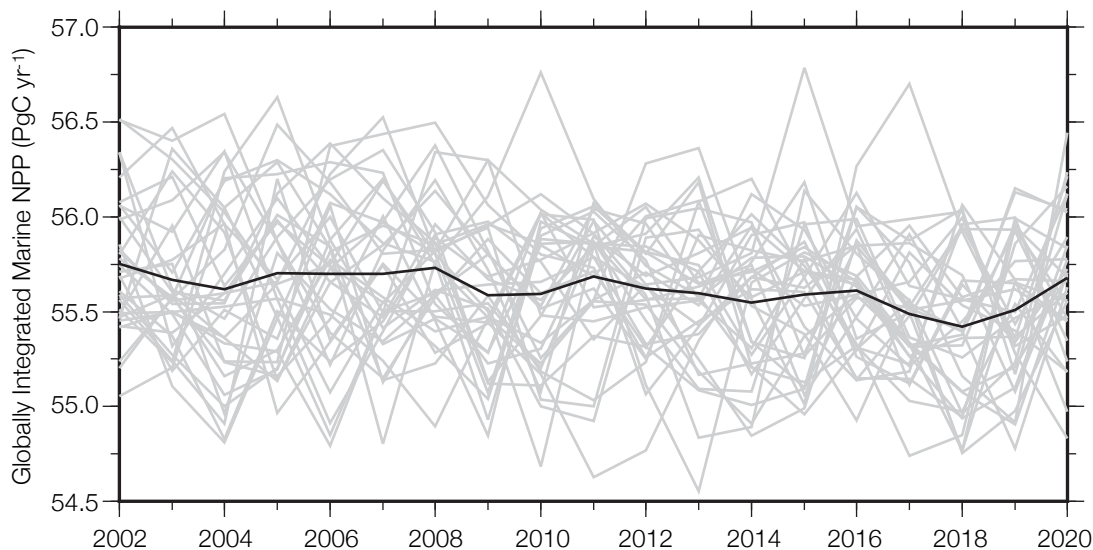


Figure 1.4: Simulated changes in net primary productivity (NPP) over the MODIS observational period (2002 to 2020) in the CESM1-LE with the ensemble mean shown in the black curve and the individual ensemble members shown in the gray curves (adapted from Krumhardt et al. [2017]). The ensemble mean represents the externally forced trend and the spread across the ensemble members approximates the range of internal variability.

surface temperatures which decrease stratification and increase upwelling nutrient flux [Chavez et al., 1998].

Phytoplankton may also be influenced by external forcing, particularly external anthropogenic forcing in the form of a warming climate. In response to a warming climate, the abundance and distribution of phytoplankton in the global ocean will likely change. Increasing global temperatures will warm the ocean surface more than the ocean interior, driving an increase in ocean stratification [Levitus et al., 2009]. An increase in stratification will reduce the upward flux of nutrients to the surface ocean and restrict phytoplankton growth, but may also alleviate light limitation [Bopp et al., 2001, Lozier et al., 2011]. In contrast, colder, nutrient-rich regions may see an increase in phytoplankton growth as increasing temperatures stimulate phytoplankton metabolism [Bopp et al., 2013, Krumhardt et al., 2017]. However, assessing disruption in the ocean biosphere in response to external forcing is challenged by the relatively short length of the observational record, restricting our ability to disentangle fluctuations due to internal climate variability from

those imposed by externally forced anthropogenic trends.

A relatively new approach to distinguishing externally forced anthropogenic signals from internal climate variability in modeled ocean phytoplankton is to analyze output from an ensemble of simulations conducted with a single Earth system model. In this context, each ensemble member has a different phasing of internal variability, but shares identical external forcing with other ensemble members [Deser et al., 2012]. An ensemble of simulations which each differ slightly in their initial conditions generates large internal variability in ocean biogeochemical variables (gray curves; Figure 1.4), while the ensemble mean demonstrates externally forced trends (black curve; Figure 1.4) [Rodgers et al., 2015, Long et al., 2016, McKinley et al., 2016, Lovenduski et al., 2016, Frölicher et al., 2016, Brady et al., 2019, Schlunegger et al., 2019].

1.3 Synopsis of the Dissertation

This dissertation examines the impact of internal climate variability on marine phytoplankton in a warming climate using both observational datasets and large ensembles of ESMs. Chapter 2 applies a novel statistical approach to construct an observationally constrained synthetic ensemble. The synthetic ensemble generated using the MODIS remotely sensed record of surface ocean chlorophyll concentration emulates observed internal variability in marine phytoplankton, providing context for the interpretation of externally derived trends over the observational record. Chapter 3 evaluates the statistical methodology of the observationally constrained synthetic ensemble in the context of a large ensemble of an ESM. When applying the statistical approach to the CESM1-LE over the historical period, the statistical method reproduces the simulated internal variability in surface ocean chlorophyll concentration. This chapter explores the interpretation of long-term trends in the presence of internal variability and identifies a wider range of possible trends in chlorophyll due to the sampling of internal variability in subpolar regions than in subtropical regions. Chapter 4 explores changes in phytoplankton internal variance with anthropogenic warming simulated by a large ensemble of an ESM. This chapter reveals global decline in phytoplankton internal variance in the CESM1-LE, which is reflected in similar declines in phytoplankton variance across

a suite of CMIP5 models. Statistical analysis reveals zooplankton grazing (top-down control) as an important contributor to declines in phytoplankton variance across several biogeochemically and ecologically important regions of the global ocean. Chapter 5 summarizes the major conclusions of this dissertation, places them into context in the marine biogeochemical observational and modeling research communities, and provides an outlook on future directions within the field.

Chapter 2

Finding the fingerprint of anthropogenic climate change in phytoplankton abundance

2.1 Abstract

We review how phytoplankton abundance may be responding to the increase in stratification associated with anthropogenic climate change, providing context on the utility of remote sensing datasets and Earth system model output to understand these perturbations. Assessing disruption in the ocean biosphere using remote sensing datasets is challenged by the relatively short length of the observational record, restricting our ability to disentangle fluctuations due to internal climate variability from those imposed by externally forced anthropogenic trends. Ensembles of Earth system models can be used to quantify past and future drivers, but may not skillfully predict observed spatial patterns and temporal dynamics in marine phytoplankton. To better understand the role of internal climate variability in the observational record, we construct a synthetic ensemble of global chlorophyll concentration over the MODIS satellite mission using statistical emulation techniques. We emphasize the use of a synthetic ensemble to illuminate the role of internal climate variability in the evolution of the ocean biosphere over time.

2.2 Introduction

The ocean biosphere is an important component of the climate system, absorbing 30% of anthropogenic carbon emissions and storing $45\times$ more carbon than the atmosphere [Friedlingstein et al., 2019]. Although phytoplankton constitute a small reservoir of carbon (3GtC), their capacity

to photosynthetically fix carbon from the atmosphere enhances the ocean’s role as a carbon sink [Falkowski, 2012]. The efficiency and strength of carbon sequestration by the biological pump in the oceanic reservoir strongly influences atmospheric carbon dioxide concentrations, with important feedbacks on the climate system [McKinley et al., 2017, Bindoff et al., 2019].

As the climate changes, the abundance and distribution of phytoplankton in the global ocean will likely also change. Increasing global temperatures will warm the ocean surface more than the ocean interior, driving an increase in ocean stratification [Levitus et al., 2009]. An increase in stratification will reduce the upward flux of nutrients to the surface ocean and restrict phytoplankton growth, but may also alleviate light limitation [Bopp et al., 2001, Lozier et al., 2011]. In contrast, colder, nutrient-rich regions may see an increase in phytoplankton growth as increasing temperatures stimulate phytoplankton metabolism [Bopp et al., 2013, Krumhardt et al., 2017].

Here, we review how phytoplankton abundance may be responding to the increase in stratification associated with anthropogenic climate change, providing context on the utility of remote sensing datasets and Earth system model (ESM) output to understand these perturbations. An ESM is a global climate or general circulation model (GCM) with explicit and interactive representation of terrestrial and marine carbon cycles and other biogeochemically important processes. Each of these methods has advantages and disadvantages in diagnosing anthropogenic change. Assessing disruption in the ocean biosphere using remote sensing datasets is challenged by the relatively short length of the observational record, restricting our ability to disentangle fluctuations due to internal climate variability from those imposed by externally forced anthropogenic trends [Henson et al., 2010]. While ensembles of ESMs can be used to quantify past and future changes in phytoplankton abundance and attribute these changes to internal or external drivers, models may not skillfully predict the observed phytoplankton chlorophyll field [Krumhardt et al., 2017, Doney et al., 2009].

To overcome these limitations, we construct a synthetic ensemble of global ocean chlorophyll concentration by applying statistical emulation techniques to the 17-year Moderate Resolution Imaging Spectroradiometer (MODIS) chlorophyll record. Much like large initial condition ensembles generated with ESMs, our synthetic ensemble represents multiple possible evolutions of ocean

chlorophyll concentration, each with a different phasing of internal climate variability (e.g., El Niño Southern Oscillation, Pacific Decadal Oscillation) but with shared external forcing (e.g., slow declines driven by increasing stratification) [Deser et al., 2012, McKinnon et al., 2017, McKinnon and Deser, 2018]. Our synthetic ensemble can be used for a variety of purposes, including diagnosing patterns of internal variability in observed chlorophyll, and validating ESM representation of such variability.

2.2.1 Importance of Phytoplankton to Ocean Biogeochemical Dynamics

The distribution and abundance of phytoplankton in the global ocean is controlled by temperature and the availability of light and nutrients [Sigman and Hain, 2012]. These variables are modulated by physical, chemical, and biological processes that vary across regional ocean ecosystems. The distribution of phytoplankton at a global scale can be quantified by the remote measurement of ocean color, specifically the reflectance of the photosynthetic pigment chlorophyll *a*. Chlorophyll concentration varies spatially and temporally by orders of magnitude across the global ocean (Figure 2.1a). Variations in chlorophyll concentration may be attributed to changes in the physical environment, as well as phytoplankton physiology [Behrenfeld et al., 2016]. Annual-mean chlorophyll concentration is elevated in the subpolar, polar, equatorial, and eastern boundary upwelling regions; high concentrations in these regions result from the upwelling of deep, nutrient-rich waters to the surface ocean. In contrast, regions such as the subtropical gyres display relatively lower chlorophyll concentrations due to restrictions in nutrient supply (Figure 2.1a).

The global distribution of chlorophyll is also tightly coupled to light availability. Mean annual light availability decreases from the equator to the poles. In nutrient-replete subpolar and polar regions, phytoplankton growth is restricted in the winter when light is limited and enhanced in the spring, summer, and autumn when light is more abundant, creating a strong seasonal cycle in chlorophyll. In contrast, subtropical oceanic regions with ample light tend to be instead limited by the supply of nutrients due to a permanent thermocline, showing only moderate seasonality [Lalli and Parsons, 1997, Giovannoni and Vergin, 2012]. Thus, the spatiotemporal distribution of

chlorophyll in the global ocean varies primarily as a function of both light and nutrient availability. Further, satellite-derived chlorophyll measurements are frequently used in combination with other ocean variables (e.g., mixed layer depth, sea surface temperature) to estimate depth integrated net primary production (NPP) of ocean phytoplankton [Saba et al., 2011]. While various NPP algorithm solutions differ substantially, these aim to relate ocean color observations of chlorophyll to oceanic carbon cycling.

Phytoplankton harvest light to convert inorganic carbon to organic carbon through the process of photosynthesis. Oxygenic photosynthesis by phytoplankton in the surface ocean (between 0 and 200 m depth) is responsible for the consumption of carbon dioxide and the biochemical production of organic matter [Sarmiento and Gruber, 2006]. A high proportion ($\sim 99\%$) of this organic matter is respired by heterotrophic organisms in the surface ocean rather than exported to depth [Emerson and Hedges, 2008]. The sinking of a small fraction of organic carbon through the water column forms the basis of the biological pump, a biologically driven process which sequesters carbon from the atmosphere to the ocean interior [McKinley et al., 2017]. The efficiency and strength of the biological pump strongly influences the global carbon cycle by contributing to the amount of carbon removed from the surface ocean and transported to depth [Sarmiento and Gruber, 2006].

The consumption of nutrients by phytoplankton influences the concentration and distribution of chemical species in the global ocean. When phytoplankton photosynthetically fix carbon in the surface ocean, they require a variety of nutrients. Nitrate, phosphate, and iron are among the nutrients required by phytoplankton and the assimilation of these nutrients in the surface ocean alters their vertical and lateral distribution [Sarmiento and Gruber, 2006]. Nutrients such as nitrate, phosphate, and silicate are considered macronutrients, which are required by phytoplankton in large amounts to support cellular growth and metabolism. In contrast, micronutrients such as iron, zinc, and cobalt are required in small amounts for the activity of enzymes and other intracellular functions [Sunda, 2013]. In the global ocean, phytoplankton can be limited by either macronutrients or micronutrients. In polar regions, particularly the Southern Ocean, phytoplankton are limited by micronutrients, such as iron, and there is an abundance of macronutrients [Moore et al., 2002].

In contrast, in regions of the subtropical gyres, phytoplankton are limited by low concentrations of macronutrients such as nitrate and phosphate.

In addition to influencing nutrient and carbon distributions in the ocean, phytoplankton also serve as the base of the marine food web [Falkowski, 2012]. Heterotrophic zooplankton graze on phytoplankton and act as primary consumers in oceanic ecosystems. Phytoplankton productivity supports complex food webs and diverse marine ecosystems by providing sustenance for higher trophic levels. Perturbations to phytoplankton productivity by anthropogenic climate change have the potential to trigger trophic cascades, dramatic reorganizations of the marine food web [Cheung et al., 2010, Pörtner et al., 2014]. However, the exact manifestations of these dramatic reorganizations in the ocean biosphere remain uncertain.

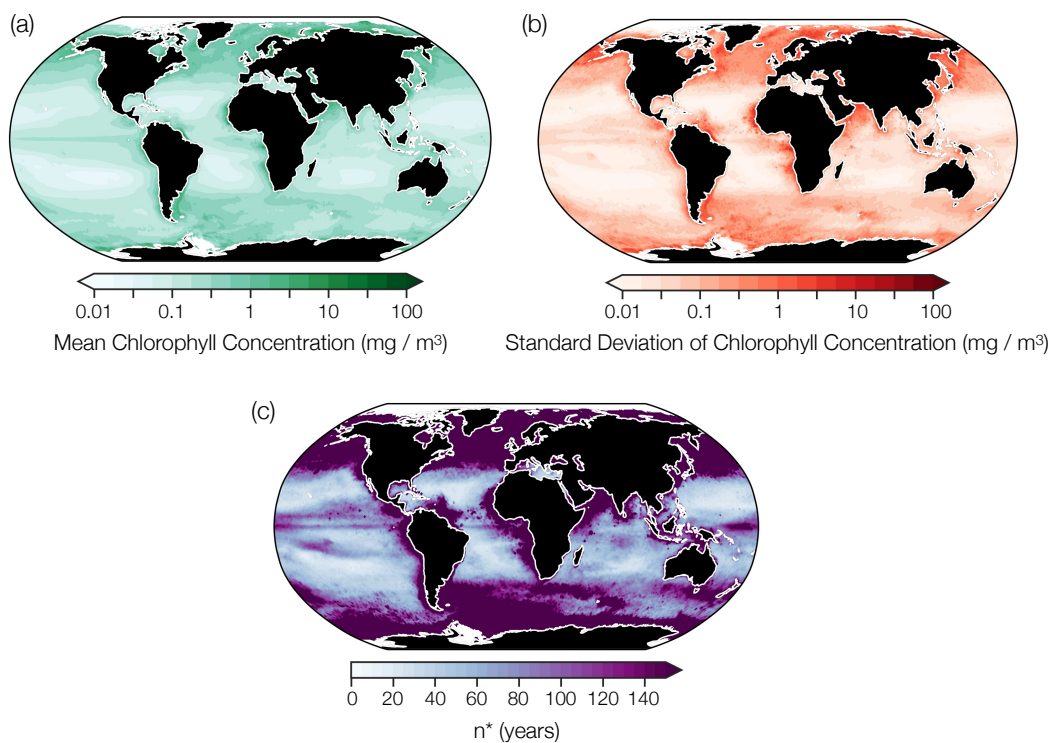


Figure 2.1: (a) Spatial distribution of chlorophyll concentration in milligrams of carbon per cubic meter over the MODIS satellite record (2002 to 2019). (b) Standard deviation of detrended and deseasonalized chlorophyll concentration over the MODIS satellite record (2002 to 2019). (c) Number of years of continuous ocean color data required to distinguish a climate change driven trend in chlorophyll concentration from natural climate variability over the MODIS satellite record. Calculated following the method of Tiao et al. [1990] and Weatherhead et al. [1998]

2.2.2 Anthropogenic Stratification and Ocean Phytoplankton

Anthropogenic climate change is heating the global ocean [Levitus et al., 2009]. Due to direct contact with a warming atmosphere, the ocean’s surface is warming more rapidly than deeper waters, with temperatures in the upper 75 m increasing at a rate of 0.11 °per decade [Rhein et al., 2013]. As a result, the thermal stratification (the strength of the vertical density gradient) of the upper ocean (0 to 200 m depth) has increased by approximately 4% since the 1970s, shoaling the depth of the mixed layer [Rhein et al., 2013].

Enhanced stratification of the upper ocean restricts the transport of nutrients to the euphotic zone, limiting phytoplankton growth [Bopp et al., 2001]. This trend is corroborated by both remote sensing datasets and ESM output. Remote sensing datasets suggest low-nutrient regions have expanded at rates of 0.8 to 4.3% per year between 1998 and 2006, consistent with a reduction in nutrient availability due to enhanced stratification [Polovina et al., 2008, Irwin and Oliver, 2009]. A variety of ESMs predict a reduction in net primary productivity (NPP) in low- to mid-latitude regions under twenty-first century global warming simulations [Bopp et al., 2001, 2013, Krumhardt et al., 2017, Schmittner et al., 2008, Steinacher et al., 2010, Marinov et al., 2013, Laufkötter et al., 2015, Kwiatkowski et al., 2017]. The primary mechanism explaining this change is enhanced stratification and the subsequent restriction in vertical nutrient supply.

2.3 Observing Changes in Ocean Phytoplankton

Particles in the ocean, such as the photosynthetic pigment chlorophyll *a*, can absorb and scatter sunlight, altering the ocean’s color. This color can be remotely observed by satellite imaging radiometers which measure the wavelength and intensity of any reflected electromagnetic radiation [Neville and Gower, 1977]. Chlorophyll reflects identifiable wavelengths and intensities, which can be used to infer certain phytoplankton properties and activities [Meister et al., 2012, Siegel et al., 2013]. Fluctuations in the relative intensity of the blue and green bands are driven by both changes in phytoplankton abundance in the surface water column and physiological responses to light and

nutrient levels, allowing changes in the ocean biosphere to be observed on a variety of spatial and temporal scales [Behrenfeld et al., 2016]. Although the reflected signal may provide incomplete spatial coverage due to obscuring clouds and sun glint, 8-day and longer composites constructed from daily datasets which incorporate an atmospheric correction provide a near-complete image [Feng and Hu, 2016].

Algorithms which convert ocean color to phytoplankton chlorophyll *a* concentration (mg m^{-3}) have evolved from simple empirical regressions [Gordon and Morel, 1983] to complex radiative transfer equation inversions [Maritorena et al., 2002]. While each approach can be applied to a specific range of conditions, historically an algorithm based on the spectral ratio of remote sensing reflectance has been used to produce global chlorophyll *a* products from measurements made remotely by satellites. A commonly used algorithm to generate chlorophyll *a* products is the ocean color index (OCI), which measures the difference between reflectance measured in the green wavelengths and a linear reference between the blue and red wavelengths [Hu et al., 2012]. The OCI is particularly effective in the measurement of chlorophyll concentration below 0.25 mg m^{-3} which constitutes approximately three quarters of the global ocean [Hu et al., 2012]. These areas of relatively low chlorophyll concentration are concentrated in regions of the oligotrophic open ocean. Over the past several decades geospatial datasets of chlorophyll concentration have been generated by multiple satellite instruments with varying spatial and temporal coverage. These include the Coastal Zone Color Scanner (CZCS), the Ocean Color and Temperature Sensor (OCTS), the Sea-viewing Wide Field-of-view Sensor (SeaWiFS), the Moderate Resolution Imaging Spectroradiometer (MODIS), the Medium Resolution Imaging Spectrometer (MERIS), and the Visible Infrared Imaging Radiometer Suite (VIIRS). The MODIS satellite mission provides the longest continuous record of global ocean chlorophyll concentration, with coverage from 2002 to present. Figure 1a illustrates the mean of monthly averaged surface ocean chlorophyll concentrations calculated using the OCI algorithm at $1^\circ \times 1^\circ$ resolution over the MODIS satellite mission (2002 to 2019).

Although there is a mechanistic understanding of how anthropogenic change may affect the

ocean biosphere over time, there is debate about whether these changes are already detectable from remotely sensed observations [Henson et al., 2010, Beaulieu et al., 2013, Henson, 2014, Henson et al., 2016, Hammond et al., 2017]. Assessing changes in the ocean biosphere using remote sensing data is challenged by the relatively short length of the continuous observational record and high temporal variability [Beaulieu et al., 2013, Henson et al., 2016]. Figure 2.1b displays the standard deviation of monthly averaged surface ocean chlorophyll concentrations at $1^\circ \times 1^\circ$ resolution from the MODIS record, illustrating that in addition to the spatial variability in chlorophyll (Figure 2.1a), there is also substantial temporal variability.

The short length of the observed chlorophyll record restricts our ability to disentangle fluctuations due to internal climate variability from those imposed by externally forced anthropogenic trends [Beaulieu et al., 2013, Henson et al., 2016]. In this context, *internal variability* refers to variability of the climate system which occurs in the absence of external forcing, and includes processes related to the coupled ocean-atmosphere system (e.g., El Niño Southern Oscillation (ENSO), Pacific Decadal Oscillation (PDO)) [Santer et al., 2011, Deser et al., 2012, Meehl et al., 2013]. *External forcing*, in contrast, refers to the signal imposed by processes external to the climate system, such as solar variability, volcanic eruptions, and rising greenhouse gas concentrations from fossil fuel combustion [Deser et al., 2012, 2010, Schneider and Deser, 2018]. While not all external forcing is *anthropogenic*, the long-term rise in global temperature that leads to stratification and possible declines in chlorophyll concentration is anthropogenic, rather than *natural* [Rhein et al., 2013].

A small number of studies suggest that the influence of anthropogenic global warming on the ocean biosphere can be detected over an observational period as short as a decade [Behrenfeld et al., 2007]. A decline in global chlorophyll concentration by $0.01 \text{ Tg year}^{-1}$ between 1999 and 2006 was inferred by Behrenfeld et al. [2007] to reflect a response of the ocean biosphere to global climate change. An inverse relationship between chlorophyll concentration and sea surface temperature in the tropics and subtropics suggested that enhanced thermal stratification was restricting surface nutrient supply and limiting phytoplankton growth in these regions. Several recent studies using remote-sensing datasets have identified changes in satellite-derived chlorophyll or phytoplankton

productivity in specific oceanic regions, such as the Southern Ocean [Castillo et al., 2019], and the Pacific and Indian Oceans [Gregg and Rousseaux, 2019].

Studies of phytoplankton biomass or productivity over longer timescales have also attributed changes in phytoplankton abundance to anthropogenic climate change [Boyce et al., 2010, Osman et al., 2019]. An integrated dataset of remote sensing observations and in situ chlorophyll measurements compiled since 1899 revealed a decrease in phytoplankton biomass by approximately 1% per year, attributable to enhanced thermal stratification [Boyce et al., 2010]. However, observational datasets from the Hawaii Ocean Time Series (HOTS), Bermuda Atlantic Ocean Time Series (BATS), and the California Cooperative Oceanic Fisheries Investigations (CalCOFI) indicated increased phytoplankton biomass over the last 20 to 50 years [Saba et al., 2010]. These conflicting findings demonstrate the sensitivity of phytoplankton trends to the methodology and length of record.

A majority of studies which incorporate a variety of ESMs and remotely sensed datasets of phytoplankton abundance suggest that a continuous observational record of between 20 and 60 years is required to detect a statistically significant trend in remote sensing datasets of chlorophyll concentration [Krumhardt et al., 2017, Beaulieu et al., 2013, Henson, 2014, Henson et al., 2016, Gregg and Rousseaux, 2014]. Long-term changes in the ocean biosphere are detectable if the trend is appreciably larger than the noise generated by internal climate variability and a sufficient length of continuous observations is available. However, in the majority of the global ocean the expression of internal variability obscures identification of possible forced secular trends in the climate record. The duration of observational time-series required varies regionally in the global ocean as a function of the regional secular signal to noise ratio [Henson et al., 2010]. The number of years required to distinguish a trend from variability is calculated using the method of Tiao et al. [1990] and Weatherhead et al. [1998]. The number of years, n^* , required to detect a linear trend with a probability of 90% is

$$n^* = \left[\frac{3.3\sigma_N}{|\omega|} * \sqrt{\frac{1+\varphi}{1-\varphi}} \right]^{2/3} \quad (2.1)$$

where σ_N is the standard deviation of the noise (chlorophyll anomalies with linear trend and seasonal cycle removed), ω is the trend (the global average trend in chlorophyll concentration over the observational period), and φ is the autocorrelation (the lag-1 autocorrelation of chlorophyll anomalies over the observational period). Figure 2.1c illustrates the number of years of continuous remote sensing data required to distinguish a trend in chlorophyll concentration from variability over the MODIS satellite mission. The length of the time series required to detect a statistically significant trend varies regionally, with relatively short time series required in regions with low temporal variability (subtropics) and relatively longer time series required in regions with high temporal variability (coastal upwelling zones and polar regions).

Using Equation 2.1, with σ_N and φ estimated from satellite observations at $1^\circ \times 1^\circ$ resolution, we find approximately 40 years of continuous remote sensing observations are required to detect a statistically meaningful trend in global chlorophyll concentrations, while detection times are predicted to be shorter (20 to 30 years) in regions with relatively lower temporal variability (Figure 2.1c) [Henson et al., 2010]. This is in agreement with previous modeling studies which also used Equation 2.1 to determine detection timescales for anthropogenic changes in surface chlorophyll concentrations but estimated the parameter values with ESMs [Henson et al., 2016].

2.4 Modeling Changes in Ocean Phytoplankton

Earth system models (ESMs) can be used as a predictive tool to identify long-term changes in phytoplankton abundance and productivity under different emission scenarios. In simulations under twenty-first century global warming conditions, phytoplankton abundance is predicted to decrease globally [Bopp et al., 2013, Steinacher et al., 2010, Henson et al., 2013]. Most models included in the Coupled Model Intercomparison Project Phase 5 (CMIP5) show consistent declines in phytoplankton abundance by 2100, though the magnitude of the decrease varies substantially

between models [Bopp et al., 2013, Cabre et al., 2014]. The majority of models project an increase in phytoplankton abundance in the high latitude ocean as light limitation is alleviated from thermal stratification, increasing temperature stimulates photosynthesis, and sea ice cover declines. In contrast, a decrease in the low latitude oceans is projected as nutrient limitation from thermal stratification is enhanced [Bopp et al., 2013, Steinacher et al., 2010, Kwiatkowski et al., 2017].

A warming ocean can both enhance phytoplankton growth rate as increased temperatures accelerate metabolic reactions and restrict phytoplankton abundance due to enhanced thermal stratification resulting in surface nutrient reductions [Marinov et al., 2013]. These conflicting controls on phytoplankton growth may generate regional differences in simulated phytoplankton abundance projections depending on the predominant effect [Marinov et al., 2013, Laufkötter et al., 2015]. For example, in CMIP5 models, integrated phytoplankton abundance projections with climate change vary latitudinally depending on whether temperature, light, micronutrients, or macronutrients are limiting, with macronutrient and temperature controls dominant between 45°S to 45°N latitude [Leung et al., 2015].

Regional biome changes under climate warming scenarios are also predicted to shift phytoplankton community structure. Thermal stratification and subsequent nutrient reduction are predicted to favor the success of small phytoplankton relative to large phytoplankton [Marinov et al., 2010, Moore et al., 2013]. Due to a relatively larger surface area-to-volume ratio, smaller phytoplankton more efficiently assimilate nutrients than larger phytoplankton. The parameterization of this effect in the Community Earth System Model (CESM1) generates biogeochemical regime boundaries at 45°N and 45°S latitude, where a specific threshold surface nutrient concentration occurs; within the lowlatitude region demarcated by these boundaries, decreases in surface nutrient supply result in greater decreases in large phytoplankton biomass because smaller phytoplankton are less impacted by nutrient decreases in low-nutrient conditions [Marinov et al., 2010].

A relatively new approach to distinguishing externally forced anthropogenic signals from internal climate variability in modeled ocean phytoplankton is to analyze output from an ensemble of simulations conducted with a single Earth system model; here, each ensemble member has a

different phasing of internal variability, but shares identical external forcing with other ensemble members [Deser et al., 2012]. An ensemble of simulations which each differ slightly in their initial conditions generates large internal variability in ocean biogeochemical variables, while the ensemble mean demonstrates externally forced trends [Rodgers et al., 2015, Long et al., 2016, McKinley et al., 2016, Lovenduski et al., 2016, Frölicher et al., 2016, Brady et al., 2019, Schlunegger et al., 2019]. The Community Earth System Model large ensemble (CESM1-LE) is a fully coupled global climate model that provides reconstructions of Earth’s past climate and projections of Earth’s future climate under different forcing scenarios, simulating the temporal evolution of the climate system of multiple ensemble members, each with slightly different initial conditions [Kay et al., 2015]. Many other fully coupled climate models also utilize the large ensemble framework, including the GFDL Earth System Model 2M (ESM2M [Rodgers et al., 2015, Frölicher et al., 2016, Schlunegger et al., 2019]).

In order to quantify timescales over which externally forced trends in multiple ocean biogeochemical variables can emerge from internal variability, Rodgers et al. [2015] employed a perturbed initial condition ensemble of ESM2M to simulate changes under a historical emission scenario and representative concentration pathway 8.5 (RCP 8.5), which is considered a high emissions or business-as-usual scenario. This analysis revealed that anthropogenic changes to global mean marine NPP would be the last of four biogeochemical variables analyzed to emerge from internal variability after changes in acidification, SST, and oxygen concentrations, respectively. A complementary study with the same model framework that incorporated several additional biogeochemical variables also found that global warming-induced changes in marine NPP would be slowest to emerge [Schlunegger et al., 2019]. Taken together, these two studies suggest that significant changes in phytoplankton biomass may take a longer time to detect compared with other biogeochemical variables [Rodgers et al., 2015, Schlunegger et al., 2019].

In addition to diagnosing timescales of emergence for biogeochemical parameters, perturbed initial condition ensembles can be used to constrain the contribution of internal climate variability on uncertainty in projections of marine NPP. Simulations forced with radiative forcing scenarios RCP 2.6 and RCP 8.5 using CMIP5 models revealed that internal climate variability in ESMs

can contribute significant uncertainty to future projections of marine NPP, especially on regional scales [Krumhardt et al., 2017, Frölicher et al., 2016]. Krumhardt et al. [2017] identified avoidable impacts of anthropogenic climate change on declining phytoplankton abundance by comparing ensemble integrations of the CESM1-LE forced with two different radiative forcing scenarios: RCP 4.5 (mitigation emission scenario) and RCP 8.5 (high emissions scenario). Their study suggests that if we follow a mitigation emission scenario (RCP 4.5), large-scale regional declines in NPP are only avoidable in the Atlantic sector, whereas large internal climate variability precludes statistical separation of the externally forced NPP response elsewhere.

Although ESMs are an effective tool for projecting the response of the ocean biosphere to anthropogenic climate change, it is essential to consider how the ESM representation of phytoplankton abundance compares to observed records of phytoplankton over time. Phytoplankton concentrations have been measured continuously over multiple decades at several ocean time series locations in the global ocean. Saba et al. [2010] compared the representation of chlorophyll concentration from 36 ESMs with embedded biogeochemistry to observational datasets collected at the ocean time series of HOTS and BATS between 1989 and 2007. At both sites, time-series observations of monthly mean chlorophyll concentration are larger than those produced by 90% of current generation ESMs, motivating further evaluation of the ESM representation of chlorophyll on both monthly and interannual timescales; the models also performed relatively poorly at producing an observed increasing NPP trend, indicating that ESMs may not accurately simulate multiannual changes in phytoplankton abundance over short time periods.

2.5 Synthetic Ensemble of Ocean Chlorophyll Concentration

A complementary approach to quantifying internal variability in phytoplankton abundance is to construct an observationally constrained synthetic ensemble by statistically emulating the satellite-derived chlorophyll record. Observations can provide a strong constraint on uncertainty related to internal climate variability over time in cases where the dominant timescales of variability are resolved within the observed record. With this constraint, the synthetic ensemble consists of

alternate evolutions of the observed spatiotemporal field that preserve the statistical properties of the single observational record.

In order to generate a synthetic ensemble of global chlorophyll concentration, we build upon the statistical model developed in McKinnon et al. [2017] and McKinnon and Deser [2018] for temperature, precipitation, and sea level pressure. In our case, we model chlorophyll concentration as

$$X^{i,t} = \beta_0^i + \beta_S^{i,m} + \beta_F^t + \beta_{ENSO}^{i,m} M_{ENSO}^t + \beta_{PDO}^{i,m} M_{PDO}^t + \epsilon^{i,t} \quad (2.2)$$

where $X^{i,t}$ is the chlorophyll concentration at location i and time t . We model chlorophyll as a linear combination of the mean state (β_0^i), seasonality ($\beta_S^{i,t}$), response to external forcing (β_F^t), response to two dominant climate modes ($\beta_{ENSO}^{i,m(t)} M_{ENSO}^t$, $\beta_{PDO}^{i,m(t)} M_{PDO}^t$), and residual internal climate variability ($\epsilon^{i,t}$). Importantly, the β_F^t term in Equation 2.2 represents the chlorophyll response to external forcing, while the last three terms represent internal climate variability. The two time series M_{ENSO}^t and M_{PDO}^t represent the evolution of the climate modes ENSO and PDO respectively, which have been shown to influence chlorophyll concentration [Gregg and Conkright, 2002, Yoder and Kennelly, 2003, Radenac et al., 2012]. Due to covariance between ENSO and PDO, we have created two orthogonalized time series via principal component analysis of the original observed temporal evolution of ENSO and PDO over 1880 to 2019. Chlorophyll anomalies are calculated by removing the mean state (β_0^i), monthly climatology ($\beta_S^{i,t}$), and linear trend in global mean chlorophyll (β_F^t) from the original MODIS dataset of chlorophyll concentration at monthly, $1^\circ \times 1^\circ$ resolution (Figure 2.2b). $\beta_{ENSO}^{i,m(t)}$ and $\beta_{PDO}^{i,m(t)}$ are estimated by calculating the ordinary least squares regression of the MODIS chlorophyll anomalies against time series of ENSO and PDO to determine the sensitivity of chlorophyll concentration to these modes. The spatially varying regression coefficients are multiplied by the observed indices and subtracted from the chlorophyll anomalies to remove the direct influence of the climate modes from the time series (Figure 2.2b), leaving us with the residual internal climate variability, $\epsilon^{i,t}$.

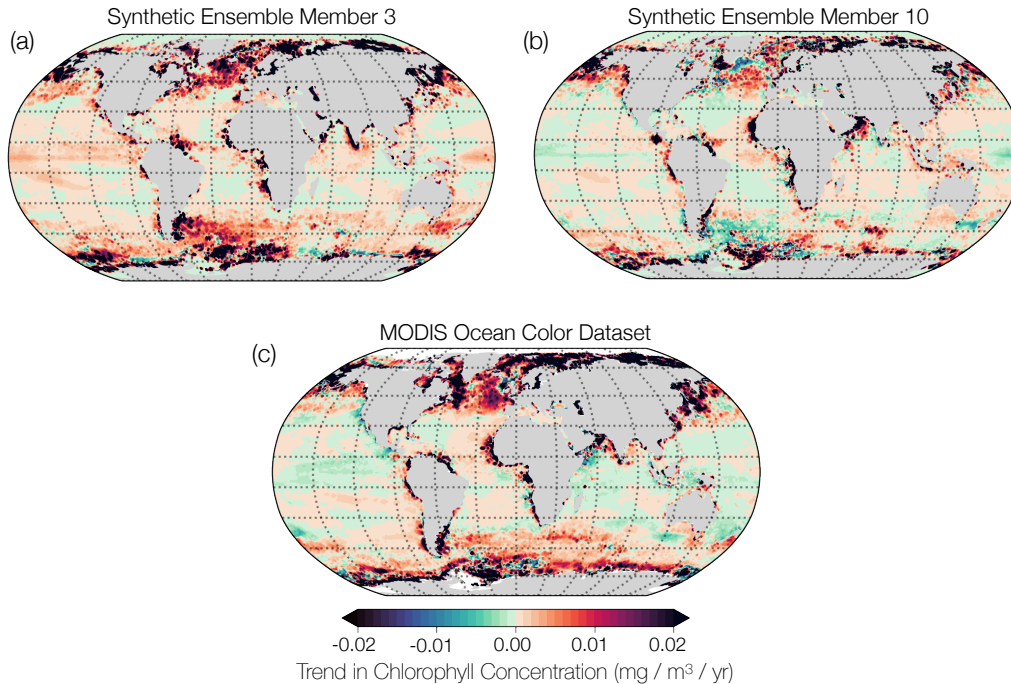


Figure 2.2: Schematic representation of the construction of a synthetic ensemble of regional ocean chlorophyll concentration in the Eastern Equatorial Pacific. (a) Original MODIS observed time series. (b) Remove mean, linear trend, monthly climatology, and scaled climate modes from original time series. (c) Block bootstrap residuals 1000 times using the moving block bootstrap method. (d) Generate 1000 surrogate climate modes of ENSO and PDO using the iterative adjusted amplitude Fourier transformation method. (e) Generate distinct ensemble members by combining the mean, the trend, the seasonal cycle, the block bootstrapped anomalies, and the response to surrogate climate modes. Synthetic ensemble member 3 is shown in the light blue line, and synthetic ensemble 10 is shown in the orange line. Dashed red lines represent the trend of each synthetic ensemble member over the observational period.

We take a two-step process to create the synthetic ensemble. First, the residuals, $\epsilon^{i,t}$, are resampled 1000 times using the nonparametric moving block bootstrap (MBB) in time, retaining their spatial structure (Figure 2.2c) [Wilks, 1997]. The residuals are resampled using a block length of 12 months which fully encapsulates the seasonal cycle in global chlorophyll concentration variability. Second, the response of chlorophyll concentration to different possible evolutions of climate modes over time is incorporated by generating 1000 surrogate climate modes of ENSO and PDO using the iterative adjusted amplitude Fourier transformation (IAAFT) method (Figure 2.2d) [Theiler et al., 1992, Schreiber and Schmitz, 2000]. This surrogate data approach produces an

ensemble of time series with the same spectral characteristics as the original climate mode time series. The surrogate climate modes are multiplied by the regression coefficients, $\beta_{ENSO}^{i,m(t)}$ and $\beta_{PDO}^{i,m(t)}$, estimated from the observed record to create time series of chlorophyll that could have occurred given a different temporal evolution of ENSO and PDO. We combine the block bootstrapped anomalies and the response to the surrogate climate modes with β_0^i , $\beta_S^{i,t}$, and β_F^t to produce multiple distinct synthetic ensemble members (Figure 2.2e). Figure 2.2e illustrates the temporal evolution of two synthetic ensemble members in the Eastern Equatorial Pacific. Each member displays a different long-term trend at this location due to different sampling of climate variability.

Figure 2.3 displays the spatial pattern of the trend in annual-mean chlorophyll concentration over 2002 to 2019 for two distinct synthetic ensemble members. Synthetic ensemble members 3 (Figure 2.3a) and 10 (Figure 2.3b) exhibit trends of opposite sign in many regions of the ocean. For example, in the Eastern Equatorial Pacific, synthetic ensemble member 3 depicts a trend toward increasing chlorophyll concentrations over time, while synthetic ensemble member 10 displays a trend toward decreasing chlorophyll. This behavior is also apparent in the California Current Eastern Boundary Upwelling System, the subpolar North Atlantic, the subtropical Pacific, and the Southern Ocean. Thus, results from our synthetic ensemble suggest that internal variability plays an important role in chlorophyll concentration in these regions, consistent with previous studies [Henson et al., 2010, Schneider and Deser, 2018, Schlunegger et al., 2019].

Observed trends in real-world chlorophyll concentration from the MODIS record (Figure 2.3c) show decreasing chlorophyll over time in the subtropical oceans and the California Current Eastern Boundary Upwelling System, with increasing chlorophyll over time in the subpolar North Atlantic, parts of the Southern Ocean, and other Eastern Boundary Upwelling Systems. The real world is a single realization (or ensemble member) in our ensemble framework. As such, the observational record is equally affected by the phasing of internal climate variability in the real world. That the negative trend in observed chlorophyll in the California Current Eastern Boundary Upwelling System is captured in synthetic ensemble member 3 but not member 10 implies that the observed trend is driven by the phasing of internal variability, for example. Our synthetic ensemble thus

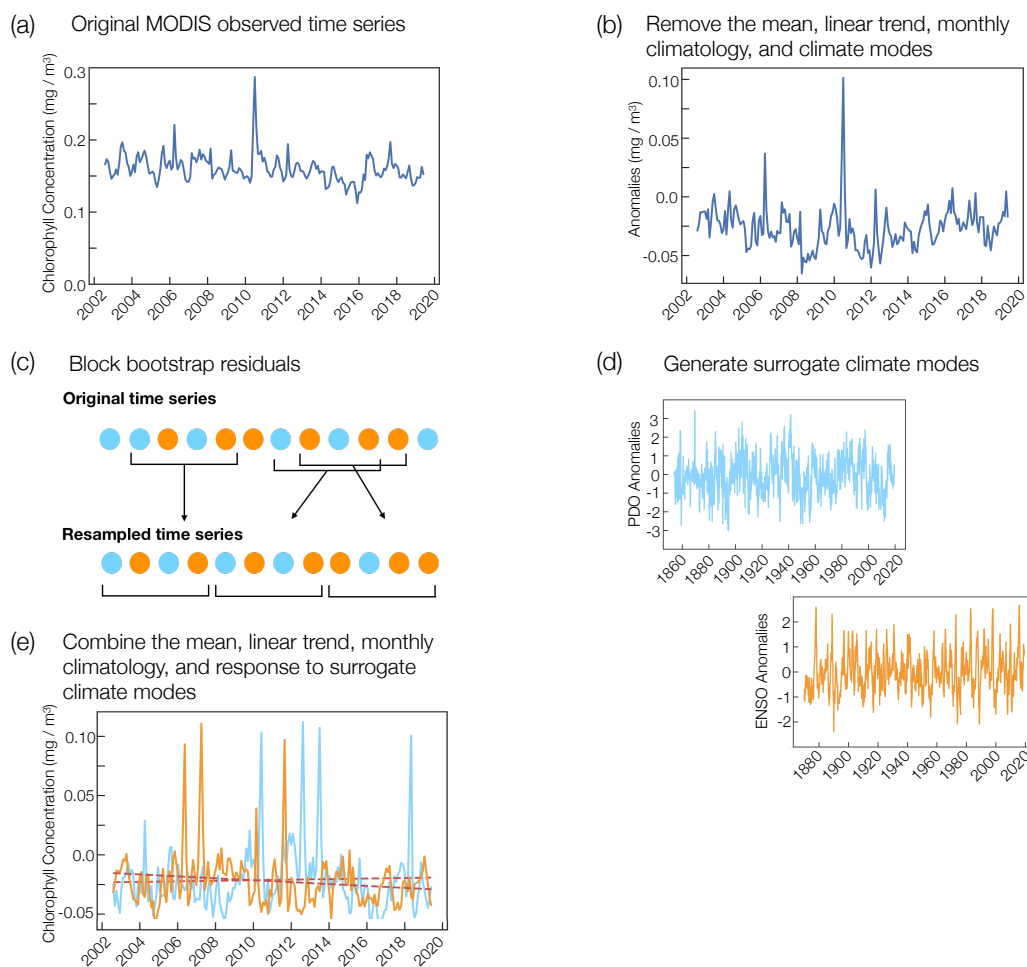


Figure 2.3: (a) Annual trend in global chlorophyll concentration from 2002 to 2019 of synthetic ensemble member 3. (b) Annual trend in global chlorophyll concentration from 2002 to 2019 of synthetic ensemble member 10. (c) Annual trend in global chlorophyll concentration from 2002 to 2019 over the MODIS ocean color record.

cautions against interpreting trends as externally driven across much of the global ocean.

2.6 Conclusions

The abundance and distribution of phytoplankton in the global ocean are controlled by both internal climate variability and external anthropogenic forcing. Our understanding of the ocean biosphere has been informed by the analysis of remote sensing datasets and ESM output. Each of these methods has advantages and disadvantages to diagnosing changes in marine phytoplankton over time. Assessing disruption in the ocean biosphere using remote sensing datasets is challenged

by the relatively short length of the observational record, restricting our ability to disentangle fluctuations in internal climate variability from externally forced anthropogenic trends. Ensembles of Earth system models can be used to confidently isolate the response due to internal climate variability and external forcing, but may not skillfully represent observed spatial patterns in marine phytoplankton.

To reconcile these differences between the satellite-derived observational record and ESM output, we implement the novel approach of constructing a synthetic ensemble of global chlorophyll concentration using data from the MODIS satellite mission. Our synthetic ensemble reveals an important role for internal variability in surface ocean chlorophyll across the global ocean. It further cautions against interpreting long-term trends from the observed record as driven by externally forced anthropogenic climate change.

Chapter 3

Alternate history: A synthetic ensemble of ocean chlorophyll concentrations

3.1 Abstract

Internal climate variability plays an important role in the abundance and distribution of phytoplankton in the global ocean. Previous studies using large ensembles of Earth system models (ESMs) have demonstrated their utility in the study of marine phytoplankton variability. These ESM large ensembles simulate the evolution of multiple alternate realities, each with a different phasing of internal climate variability. However, ESMs may not accurately represent real world variability as recorded via satellite and in situ observations of ocean chlorophyll over the past few decades. Observational records of surface ocean chlorophyll equate to a single ensemble member in the large ensemble framework, and this can cloud the interpretation of long-term trends: are they externally forced, caused by the phasing of internal variability, or both? Here, we use a novel statistical emulation technique to place the observational record of surface ocean chlorophyll into the large ensemble framework. Much like a large initial condition ensemble generated with an ESM, the resulting synthetic ensemble represents multiple possible evolutions of ocean chlorophyll concentration, each with a different sampling of internal climate variability. We further demonstrate the validity of our statistical approach by recreating an ESM ensemble of chlorophyll using only a single ESM ensemble member. We use the synthetic ensemble to explore the interpretation of long-term trends in the presence of internal variability and find a wider range of possible trends in chlorophyll due to the sampling of internal variability in subpolar regions than in subtropical regions.

3.2 Introduction

The ocean biosphere strongly influences biogeochemical cycling, carbon export, and air-sea carbon flux. Although phytoplankton constitute a relatively small reservoir of carbon, their ability to photosynthetically fix carbon from the atmosphere enhances the ocean's role as a carbon sink, allowing the ocean to store 45 times more carbon than the atmosphere [Friedlingstein et al., 2019]. The efficiency and strength of the ocean biological pump can influence atmospheric carbon dioxide concentrations; in the absence of the ocean biosphere, atmospheric carbon dioxide concentrations would increase by approximately 50% of preindustrial values [McKinley et al., 2017].

Internal climate variability plays an important role in the abundance and distribution of phytoplankton in the global ocean. Modes of internal climate variability, such as the El Niño Southern Oscillation (ENSO), the Southern Annular Mode (SAM), and the North Atlantic Oscillation (NAO), alter the physical and chemical environment for, and thus the abundance of, phytoplankton on timescales ranging from interannual to multi-decadal [Chavez et al., 1998, Lovenduski and Gruber, 2005, Thomas et al., 2009, Zhai et al., 2013]. Correlations between these climate indices and marine phytoplankton have been demonstrated on regional and local scales using several decades of remotely sensed and in situ observations [Chavez et al., 1998, Behrenfeld et al., 2001, Lovenduski and Gruber, 2005, Thomas et al., 2009, Zhai et al., 2013]. For example, bio-optical data from moorings in the Central Equatorial Pacific revealed a reduction in phytoplankton biomass coincident with the 1997-98 El Niño event, driven by the reduced upwelling of nutrients and subsequent declines in phytoplankton productivity [Chavez et al., 1998]. Modes of internal climate variability have also been shown to affect regional upwelling, and thus phytoplankton productivity, in Eastern Boundary Upwelling Systems such as the California and Humboldt Current Systems [Thomas et al., 2009]. These studies demonstrate that the phasing and magnitude of internal climate variability has a measurable imprint on the ocean chlorophyll record.

Multiple studies have used coupled Earth System Models (ESMs) or stand-alone ocean biogeochemical models to illustrate the influence of internal climate variability on biological processes,

often through the lens of air-sea carbon flux [Le Quéré et al., 2000, Lenton and Matear, 2007, Wang and Moore, 2012, Hauck et al., 2013, Bopp et al., 2013, McKinley et al., 2018]. For example, several modeling studies suggest that SAM has a marked influence on phytoplankton productivity in the Southern Ocean [Lenton and Matear, 2007, Wang and Moore, 2012, Hauck et al., 2013] while ENSO has been demonstrated to impact net primary production (NPP) in tropical regions [Kwiatkowski et al., 2017]. Globally, an analysis of upper ocean dissolved inorganic carbon (DIC) revealed correlations between modelled phytoplankton abundance and ENSO, SAM, and NAO [Long et al., 2013]. Mechanisms of the connection between modes of variability and phytoplankton biomass have been explored using biogeochemical models to attribute regional changes in biomass to internal variability driven fluctuations in nutrient supply and light availability [McKinley et al., 2018]. Thus, ESMs are an important tool for developing an understanding of the impact of internal variability on the abundance and distribution of marine phytoplankton.

Large initial condition ensembles of ESMs are a recently developed research tool for the representation and analysis of internal variability in the climate system [Kumar and Ganguly, 2018, Bengtsson and Hodges, 2019, Dai and Bloecker, 2019, Deser et al., 2020]. In this approach, each ESM simulation or ensemble member is initialized slightly differently and thus produces a phasing of internal climate variability that is not identical to the other ensemble members. Analyses of variability in global air temperature and precipitation using a subset of initial condition large ensembles conducted with the Coupled Model Intercomparison Project Version 5 (CMIP5) models reveal that internal variability accounts for approximately half of the spread in projected climate trends across North America and Europe over the next half century [Hawkins and Sutton, 2009, 2011, Deser et al., 2020]. Additionally, regional differences in the range of internal variability have also been reported from large ensembles, with subtropical regions experiencing a relatively lower range of coupled ocean-atmosphere variability [Deser et al., 2010, 2020].

Several recent studies have demonstrated the utility of large ensembles of ESMs for the study of marine phytoplankton [Rodgers et al., 2015, Frölicher et al., 2016, Krumhardt et al., 2017]. Krumhardt et al. [2017] used the Community Earth System Model 1 Large Ensemble (CESM1-LE)

to quantify the contribution of internal climate variability to uncertainty in projections of NPP. Their analysis revealed that internal climate variability challenges our ability to quantify the role of emissions mitigation for end-of-century NPP changes, especially at regional scales. Other studies have identified NPP as a biogeochemical quantity whose anthropogenic signal is slow to emerge from internal variability using the GFDL Earth System Model 2M (ESM2M) [Rodgers et al., 2015, Frölicher et al., 2016, Schlunegger et al., 2019]. The important role of internal variability in NPP contributes to improved predictability of NPP relative to other biogeochemical variables [Séférian et al., 2014]. Thus, large initial condition ensembles of ESMs demonstrate the important role of internal variability in the long-term changes in marine phytoplankton abundance and productivity.

Observational records of surface ocean chlorophyll concentration from satellite and in situ datasets equate to a single ensemble member in the large ensemble framework. As such, the observational record captures only one of the many possible trajectories through climate space that could have occurred, even given the same physical constraints and boundary conditions. For example, the multi-decade record of remotely sensed ocean color from the Moderate Resolution Imaging Spectroradiometer (MODIS) recorded the reduction in chlorophyll concentration in the Eastern Equatorial Pacific associated with the dramatic 2015-2016 El Niño event [Coria-Monter et al., 2018]. Due to this event occurring towards the end of our observational record, it will have an outsized impact on our estimation of a linear trend. However, had a La Niña event occurred, rather than an El Niño event, the linear trend estimated over the same period may have been positive. With a single observational record it can thus be challenging to interpret changes in chlorophyll concentration or phytoplankton productivity even over long-term (multi-decadal) timescales due to sampling of internal variability. A complementary approach to quantifying internal variability in phytoplankton abundance is to construct an observationally constrained synthetic ensemble by statistically emulating the observational record. This "observational large ensemble" allows us to simulate how phytoplankton would respond given a different phasing of internal variability, illustrating a range of possible long-term chlorophyll trends.

In this paper, we place the observational record of surface ocean chlorophyll concentration into

the large ensemble framework by constructing a synthetic ensemble of observed chlorophyll. Much like a large initial condition ensemble generated with an ESM, the synthetic ensemble represents multiple possible evolutions of ocean chlorophyll concentration, each with a different phasing of internal climate variability (ENSO, PDO, and other climate noise). We use statistical emulation techniques to illustrate the importance of internal climate variability for the interpretation of trends in the observational record. We further evaluate our synthetic ensemble methodology in the context of a large initial condition ensemble generated with an ESM to demonstrate that our approach is valid.

3.3 Data and Model Output

In our analysis, we construct a synthetic ensemble of surface ocean chlorophyll concentration using both remotely sensed and in situ observations. We then evaluate our statistical method using a large initial condition ensemble of an ESM as a testbed. Here, we describe the observational data and the model testbed. We describe the generation of the synthetic ensemble in Section 3.4.

3.3.1 Observations

3.3.1.1 Ocean color datasets

Marine phytoplankton have been observed over the past several decades by multiple satellite instruments with varying spatial and temporal coverage. Here, we utilize the global ocean chlorophyll concentration estimated by the Moderate Resolution Imaging Spectroradiometer (MODIS) ocean color dataset, as it provides the longest continuous record of global ocean chlorophyll concentration, with coverage from 2002 to present. Analyses of the MODIS ocean color dataset were conducted using Level 3 composites of 8 day mean output at 9 kilometer resolution of chlorophyll a concentration (mg m^{-3}) obtained from the NASA Ocean Color Archive (<http://oceancolor.gsfc.nasa.gov/>). The OCI algorithm was used to convert ocean color measurements to total chlorophyll concentration in mg m^{-3} . The dataset was averaged to monthly and coarsened to 1° resolution for comparison

with output from the CESM-LE.

3.3.1.2 Ocean time-series measurements

We additionally use in situ surface ocean chlorophyll measurements from the Hawaii Ocean Time Series (HOT). Photosynthetic pigment concentrations are measured both in situ using a fluorescence sensor attached to a CTD instrument which is lowered through the water column and through High Performance Liquid Chromatography (HPLC) analysis of water samples which are collected at discrete depth intervals in the water column [Tupas et al., 1997]. This observational dataset provides the longest continuous record of surface ocean chlorophyll, with coverage from 1989 to 2018 [Karl and Lukas, 1996]. In contrast to the MODIS ocean color dataset which provides a shorter record and global coverage, the HOT dataset provides a longer record at a discrete location. Analyses of the HOT dataset were conducted using chlorophyll a concentration (mg m^{-3}) obtained from the HOT Data Organization and Graphical System (<https://hahana.soest.hawaii.edu/hot/>). Chlorophyll a concentration is measured using HPLC analysis. The dataset has been resampled at monthly intervals using linear interpolation between measurements and averaged over the upper 10 meters for comparison with output from our modeling tool, described next.

3.3.2 Community Earth System Model Large Ensemble

We evaluate our statistical methodology using output from the Community Earth System Model 1 Large Ensemble (CESM1-LE) [Kay et al., 2015]. CESM1 is a fully-coupled climate model that provides simulations of Earth’s past climate and projections of Earth’s future climate under historical and Representative Concentration Pathway 8.5 external forcing by simulating the evolution of the atmosphere, ocean, land, and sea ice component models [Hurrell et al., 2013]. The ocean physical model is the ocean component of the Community Climate System Model version 4 [Danabasoglu et al., 2012]. The model has a nominal 1° resolution and 60 vertical levels. The biogeochemical-ecosystem ocean model consists of an upper-ocean ecological module which incorporates multi-nutrient co-limitation on phytoplankton growth and specific phytoplankton functional

groups [Moore et al., 2004], and a full-depth ocean biogeochemistry module which incorporates full carbonate system thermodynamics and a dynamic iron cycle [Doney et al., 2006, Moore and Braucher, 2008].

The CESM1-LE models the spatiotemporal evolution of the climate system by simulating multiple ensemble members, each with slightly different initial conditions. Each member is branched from a multi-century 1850 control simulation with constant pre-industrial forcing [Lamarque et al., 2010]. The ocean model in the control simulation was initialized from observations (January mean climatological potential density and salinity data from the Polar Science Center Hydrographic Climatology), while the other component models were initialized from previous CESM1 simulations [Danabasoglu et al., 2012]. Once the control simulation climate achieved quasi-equilibrium with the 1850 forcing, the first ensemble member was initialized from a January 1, year 402 in the control run. Ensemble member 1 was integrated forward from 1850 to 2100. The remaining ensemble members were integrated from 1920 to 2100 using slightly different initial conditions generated by round-off level differences in their initial air temperature fields from January 1920 of ensemble member 1 [Kay et al., 2015]. Due to the chaotic nature of the atmosphere, the small differences in initial conditions quickly propagate through the atmosphere and lead to each ensemble member experiencing a different evolution of internal variability. A total of 40 ensemble members were generated in this fashion for the CESM1-LE experiment. Six CESM1-LE members had corrupted ocean biogeochemistry, therefore, we use the 34 CESM1-LE members with valid ocean biogeochemistry. Analyses of model output were conducted using monthly mean output at 1° resolution over the historical period (1920 to 2005) due to its realistic volcanic forcing. We consider chlorophyll concentration in the uppermost model layer (10 meters) by summing each of the three phytoplankton functional types (diatoms, diazotrophs, and small phytoplankton).

3.4 Creating a synthetic ensemble of the observational record

We create a synthetic ensemble to highlight the role of internal variability in historical, observed surface ocean chlorophyll. To generate the synthetic ensemble, we build upon the statistical

model developed in McKinnon et al. [2017] and McKinnon and Deser [2018] and additionally described in Elsworth et al. [2020], with slight modifications to the approach. We model chlorophyll concentration as:

$$X^{i,t} = \beta_0^i + \beta_S^{i,m(t)} + \beta_F^t + \beta_{ENSO}^{i,m(t)} M_{ENSO}^t + \beta_{PDO}^{i,m(t)} M_{PDO}^t + \epsilon^{i,t}, \quad (3.1)$$

where X is the chlorophyll concentration at location i and time t , and $m(t)$ indicates the month associated with time t . In this model, chlorophyll is described as a linear combination of the mean state β_0^i , seasonality $\beta_S^{i,m(t)}$, the assumed spatially-uniform response to external forcing β_F^t , response to climate modes $\beta_{ENSO}^{i,m(t)} M_{ENSO}^t$ and $\beta_{PDO}^{i,m(t)} M_{PDO}^t$, and residual internal climate variability $\epsilon^{i,t}$. Importantly, the β_F^t term in Equation 3.1 represents the response to external forcing, while $\beta_{ENSO}^{i,m(t)} M_{ENSO}^t$, $\beta_{PDO}^{i,m(t)} M_{PDO}^t$, and $\epsilon^{i,t}$ capture the role of internal climate variability in chlorophyll concentration. The time series M_{ENSO}^t and M_{PDO}^t represents the evolution of the climate modes ENSO and PDO respectively, which have been shown to influence chlorophyll concentration [Gregg and Conkright, 2002, Yoder and Kennelly, 2003, Radenac et al., 2012]. The Niño 3.4 and PDO indices were obtained from the National Oceanographic and Atmospheric Administration Climate Prediction Center. As in McKinnon and Deser [2018], we address the covariance between ENSO and PDO by creating two orthogonal time series via principal component analysis of the original observed temporal evolution of ENSO and PDO from 1880 to 2020.

3.4.1 HOT

To illustrate our approach, we create a synthetic ensemble of chlorophyll concentration averaged over the upper 10 meters of the water column at HOT, a discrete location in the Subtropical North Pacific. The synthetic ensemble is created in a two-step process (Figure 3.1). First, we estimate the parameters (β 's in Equation 3.1) (top panel, Figure 3.1). Second, we simulate alternate evolutions of chlorophyll over time given different phasings in the climate modes (ENSO, PDO) and by resampling the residuals (ϵ in Equation 3.1) (bottom panel, Figure 3.1).

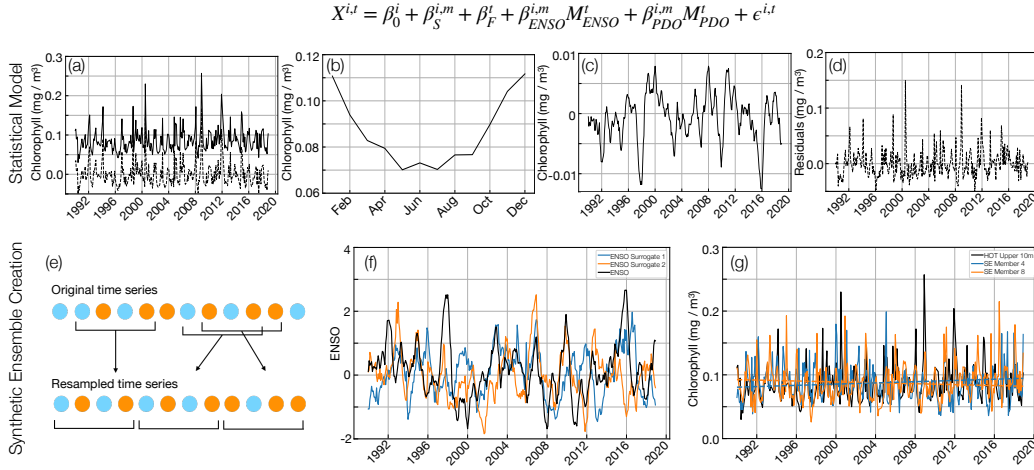


Figure 3.1: Schematic illustrating the creation of a synthetic ensemble using the HOT dataset of chlorophyll concentration averaged over the upper 10 meters. The statistical model is displayed above with specific terms corresponding to a graphic representation below. In our statistical approach, we model and remove (a) the mean state, β_0^i , (b) the monthly climatology, $\beta_S^{i,m}$, and (c) the dependence on climate modes such as ENSO, $\beta_{ENSO}^{i,m(t)} M_{ENSO}^t$, before arriving at (d) the chlorophyll residuals, $\epsilon^{i,t}$. The β_F^t term represents external forcing, while $\beta_{ENSO}^{i,m(t)} M_{ENSO}^t$, $\beta_{PDO}^{i,m(t)} M_{PDO}^t$, and $\epsilon^{i,t}$ capture the role of internal climate variability in chlorophyll concentration. The synthetic ensemble is then generated by (e) block bootstrapping the residuals, (f) generating surrogate climate modes, and (g) generating distinct synthetic ensemble members by incorporating the the mean, the seasonal cycle, the block bootstrapped anomalies, and the response to surrogate climate modes.

To develop the synthetic ensemble of chlorophyll at HOT, we first remove the mean state, β_0 , from the time-varying chlorophyll, such that the resulting anomaly time series centers around zero (Figure 3.1a). We then remove the monthly climatology, β_S^m , by removing the monthly average in chlorophyll concentration from the anomaly time series (Figure 3.1b). Note that for this illustration, we assume that the externally forced trend, β_F^t , is zero. Finally, we estimate the dependence of chlorophyll on the climate modes ENSO and PDO, $\beta_{ENSO,PDO}$, by assuming a linear relationship and calculating the ordinary least squares regression of the deseasonalized anomalies with the ENSO and PDO indices (Figure 3.1c). The regression coefficients, $\beta_{ENSO,PDO}$, are then multiplied by the observed indices, $M_{ENSO,PDO}^t$, and subtracted from the deseasoned anomalies, leaving us with chlorophyll residuals, $\epsilon^{i,t}$ (Figure 3.1d).

We apply two techniques to simulate alternate evolutions of chlorophyll concentration over

time at HOT. First, the residuals, $\epsilon^{i,t}$, are resampled 1000 times using the nonparametric moving block bootstrap (MBB) in time (Figure 3.1e). The MBB captures high frequency temporal variability by resampling the dataset with a block length sufficiently large compared to the temporal autocorrelation scale but sufficiently small to generate variability between bootstrapped samples. In this context, the residuals are resampled using a block length of 12 months which encapsulates the seasonal cycle in global chlorophyll concentration variability. Although block bootstrapping tends to underestimate trend variability when the data are positively correlated and the data record is short, the validation of the statistical method using a large ensemble of an Earth system model suggests that the methodology does not generally underestimate trend variability [McKinnon et al., 2017]. Second, the response of chlorophyll concentration to different possible evolutions of the climate modes over time is incorporated by generating 1000 surrogate climate modes of ENSO and PDO using the iterative adjusted amplitude Fourier transformation (IAAFT) method (Figure 3.1f) [Schreiber and Schmitz, 1996]. This surrogate data approach produces an ensemble of time series with the same amplitude distribution and spectra as the original climate mode time series. The surrogate climate modes are multiplied by the regression coefficients, $\beta_{ENSO}^{i,m(t)}$ and $\beta_{PDO}^{i,m(t)}$, estimated from the observed record to create time series of chlorophyll that could have occurred given a different temporal evolution of ENSO and PDO. We combine the block bootstrapped anomalies and the response to the surrogate climate modes with β_0 and $\beta_S^{i,m(t)}$ to produce multiple distinct synthetic ensemble members at HOT (Figure 3.1g).

Figure 3.2 illustrates the temporal evolution of 10 synthetic ensemble members for the surface ocean chlorophyll concentration at HOT. Each ensemble member has a unique phasing of internal climate variability that results in a distinct temporal evolution for surface ocean chlorophyll at this location. Yet, our method ensures that each ensemble member has similar statistical properties as the original observed time-series. This synthetic ensemble can thus inform our interpretation of the chlorophyll record at HOT by simulating how phytoplankton would respond given a different phasing of internal variability. The phasing of such variability will influence trend estimates of chlorophyll, potentially moderating conclusions regarding the observed trend over the observational

record. However, a limitation of the statistical methodology remains that the variability in the observational record will be emulated in the synthetic ensemble by the statistical model. It is appropriate for us to expand the method to a broader spatial scale, and we explore this using satellite chlorophyll observations in the next section.

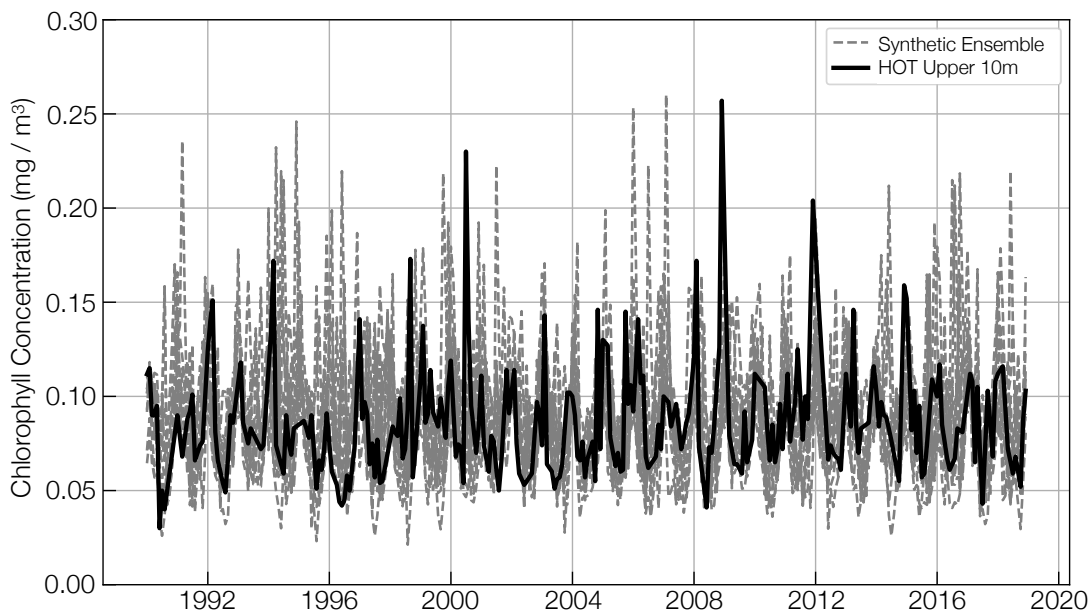


Figure 3.2: Temporal evolution of chlorophyll a concentration in mg m^{-3} averaged over the upper 10 m at the Hawaii Ocean Time-Series (HOT). The original time series is shown in the black line and ten synthetic ensemble members generated from the record are shown in the gray dashed lines. The range of possible evolutions displayed by the synthetic ensemble members illustrates the importance of internal climate variability on observational records, even over relatively short timescales.

3.4.2 MODIS

We demonstrate the role of internal variability on chlorophyll across the global ocean by generating a synthetic ensemble at every $1^\circ \times 1^\circ$ grid cell. We begin with monthly chlorophyll concentration collected over the MODIS mission from 2002 to 2020. In regions with high cloud coverage such as the high latitudes, chlorophyll concentration is linearly interpolated to prevent a sparsity of observations. Although the method of modeling internal variability over the full spatial grid is similar to modeling internal variability at a discrete location, there are two key differences.

First, we approximate the externally forced signal, β_F^t , as the linear trend in global mean chlorophyll concentration ($2.75 \times 10^{-5} \text{ mg m}^{-3} \text{ yr}^{-1}$ from 2002-2020), assuming that the global mean trend is most representative of the externally forced component. Second, our method produces spatially varying regression coefficients, $\beta_{ENSO,PDO}^{i,m(t)}$ (Figure S1), that can then be multiplied by the observed indices, $M_{ENSO,PDO}^t$, to model the direct influence of climate modes. Due to the sparsity of the ocean color record at high latitudes, the estimation of $\beta_{ENSO}^{i,m(t)}$ and $\beta_{PDO}^{i,m(t)}$ may be less reliable in these regions. The coefficients are combined with the synthetic climate mode time series to produce a spatially coherent pattern in the synthetically generated chlorophyll for a given time in a given ensemble member. The synthetic ensemble of the MODIS ocean color record thus represents multiple possible alternative evolutions of ocean chlorophyll over time at every $1^\circ \times 1^\circ$ grid cell.

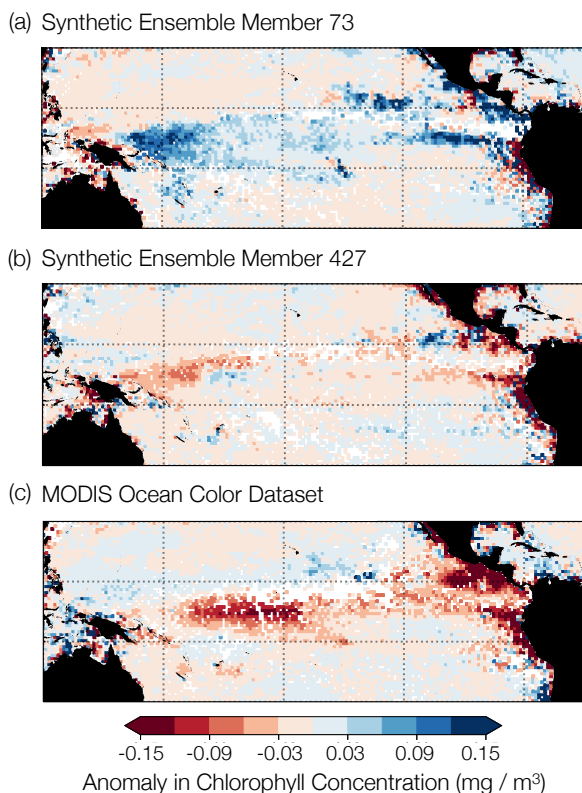


Figure 3.3: Anomalous, monthly mean chlorophyll concentration in December 2015 (mg m^{-3}): (a) derived from synthetic ensemble member 73 (La Niña-like event), (b) derived from synthetic ensemble member 427 (ENSO neutral conditions), and (c) derived from the the MODIS satellite observations (El Niño event).

We showcase the synthetic ensemble by mapping the anomalous chlorophyll concentration in the Equatorial Pacific Ocean in December 2015, during the observed 2015-16 El Niño event (Figure 3.3). Anomalous chlorophyll concentrations are calculated as the difference between the December chlorophyll concentration in 2015 and the average December chlorophyll concentration over the period 2002 to 2020. Observed anomalies in chlorophyll concentration from the MODIS ocean color record show anomalously low chlorophyll concentrations in the Eastern Equatorial Pacific due to regional changes in the distribution of nutrients (Figure 3.3c). In contrast, synthetic ensemble member 73 displays anomalously high chlorophyll concentrations in this region, as this ensemble member experiences a La Niña-like event during December 2015, promoting an influx of nutrients to the surface and enhanced phytoplankton productivity (Figure 3.3a). Synthetic ensemble member 427 displays an intermediate magnitude of anomalous concentration, reflective of its ENSO neutral conditions (Figure 3.3b). Differences between the synthetic ensemble members and the observational record illustrate how internal variability can play an important role in chlorophyll concentration in this region. We also observe large differences between the synthetic ensemble and the observational record outside of this region, where other components of internal variability such as the PDO or other climate noise dominate (not shown).

3.5 Evaluating the synthetic ensemble methodology using CESM1-LE

Supplied with chlorophyll concentration from only a single ensemble member of an ESM large ensemble, can we reproduce the variability in the other ESM large ensemble members using our statistical methodology? In other words, can we produce a valid ensemble from a single record, analogous to producing an ensemble from our single observational record? To answer this question, we apply the statistical approach outlined above (Figure 3.1) to the surface ocean chlorophyll concentration from individual ensemble members of the CESM1-LE over the historical period (1920-2005). We generate 1000 synthetic ensemble members for each of the 34 members of the model ensemble by removing the global mean ensemble mean linear trend ($-4.88 \times 10^{-6} \text{ mg m}^{-3}$ from 1920-2005) (β_F^t), the monthly climatology ($\beta_S^{i,m(t)}$) of each individual ensemble member, and

the contribution linearly related to the climate modes ENSO and PDO ($\beta_{ENSO,PDO}^{i,m(t)} M_{ENSO,PDO}^t$). Climate modes are sourced for each individual ensemble member using the Climate Variability Diagnostics Package (CVDP), an analysis tool that calculates major modes of climate variability in the CESM1-LE [Phillips et al., 2014]. Synthetic ensemble members are generated by combining the block bootstrapped residuals and the surrogate climate modes with the terms previously removed. The synthetically generated ensembles are then evaluated against the full model ensemble to determine the robustness of the statistical method.

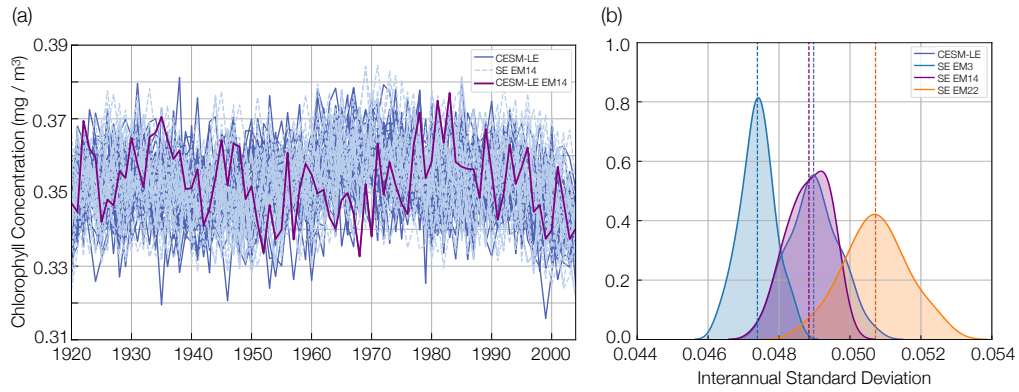


Figure 3.4: (a) The evolution of global-mean surface ocean chlorophyll concentration in mg m^{-3} in the Community Earth System Model Large Ensemble (CESM-LE) and a synthetic ensemble generated from model large ensemble member 14 over the historical period from 1920 to 2005. 34 members of the CESM-LE are shown in the solid dark blue lines while 30 members of the synthetic ensemble are shown in the dashed light blue lines. (b) A probability density function comparing the range of interannual standard deviation in global-mean surface ocean chlorophyll concentration between the CESM-LE (dark blue curve) and synthetic ensembles created from ensemble member 3 (light blue curve), ensemble member 14 (purple curve), and ensemble member 22 (orange curve). Vertical dashed lines in the corresponding colors show the interannual standard deviation from each original CESM1 member.

The interannual standard deviation in global-mean surface ocean chlorophyll concentration from the model-based, synthetically generated ensemble members exhibits a close correspondence to that of the full CESM1-LE. This is illustrated by similarities in the temporal evolution of global-mean chlorophyll concentration of the synthetic ensemble generated from ensemble member 14 (solid purple line and dashed light blue lines) and the original CESM1-LE ensemble (solid dark blue lines) over the historical period (Figure 3.4a). However, the statistical model mimics the internal

variability in the CESM1-LE ensemble member used to create the synthetic ensemble, highlighting a limitation of applying our approach to a limited record. As such, ensemble members with relatively narrower ranges of internal variability, such as CESM1-LE ensemble member 3, produce synthetic ensembles with relatively narrower ranges of internal variability (light blue curve) compared to the full CESM1-LE model ensemble (dark blue curve) (Figure 3.4b). In contrast, CESM1-LE ensemble members with relatively wider ranges of internal variability, such as ensemble member 22, produce synthetic ensembles with relatively wider ranges of internal variability (orange curve) compared to the full CESM1-LE model ensemble (dark blue curve; Figure 3.4b). This mismatch in interannual standard deviation is 0.002 mg m^{-3} at its largest (Figure 3.4b), which is small (4.1%) compared to the mean interannual standard deviation.

The interannual standard deviation in the surface ocean chlorophyll produced synthetically from the CESM1-LE compares favorably to that of the original CESM1-LE across a large fraction of the global ocean (Figure 3.5a). To illustrate this point, we estimate the fractional error in interannual standard deviation between the CESM1-LE and the synthetic ensemble generated from a randomly selected ensemble member (number 10) as $(\sigma_{CESM1-LE} - \sigma_{SE}) / \sigma_{SE}$. Although regional differences exist in the relative underestimation (blue regions) or overestimation (red regions) of the standard deviation in our synthetic ensemble when compared to the original CESM1-LE, the fractional error of the synthetic ensemble is relatively low over the historical period (Figure 3.5a). Similarly low fractional errors are found for synthetic ensembles generated from other CESM1-LE members (not shown).

We repeat our approach for a period of 20 years near the end of the historical period (1987-2005) of the CESM1-LE, which is comparable to the length of the MODIS ocean color dataset and the HOT record. When compared to the model ensemble, the synthetic ensemble generated from ensemble member 10 exhibits a relatively higher fractional error over shorter time scales than longer time scales (Figure 3.5b). This result illustrates the limitations in applying this statistical method over shorter periods of time. Observations can provide a strong constraint on uncertainty related to internal climate variability over time, but only in cases where the dominant timescales

of variability are resolved within the observed record.

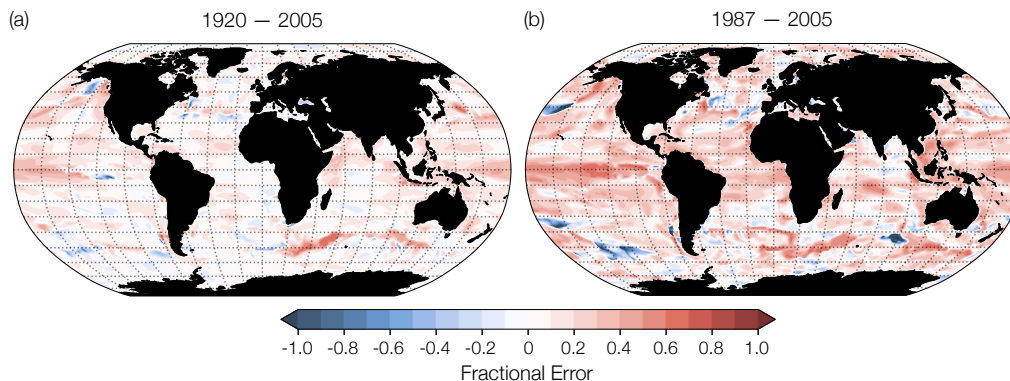


Figure 3.5: Fractional error of the interannual standard deviation in the synthetic ensemble generated from ensemble member 10 as compared to the original CESM1-LE, estimated as $(\sigma_{CESM1-LE} - \sigma_{SE}) / \sigma_{SE}$ for (a) the period 1920 to 2005 and (b) the period 1987 to 2005. Regions of blue indicate the synthetic ensemble methodology is underestimating the variance when compared to the full model ensemble while regions of red indicate the synthetic ensemble methodology is overestimating the variance when compared to the full model ensemble.

3.6 Implications for the interpretation of observational records

The synthetic ensemble can be used to illustrate how variable phasing in climate modes can produce different trends over the observational period, both at a discrete location and across the full spatial grid as in Elsworth et al. [2020]. For example, Figure 3.6 illustrates the temporal evolution of two synthetic ensemble members generated from the HOT dataset. Each member displays a trend of opposite sign over the observational period due to a different sampling of climate variability. Synthetic ensemble member 4 displays a trend of $4.01 \times 10^{-5} \text{ mg m}^{-3} \text{ yr}^{-1}$ while member 8 displays a trend of $-3.00 \times 10^{-5} \text{ mg m}^{-3} \text{ yr}^{-1}$. The range of trends for 1000 synthetic ensemble members is between $6.40 \times 10^{-5} \text{ mg m}^{-3} \text{ yr}^{-1}$ to $-5.43 \times 10^{-5} \text{ mg m}^{-3} \text{ yr}^{-1}$. Differing linear trends across the various synthetic ensemble members demonstrate an important role for internal variability in HOT chlorophyll trends.

Figure 3.7 displays the spatial pattern of the linear trend in annual-mean chlorophyll concentration for two distinct synthetic ensemble members generated from the MODIS record. Observed

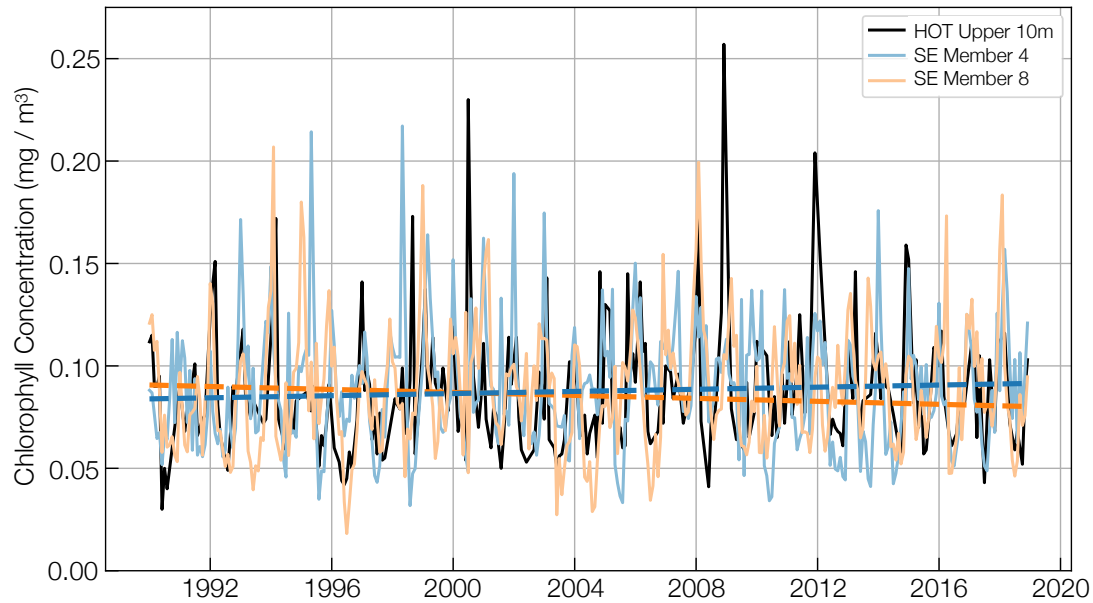


Figure 3.6: A comparison between the temporal evolution of chlorophyll a concentration in mg m^{-3} between the HOT record and synthetic ensemble members created from the original dataset. Synthetic ensemble member 4 is shown in the blue line and synthetic ensemble member 8 is shown in the orange line. Dashed red lines represent the trend of each synthetic ensemble member and illustrate trends of opposite sign over the observational period.

trends in real-world chlorophyll concentration (Figure 3.7c) show decreasing chlorophyll over time in the subtropical oceans and the California Current Eastern Boundary Upwelling System, increasing chlorophyll over time in parts of the subpolar North Atlantic and Southern Oceans, and a statistically significant (hatched; determined by a t-test with a p value less than 0.05) negative trend in the Equatorial Pacific. In contrast, synthetic ensemble members 16 (Figure 3.7a) and 45 (Figure 3.7b) exhibit trends of opposite sign from the observations across much of the ocean. For example, in the Eastern Equatorial Pacific, synthetic ensemble member 16 displays a trend toward increasing chlorophyll concentrations over time, while synthetic ensemble member 45 displays a statistically significant trend toward decreasing chlorophyll. This mismatch of trends is also apparent in the California Current Eastern Boundary Upwelling System, and parts of the subpolar North Atlantic, Indian, and Southern Oceans. Thus, results from our synthetic ensemble suggest that internal variability can cloud the interpretation of chlorophyll trends across much of the ocean,

consistent with Elsworth et al. [2020], even when the trends are deemed statistically significant (as in the Equatorial Pacific), although we note that our MODIS results rely on a short record, which affects the performance of our method (Fig. 5b).

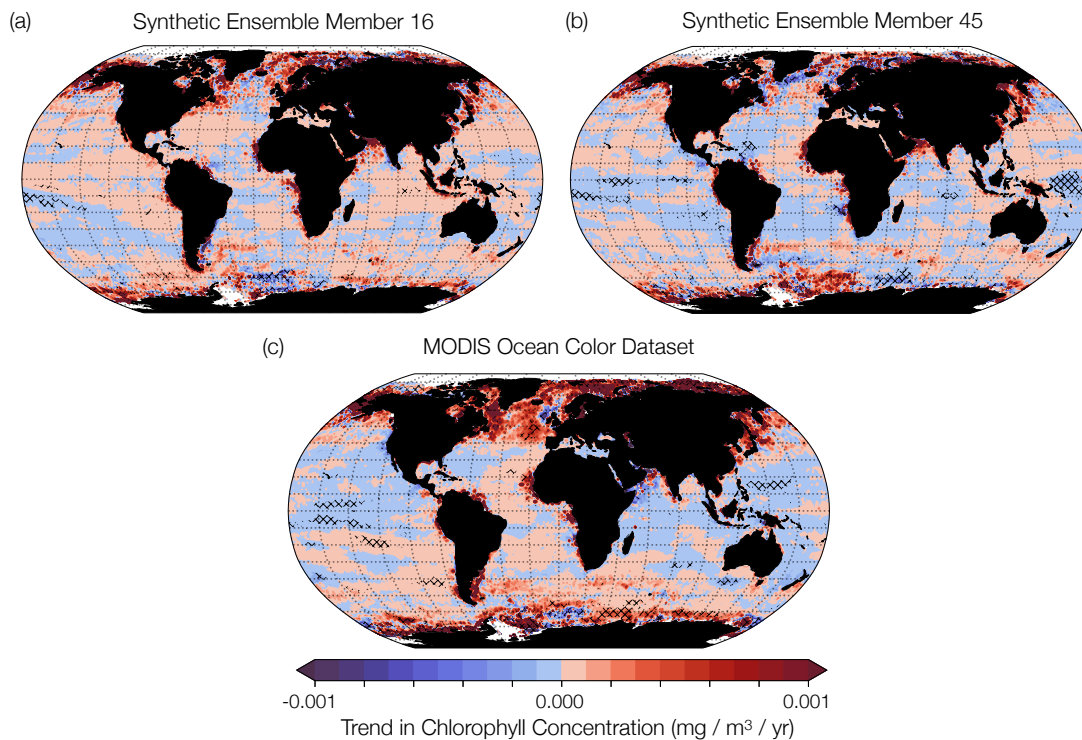


Figure 3.7: (a) Annual trend in global chlorophyll concentration from 2002 to 2020 in $\text{mg m}^{-3} \text{yr}^{-1}$ of synthetic ensemble member 16. (b) Annual trend in global chlorophyll concentration from 2002 to 2020 of synthetic ensemble member 45. (c) Annual trend in global chlorophyll concentration from 2002 to 2020 over the MODIS ocean color record. Hatched areas indicate regions of trend significance determined by a t-test with a p value less than 0.05. Adapted from Elsworth et al. [2020], with a newly generated synthetic ensemble.

Across much of the global ocean, different synthetic ensemble members produce dramatically different long-term trends (Figure 3.7). From this, we can infer that processes external to the climate system are challenging to detect in the observational record of chlorophyll in the majority of the ocean. Our findings thus complement those of several other studies that use a range of statistical methods to comment on detectability of the effects of anthropogenic climate change in the ocean biosphere [Beaulieu et al., 2013, Henson et al., 2010, Henson, 2014, Gregg and Rousseaux,

2014, Henson et al., 2016, Hammond et al., 2020].

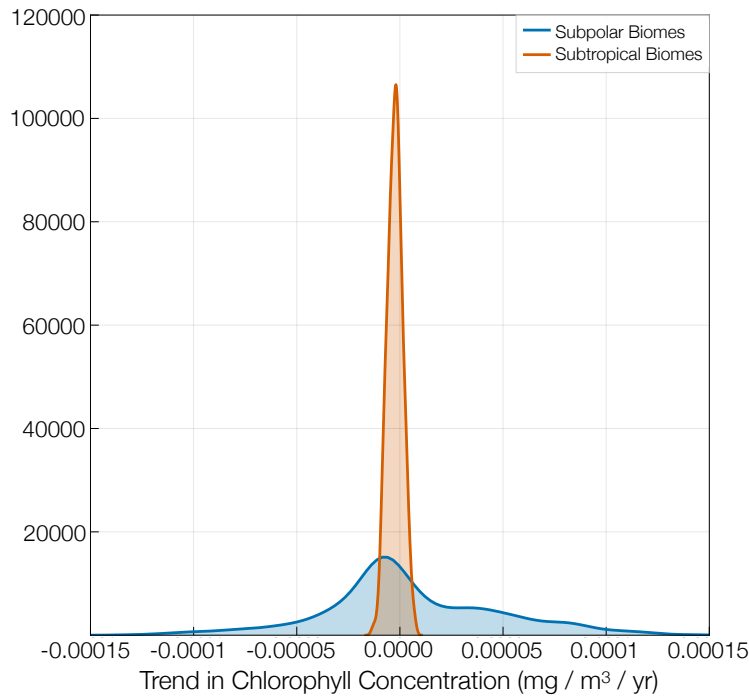


Figure 3.8: Probability density functions of linear trends over 2002-2020 in 1,000 synthetic ensemble members generated from observed chlorophyll concentrations averaged over (blue) the subpolar biomes, and (orange) the subtropical permanently stratified biomes [biomes defined as in Fay and Mckinley, 2014].

Internal variability creates a wider range of possible chlorophyll trends in subpolar regions than in subtropical regions (Figure 3.8). A synthetic ensemble generated from the observed chlorophyll concentration averaged over the subpolar biomes generates a broader distribution of linear trends than a synthetic ensemble generated from observed chlorophyll concentration averaged over the subtropical permanently stratified biomes [cf. blue and orange curves in Figure 3.8; biomes defined as in Fay and Mckinley, 2014], due to higher $\epsilon^{i,t}$ at high latitudes in our statistical model. This means that if we observe large absolute magnitude trends in chlorophyll in subpolar regions, they are much more likely to be driven by internal processes than in subtropical regions. This regional variation in internal trends can help to decode the likely causes of trends in chlorophyll from the observational record [e.g., Behrenfeld et al., 2007], especially between regions of relatively high

productivity (subpolar regions) and regions of relatively low productivity (subtropical regions).

3.7 Conclusions

We place the observational record of surface ocean chlorophyll into the large ensemble framework by constructing a synthetic ensemble of observed chlorophyll using the HOT and MODIS datasets. The synthetic ensembles represent multiple possible evolutions of ocean chlorophyll concentration, each with a different phasing of internal climate variability. Our approach illustrates the importance of internal climate variability for the interpretation of trends in the observational record, and our findings can help to decode the causes of observed changes in chlorophyll across various oceanic regions. When applied to the CESM1-LE from 1920-2005, we are able to reproduce the variability in surface ocean chlorophyll concentration of the full model ensemble using our statistical methodology. However, our assumption that ENSO and PDO are linearly related to chlorophyll may not be a robust assumption. Additional assumptions underpinning our statistical model, such as the approximation of the global mean being representative of the externally forced trend and the residual variability being encapsulated by a block length of 12 months, may affect the interpretation of our results.

Limitations exist when applying this statistical method over shorter timescales, especially those comparable to the length of existing continuous observational datasets for surface ocean chlorophyll. Additionally, the approach assumes internal variability does not change with time, which may not be a valid expectation as the climate continues to change due to anthropogenic influence [Resplandy et al., 2015, Thompson et al., 2015]. However, the synthetic ensemble can be used as an effective tool to illustrate the important role of internal variability in the evolution of a variety of ocean biogeochemical parameters provided a sufficient length of continuous observations are available. Future work can utilize this statistical methodology to compare the range of internal variability observed over the observational record with the range of internal variability generated in large ensemble modeling studies.

Chapter 4

Anthropogenic climate change drives non-stationary phytoplankton variance

4.1 Abstract

Multiple studies conducted with Earth system models suggest that anthropogenic climate change will influence marine phytoplankton over the coming century. Light limited regions are projected to become more productive and nutrient limited regions less productive. Anthropogenic climate change can influence not only the mean state, but also the variance around the mean state, yet little is known about how variance in marine phytoplankton will change with time. Here, we quantify the influence of anthropogenic climate change on internal variability in marine phytoplankton biomass from 1920 to 2100 using the Community Earth System Model 1 Large Ensemble (CESM1-LE). We find a significant decrease in the internal variance of global phytoplankton carbon biomass under a business-as-usual (RCP8.5) emission scenario, with heterogeneous regional trends. Decreasing variance in biomass is most apparent in the subpolar North Atlantic and North Pacific. In these high-latitude regions, zooplankton grazing acts as a top-down control in reducing internal variance in phytoplankton biomass, with bottom-up controls (light, nutrients) having only a small effect on biomass variance. Grazing-driven declines in phytoplankton variance are also apparent in the biogeochemically critical regions of the Southern Ocean and the Equatorial Pacific. Our results suggest that climate mitigation and adaptation efforts that account for marine phytoplankton changes (e.g., fisheries) should also consider changes in phytoplankton variance driven by anthropogenic warming, particularly on regional scales.

4.2 Introduction

Anthropogenic climate change has significantly impacted marine ecosystems, particularly fisheries. Research suggests that the most prominent biological responses to warming include changes in species composition [Wernberg et al., 2016, Flanagan et al., 2018], species phenology [Mills et al., 2013, Staudinger et al., 2019], geographic distribution [Perry et al., 2005, Cheung et al., 2009], and regional productivity [Cheung et al., 2010]. As the base of the marine food web, phytoplankton support diverse marine ecosystems by providing food for higher trophic levels [Falkowski, 2012]. Constraining future changes in phytoplankton with anthropogenic warming is important at regional scales for fisheries adaptation [Pauly and Christensen, 1995, Chassot et al., 2010, Link and Marshak, 2019, Marshak and Link, 2021], particularly as phytoplankton biomass is incorporated into offline fisheries models to predict changing catch potential [Christensen and Walters, 2004, Travers-Trolet et al., 2009, Lehodey et al., 2010, Maury, 2010, Blanchard et al., 2012, Christensen et al., 2015, Jennings and Collingridge, 2015, Tittensor et al., 2018]. In this context, understanding changes in both phytoplankton biomass and its variance is essential in reducing uncertainty in marine ecosystem projections.

The abundance and distribution of phytoplankton will likely change with anthropogenic warming. Future projections of climate change impacts reveal a global loss of marine net primary production (NPP) and phytoplankton biomass, particularly at middle and low latitudes [Steinacher et al., 2010, Bopp et al., 2013, Lotze et al., 2019, Tittensor et al., 2021]. A majority of Earth System Models (ESMs) project an increase in phytoplankton abundance in the high latitude ocean as light limitation is alleviated from stratification, increasing temperature stimulates photosynthesis, and sea ice cover declines. In contrast, a decrease in the low latitude oceans is projected as nutrient limitation from thermal stratification is enhanced [Steinacher et al., 2010, Kwiatkowski et al., 2020]. While bottom-up controls (e.g. nutrient flux, light availability) have been shown to affect phytoplankton growth in a changing climate, top-down controls (e.g. zooplankton grazing) also play a role. For example, analysis across a suite of Earth system models (ESMs) forced under

climate change scenarios revealed grazing pressure as a driver of biomass decline in low to intermediate latitude regions [Laufkötter et al., 2015]. Additionally, top-down controls have been shown to affect regional changes in NPP and export production [Bopp et al., 2001]. Regional redistributions of phytoplankton biomass have consequences for fisheries management and conservation [Blanchard et al., 2017, Stock et al., 2017], and may have implications for economics and policy making decisions [Moore et al., 2021].

While climate change is known to impact the mean state of phytoplankton biomass or NPP [Bopp et al., 2013, Kwiatkowski et al., 2020], little is known about how climate change will affect variability in these quantities. Several recent studies have demonstrated how other aspects of the coupled atmosphere-ocean climate system are projected to experience changes in variance in a changing climate [Resplandy et al., 2015, Landschützer et al., 2018, Kwiatkowski and Orr, 2018, Rodgers et al., 2021]. For example, Resplandy et al. [2015] examined the contribution of internal variability to air-sea pCO_2 and pO_2 fluxes with climate change using a suite of ESMs. Their analyses revealed distinct regional differences in variability of air-sea pCO_2 and pO_2 fluxes. Other studies have revealed increases in the frequency of modes of internal variability such as El Niño and La Niña events in response to greenhouse warming [Timmermann et al., 1999, Cai et al., 2014, 2015, 2022]. Clarifying how variance in phytoplankton biomass may be changing over long time scales with climate change is important for fisheries management, especially at regional scales. Near-term predictions of phytoplankton biomass may also benefit from knowledge of the projected magnitude of internal variability, as the chaotic nature of internal variability hampers near-term predictions [Meehl et al., 2009, 2014].

Here, we quantify changes in the interannual variability of phytoplankton biomass over the next century using a large ensemble of an ESM, in which each ensemble member experiences a different phasing of internal climate variability but is forced with a common emissions scenario. We illustrate the drivers of these changes in variance via statistical analysis of physical and biogeochemical model output and demonstrate their relative importance in key fisheries regions.

4.3 Methods

4.3.1 Community Earth System Model 1 Large Ensemble

4.3.1.1 Model Description

We evaluate changes in phytoplankton biomass variance using output from the Community Earth System Model 1 Large Ensemble (CESM1-LE) [Kay et al., 2015]. CESM1 is a fully-coupled climate model that simulates Earth’s climate under historical and Representative Concentration Pathway (RCP) 8.5 external forcing by simulating the evolution of coupled atmosphere, ocean, land, and sea ice component models [Hurrell et al., 2013]. The ocean physical model is the ocean component of the Community Climate System Model version 4 [Danabasoglu et al., 2012] and has a nominal 1° resolution and 60 vertical levels. The biogeochemical-ecosystem ocean model consists of an upper-ocean ecological module which incorporates multi-nutrient co-limitation of nitrate, ammonium, phosphate, dissolved iron, and silicate on phytoplankton growth and dynamic iron cycling [Moore et al., 2004, Doney et al., 2006, Moore and Braucher, 2008]. The ocean biogeochemistry component simulates three phytoplankton functional types (PFTs): diatoms, diazotrophs, and small phytoplankton. Each PFT plays a unique role in the marine ecosystem and occupies a distinct ecological niche. For example, diatoms grow faster in cool, high-nutrient environments while small phytoplankton thrive in warmer, low-nutrient environments. In contrast, diazotrophs are not limited by nitrogen availability due to their ability to biologically fix nitrogen from the atmosphere. Each PFT has a maximum growth rate, which is dictated by temperature (scaled by a temperature function with a Q10 of 2.0), and limited by nutrient and light availability [Moore et al., 2004, 2013]. Anthropogenic warming can alter these environmental variables and in turn affect phytoplankton abundance and productivity. Phytoplankton are subject to a linear mortality rate which is scaled by temperature. Photoadaptation (variable chlorophyll to carbon ratios) occurs in response to variations in irradiance and nutrient availability [Geider et al., 1998, Moore et al., 2004]. In addition to these bottom-up controls, top-down controls, such as zooplankton grazing, can also affect phytoplankton biomass. The ecosystem model simulates a single generic zooplankton functional

type (ZFT) with different grazing rates and half saturation constants prescribed for different PFTs (e.g., slower zooplankton grazing rates for larger phytoplankton). Grazing rate is computed using a Holling Type III (sigmoidal) relationship and is a function of both prey density and temperature (Figure B.1). Zooplankton loss scales with temperature (scaled by a Q10 function) and a linear mortality term which represents zooplankton losses from predation. While zooplankton growth and loss terms both scale with temperature, a quadratic parameterization of the loss term results in a relatively larger increase in loss than increase in production.

Large ensembles of ESMs are a recently developed research tool which allow us to disentangle fluctuations due to internal climate variability from those imposed by externally forced anthropogenic trends. Internal variability refers to variability in the climate system which occurs in the absence of external forcing, and includes processes related to the coupled ocean-atmosphere system (e.g. El Niño Southern Oscillation, Pacific Decadal Oscillation) [Santer et al., 2011, Deser et al., 2010, Meehl et al., 2013]. In contrast, external forcing refers to the signal imposed by processes external to the climate system, such as solar variability, volcanic eruptions, and rising greenhouse gases from fossil fuel combustion [Deser et al., 2012, 2010, Schneider and Deser, 2018]. The CESM1-LE simulates the evolution of the climate system with multiple ensemble members, each initiated with slightly different atmospheric temperature fields and branched from a multi-century 1850 control simulation with constant pre-industrial forcing [Lamarque et al., 2010, Danabasoglu et al., 2012]. Once the control simulation achieved equilibrium with the 1850 forcing, ensemble members were integrated from 1920 to 2100 using round-off level differences in the initial air temperature field [Kay et al., 2015], resulting in each ensemble member experiencing a different evolution of internal climate variability (e.g., each member has different phasing of climate modes such as El Niño Southern Oscillation). Variable phasing of internal climate variability across ensemble members can influence phytoplankton biomass variability through the propagation of physical climate variability to biologically relevant environmental variables. For example, an ensemble member with a positive phasing of ENSO may display decreased phytoplankton biomass in the Eastern Equatorial Pacific due to relatively warmer sea surface temperatures which increase stratification and decrease

upwelling nutrient flux. RCP8.5 forcing was applied from 2006 to 2100 [Meinshausen et al., 2011] with well-mixed greenhouse gases and short-lived aerosols [Lamarque et al., 2010] projected by four different Integrated Assessment Models. A total of 40 ensemble members were generated for the CESM1-LE experiment. Six CESM1-LE members had corrupted ocean biogeochemistry, therefore, we use the 34 CESM1-LE members with valid ocean biogeochemistry.

4.3.1.2 Statistical Analysis of Model Output

Analyses were conducted using annual mean output at 1° resolution from 1920 to 2100. Changes in CESM1 phytoplankton variance can be assessed via statistical analysis of chlorophyll concentration, net primary productivity (NPP), or phytoplankton carbon concentration (an indicator of total biomass). In our analysis we focus on biomass (phytoplankton carbon concentration) because it is conserved in CESM1 and is an important predictor variable in offline fisheries models [Christensen and Walters, 2004, Travers-Trolet et al., 2009, Lehodey et al., 2010, Maury, 2010, Blanchard et al., 2012, Christensen et al., 2015, Jennings and Collingridge, 2015, Tittensor et al., 2018]. Additionally, under climate change scenarios, phytoplankton biomass may be a more reliable indicator than NPP of climate change impacts [Bopp et al., 2021]. Vertical integrals (top 150m) of biomass carbon concentration from each PFT were calculated and then summed to create maps of total phytoplankton biomass.

We classified the marine environment into 11 ecologically cohesive biomes as in Tagliabue et al. [2021], which are a consolidation of the 38 ecological regions defined in Longhurst [2007] using multivariate statistical analysis [Vichi et al., 2011]. Although we consider all 11 biomes in our analysis, we analyze drivers in four biomes that are particularly relevant for fisheries production and/or of high biogeochemical interest: the subpolar Atlantic (ASP), the subpolar Pacific (SAP), the Equatorial Pacific (EQP), and the Southern Ocean (SOC). ASP is a consolidation of aggregated biogeochemical provinces 4, 11, and 15, SAP a consolidation of 50 and 51, EQP a consolidation of 61, 62, and 63, and SOC a consolidation of 21, 81, 82, and 83 [Longhurst, 2007, Vichi et al., 2011].

Internal variability at each location (x, y) is approximated as the standard deviation (σ)

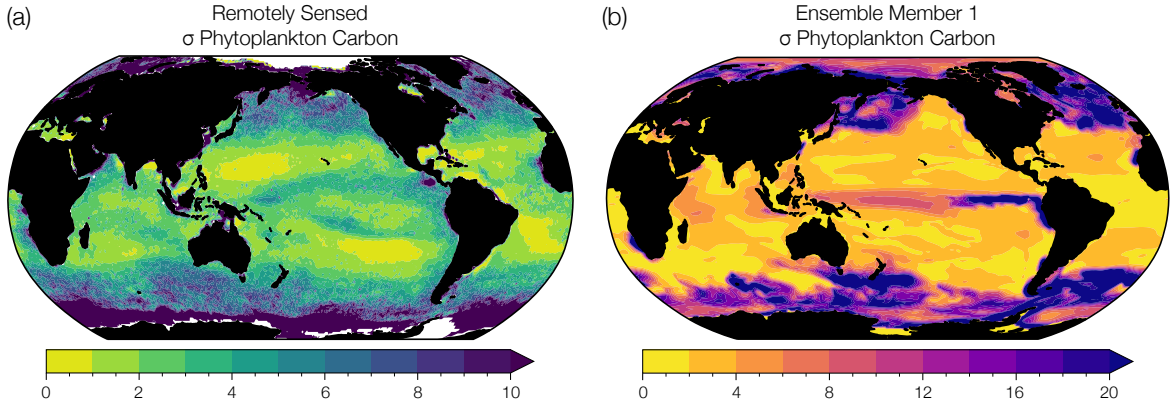


Figure 4.1: Comparison between observed and modeled phytoplankton biomass interannual variability. (a) Temporal standard deviation in annual mean phytoplankton carbon concentration reconstructed from remotely sensed chlorophyll concentrations, backscattering coefficients, and phytoplankton absorption (1998 to 2019) [Bellacicco et al., 2020] (b) Temporal standard deviation in annual mean phytoplankton carbon concentration simulated by ensemble member 1 of the CESM1-LE over the same observational period (1998 to 2019).

across ensemble members (EMs) at a given time (t),

$$\sigma(x, y, t) = \sigma(EM(x, y, t)). \quad (4.1)$$

The forced response of the large ensemble is calculated as the mean of ensemble members at a given location and time,

$$\overline{LE}(x, y, t) = \frac{\sum_1^n EM(x, y, t)}{n}, \quad (4.2)$$

where n is the number of ensemble members.

4.3.2 Model Evaluation

We used remotely sensed estimates of phytoplankton carbon to evaluate the representation of phytoplankton variance in the CESM1-LE. Although phytoplankton carbon concentrations cannot be measured directly by satellites, they can be reconstructed using algorithms that incorporate remotely sensed chlorophyll concentrations, detrital backscattering coefficients, and phytoplankton

absorption [Kostadinov et al., 2016, Martinez-Vicente et al., 2017, Roy et al., 2017, Sathyendranath et al., 2020, Brewin et al., 2021]. We use the observational phytoplankton carbon dataset of Bellaccioco et al. [2020], annually averaged and interpolated onto a 1° grid, to evaluate temporal variability in phytoplankton biomass in a single model ensemble member. Figure 4.1a shows satellite derived estimates of interannual variability in phytoplankton carbon with regions of relatively low phytoplankton variability shown in light green and regions of relatively high variability in dark blue. Remotely sensed observations capture areas of high interannual variability in the subpolar North Atlantic, North Pacific, and Southern Ocean and areas of low interannual variability in the subtropical gyre regions. Similar spatial patterns are apparent when compared to the range of phytoplankton interannual variability in ensemble member 1 of the CESM1-LE over the observational period (1998 to 2019) (Figure 4.1b). However, while the model ensemble captures regional patterns of observed variability, the CESM1-LE overestimates the magnitude of observed interannual variability. As such, estimates of interannual variability derived from the model ensemble will tend to overestimate that observed in the real world.

We compare the internal variance in chlorophyll simulated in the CESM1-LE to a synthetic ensemble generated from observed chlorophyll concentrations over the MODIS remote sensing record [Elsworth et al., 2020, 2021] (Figure B.2; chlorophyll was readily available in the CESM1-LE and can be directly compared with our synthetic ensemble of observed chlorophyll). A synthetic ensemble is a novel technique that allows the observational record to be statistically emulated to create multiple possible evolutions of the observed record, each with a unique sampling of internal climate variability [McKinnon et al., 2017, McKinnon and Deser, 2018]. Compared to the internal variability over the observational period (2002 to 2020) (purple circle, (Figure B.2), the model ensemble underestimates the magnitude of internal variability in chlorophyll observed in the real world.

4.4 Results

Annually averaged, global mean, upper-ocean (top 150m) integrated phytoplankton biomass across the model ensemble decreases from $76.1 \text{ mmol C m}^{-2}$ to $66.2 \text{ mmol C m}^{-2}$ from the historical

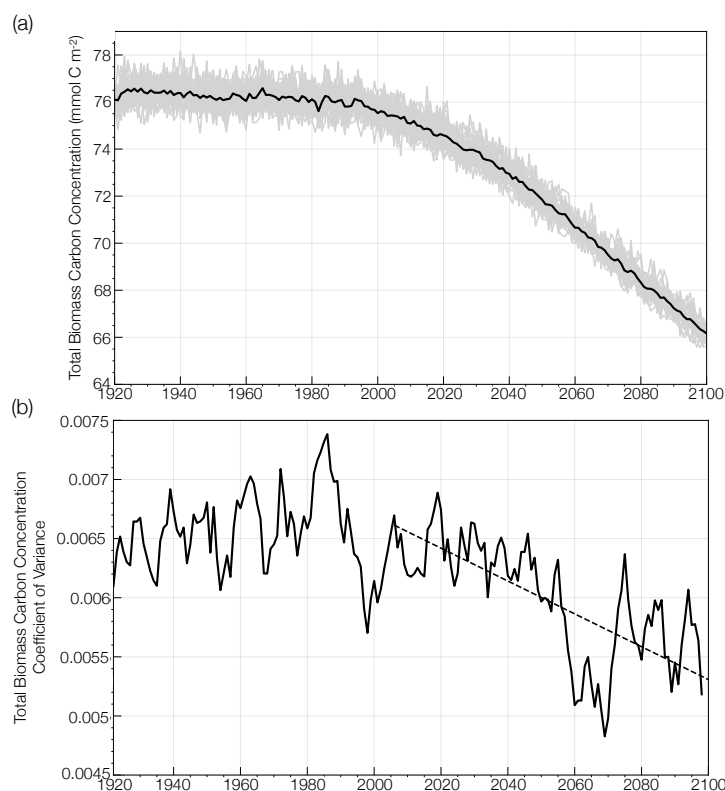


Figure 4.2: (a) Global change in annual mean total phytoplankton carbon concentration simulated by the CESM1-LE in mmol C m^{-2} from the historical period through the RCP8.5 forcing scenario (1920 to 2100). The ensemble mean is shown in the black curve and the 34 individual ensemble members are shown in the gray curves. (b) Global change in the coefficient of variance in annual mean total phytoplankton carbon concentration over the same period, smoothed using a 5 year window. Trend in the coefficient of variance over the RCP8.5 forcing scenario is shown in the black dashed line.

period through the RCP8.5 forcing scenario (1920 to 2100), a decline of 13% (black curve; Figure 4.2a). Despite a global decline in phytoplankton biomass with anthropogenic warming, changes are regionally heterogeneous (Figure 4.3a). Regional changes in mean phytoplankton biomass across the RCP8.5 forcing scenario (2006 to 2100) display increasing biomass in portions of the Arctic and the Southern Ocean that gradually become ice-free over the century (on the order of 20-40% of the mean biomass) and decreasing biomass across the subtropical gyres (on the order of 15-30% of the mean biomass; Figures 4.3a, B.3a). In the North Atlantic subpolar gyre, the phytoplankton biomass declines by 40-50% of its mean (Figures 4.3a, B.3a), likely due to weakening of the At-

lantic Meridional Overturning Circulation (AMOC) [Brander, 2010]. This result is consistent with previous modelling studies which identified a 50% reduction in North Atlantic primary production associated with AMOC weakening during the last glacial period [Schmittner, 2005]. A weakening of the AMOC is also projected with anthropogenic warming [Manabe and Ronald, 1993, Stocker and Schmittner, 1997].

Regional changes in phytoplankton biomass are dominated by changes in diatom and small phytoplankton (Table 4.1). We aggregate biomass across 11 ecological provinces [Vichi et al., 2011, Tagliabue et al., 2021], and present changes in total and PFT biomass over the RCP8.5 scenario in Table 4.1. We observe the largest decline in total phytoplankton carbon concentration in the subpolar Atlantic (ASP) region, where diatom biomass declines by $\sim 80 \text{ mmol C m}^{-2}$, and small phytoplankton biomass increases slightly ($\sim 8 \text{ mmol C m}^{-2}$). We observe moderate decreases in the subpolar Pacific (SAP) region that are again driven by declines in diatom carbon concentration, with opposing trends in small phytoplankton carbon concentration (Table 4.1). We observe a smaller decline in total carbon concentration in the Southern Ocean (SOC) region, where diatom biomass declines $\sim 3 \text{ mmol C m}^{-2}$ and small phytoplankton biomass declines $\sim 7 \text{ mmol C m}^{-2}$. In the Equatorial Pacific (EQP) region we observe the smallest decline in total phytoplankton carbon concentration, where diatom biomass declines $\sim 7 \text{ mmol C m}^{-2}$ and small phytoplankton biomass declines $\sim 5 \text{ mmol C m}^{-2}$.

Internal variability in global phytoplankton biomass, which is indicated by the spread across the individual ensemble members (gray curves; Figure 4.2a), declines over the RCP8.5 forcing period from 2006 to 2100. To quantify how the range of internal variability in phytoplankton biomass is changing with anthropogenic warming, we calculated the coefficient of variance as the standard deviation across the ensemble members for a given year (ensemble spread) divided by the ensemble mean. Figure 4.2b illustrates the change in the coefficient of variance from the historical period through the RCP8.5 forcing scenario (1920 to 2100). The coefficient of variance is relatively constant across the historical period (1920 to 2005), and then significantly declines by $\sim 20\%$ from 2006-2100.

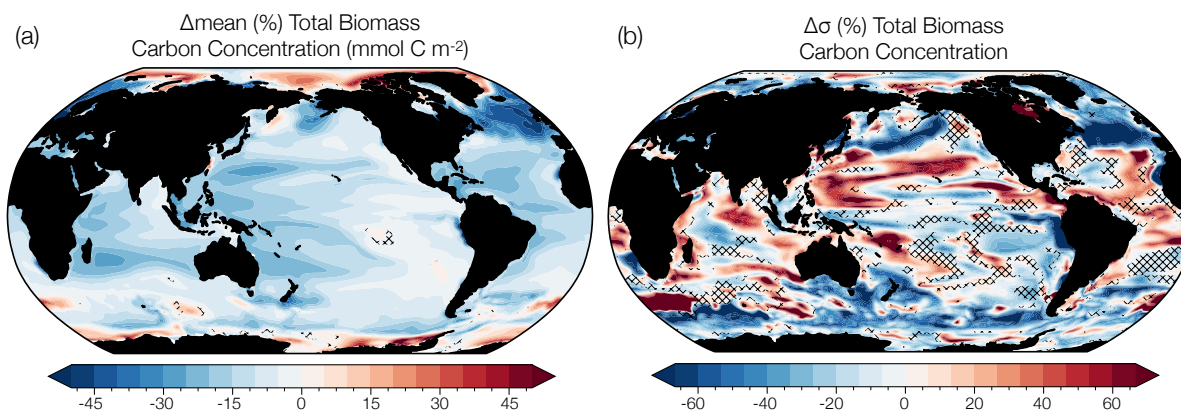


Figure 4.3: (a) Percentage change in annual total phytoplankton carbon concentration in mmol C m^{-2} over the RCP8.5 forcing scenario (2006 to 2100) simulated by the CESM1-LE. (b) Percentage change in annual total phytoplankton variability over the same period. Hatched areas indicate regions of trend insignificance determined by a t-test with a p value greater than 0.05.

A decrease in global phytoplankton internal variability with anthropogenic warming is not unique to the CESM1-LE. We illustrate this by analyzing phytoplankton chlorophyll (rather than biomass; chlorophyll was readily available in the CMIP5 archive) from three other CMIP5 ESM large ensembles which include representation of ocean biogeochemistry: the GFDL-ESM2M from the Geophysical Fluid Dynamics Laboratory [GFDL; Dunne et al., 2012, 2013], the CanESM2 from the Canadian Centre for Climate Modelling and Analysis [Christian et al., 2010, Arora et al., 2011], and the MPI-ESM-LR from the Max Planck Institute [MPI; Giorgetta et al., 2013, Ilyina et al., 2013], consisting of 30, 50, and 100 ensemble members, respectively. Similarly to the CESM1-LE, historical forcing was applied through 2005, followed by RCP8.5 forcing through 2100. While there is substantial spread in the mean coefficient of variance across the four models, a similar decline in the coefficient of variance can be observed across each of the four ESM ensembles, (Figure B.2). From 2006 to 2100, the coefficient of variance decreases by 0.0026 in the CESM1-LE, 0.064 in the MPI-ESM-LR1, 0.0064 in the CanESM2, and 0.018 in the GFDL-ESM2M. These declines are statistically significant in all model ensembles with the exception of the MPI-ESM-LR1 (Figure B.2).

In contrast to the mean change in phytoplankton biomass, changes in phytoplankton internal variability with time are spatially heterogeneous across the global ocean (Figure 4.3b). The largest

decreases in variance are apparent in the North Atlantic and North Pacific subpolar regions, with smaller declines in the Equatorial Pacific and Southern Oceans (Figure 4.3b). Changes in variance in the subtropical regions are characterized by mixed trends. We observe the largest magnitude decline in total phytoplankton carbon variance in the subpolar Atlantic (ASP) region, where diatom variance declines by ~ 2.8 and small phytoplankton variance declines by ~ 0.3 . We observe the smallest magnitude decline in total phytoplankton variance in the subpolar Pacific (SAP) region, driven by a decrease in small phytoplankton variance with a minor decrease in diatom variance (Table 4.1). In both the Southern Ocean (SOC) and the Equatorial Pacific (EQP) regions we observe moderate declines in phytoplankton variance, with a decrease in small phytoplankton variance dominating the change.

Table 4.1: Changes in phytoplankton biomass and its variability in the CESM1-LE from 2006 to 2100 for the 11 ecological provinces defined in Vichi et al. [2011] and Tagliabue et al. [2021]. Units are mmol C m^{-2} .

Biome	Region Name	Change in Mean			Change in Variance		
		Total	Diatom	Small	Total	Diatom	Small
ARC	Arctic	-21	-58	+37	-1.4	-2.8	-0.3
ASP	Arctic subpolar	-71	-79	+8.2	-5.6	-9.9	-2.2
NAS	North Atlantic subtropical gyre	-18	-15	-2.9	-1.8	-2.8	-0.3
EQA	Equatorial Atlantic	-12	-6.6	-5.9	-0.1	-0.4	+0.2
SAS	South Atlantic subtropical gyre	-10	-7.2	-3.1	-0.5	-0.6	-0.1
IND	Indian Ocean	-11	-6.1	-4.7	+0.1	0	+0.1
SAP	subarctic Pacific	-21	-15	-5.4	-0.1	-1.4	-2.4
NPS	North Pacific subtropical gyre	-11	-5.6	-4.9	-0.2	-0.4	+0.1
EQP	Equatorial Pacific	-12	-6.6	-5.0	-2.0	-2.0	-0.2
SPS	South Pacific subtropical gyre	-8.9	-4.3	-4.6	-0.1	0	-0.1
SOC	Southern Ocean	-9.3	-2.8	-6.6	-1.0	0	-1.3

To guide our attribution analysis of changing phytoplankton variability, we considered the dominant ecological assemblage across different regions of the global ocean. The CESM1-LE simulates three phytoplankton functional types, each of which thrive in distinct regions of the global ocean. Diatoms dominate in the subpolar Atlantic and Pacific, the Eastern Equatorial upwelling zone, and portions of the Southern Ocean, while small phytoplankton dominate across the subtropical gyres and portions of the Southern Ocean (Figure 4.4). In contrast, diazotrophs, a minor

contributor to total carbon biomass, are present at such low concentrations that they do not dominate anywhere in the global ocean (Figure 4.4). Using the ecologically cohesive regions defined by Tagliabue et al. [2021] and Vichi et al. [2011], we selected areas that align with the most productive fisheries regions by catch in the Atlantic and Pacific basins [FAO, 2020], as well as regions of global biogeochemical importance for further analysis. In each ecological region we identified the dominant phytoplankton functional type to include in our driver analysis. In regions where multiple phytoplankton functional types dominated, we used total carbon concentrations to reflect the mixed ecological assemblage.

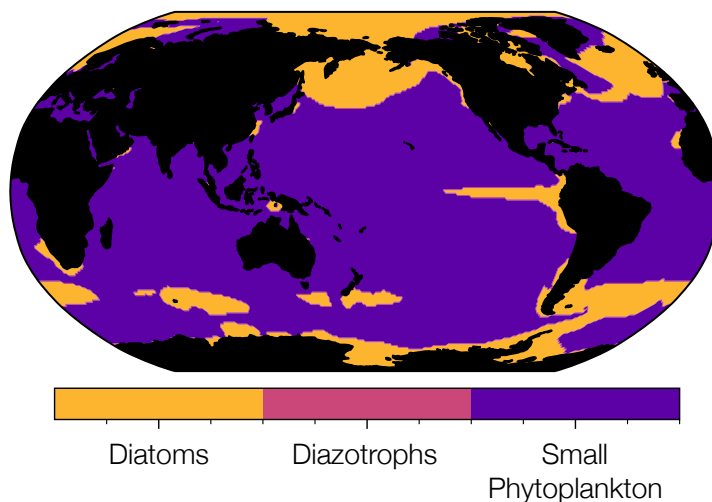


Figure 4.4: Distribution of the dominant phytoplankton functional type in biomass carbon averaged over 2006 to 2100. The CESM1-LE simulates three phytoplankton functional types: diatoms, diazotrophs, and small phytoplankton. Regions where diatoms dominate are shown in yellow, regions where diazotrophs dominate are shown in pink, and regions where small phytoplankton dominate are shown in purple.

We quantified the relationship between phytoplankton carbon and the variables which contribute to changing phytoplankton internal variance by performing a multiple linear regression (MLR) analysis. The MLR analysis was performed on linearly detrended annual anomalies using the ordinary least squares function of the Python package statsmodels.api. We then reconstructed the contribution of each driver variable to phytoplankton variance between the beginning of the century (2006 to 2016) and the end of the century (2090 to 2100) by multiplying the MLR regres-

sion coefficients by the 10-year averaged standard deviation across the model ensemble (ensemble spread) for each variable. We reconstruct phytoplankton variance as a function of light (*Solar*), temperature (*SST*), phosphate advection (*Nutrient*), mixed layer depth (*MLD*), and zooplankton grazing (*Grazing*):

$$\sigma_{C_{phyto}} = \frac{\partial C_{phyto}}{\partial Solar} \sigma_{Solar} + \frac{\partial C_{phyto}}{\partial SST} \sigma_{SST} + \frac{\partial C_{phyto}}{\partial Nutrient} \sigma_{Nutrient} + \frac{\partial C_{phyto}}{\partial MLD} \sigma_{MLD} + \frac{\partial C_{phyto}}{\partial Grazing} \sigma_{Grazing} \quad (4.3)$$

where σ_X represents the standard deviation across all ensemble members for a particular variable and $\frac{\partial C_{phyto}}{\partial X}$ represents the MLR regression coefficient describing the relationship between a particular variable and phytoplankton biomass.

We identify the drivers of changing phytoplankton internal variance in four distinct ecological regions using our statistical approach. In the subpolar Atlantic (ASP) and subpolar Pacific (SAP) ecological provinces, where diatoms dominate total biomass (Figure 4.4), diatom variance declines between the beginning and end of the century (Figure 4.5a, Table 4.1). In both provinces, the largest contributions to this decline in diatom variability derive from a decline in diatom grazing variability, while more minor contributions derive from bottom-up controls such as solar flux, sea surface temperature, nutrient advection, and mixed layer depth (Figure 4.5a).

As the Southern Ocean (SOC) and Equatorial Pacific (EQP) provinces are characterized by mixed phytoplankton assemblages where both diatoms and small phytoplankton dominate, we identify the drivers of the change in total phytoplankton variance here. In contrast to the ASP and SAP provinces, we observe a relatively smaller decline in internal phytoplankton variance between the beginning and end of the century in the Southern Ocean (Figure 4.5c). Similarly to ASP and SAP provinces, the largest contributions to the change in internal variability derive from a decline in grazing variability, with bottom-up controls playing only a small role (Figure 4.5c). In the Equatorial Pacific, total phytoplankton variance declines between the beginning and end of the century, with the largest contributions to this decline deriving from zooplankton carbon and

diatom grazing, with increasing variance in small phytoplankton grazing (Figure 4.5d).

The parameterization of zooplankton grazing in the biogeochemical ecosystem model of the CESM1 defines a single zooplankton functional type with different maximum grazing rates and half saturation constants prescribed for the three PFTs. Zooplankton grazing rate is defined as a Holling Type III (sigmoidal) function of maximum grazing rate, temperature (Q10 function), zooplankton concentration, and phytoplankton concentration (Figure B.1) [Evjemo et al., 2000, Morozov, 2010, Bemal and Anil, 2019]. To approximate the effects of climatic warming, we plot the relationship between grazing rate and diatom concentration across a series of increasing temperatures. With increasing temperature, maximum grazing rate increases across a range of diatom concentrations (Figure B.1). Changes in diatom concentration in mmol m^{-3} between the beginning and end of the century are denoted by dark and light orange circles, respectively for the ASP region (top) and the SAP region (bottom). A decline in diatom concentration across the century results in a reduction in maximum grazing rate in these regions (Figure B.1).

4.5 Conclusions and Discussion

We quantify both global and regional changes in phytoplankton internal variance across the RCP8.5, or business-as-usual forcing scenario in the CESM1-LE. We observe a global decline in phytoplankton variance in the model ensemble, which is reflected in similar declines in phytoplankton variance across a suite of CMIP5 models. Regional changes in phytoplankton variability with anthropogenic climate change in the model ensemble are spatially heterogeneous, with highly productive fisheries regions and important global biogeochemical regions experiencing large changes in variance. Statistical analysis of these specific regions reveal zooplankton grazing (top-down control) as an important contributor to changes in phytoplankton variance, consistent with previous studies [Bopp et al., 2001, Laufkötter et al., 2015].

While the CESM1-LE represents regional patterns of observed variability, the model ensemble tends to underestimate the magnitude of observed internal variance in phytoplankton carbon. As such, the magnitude of changes in phytoplankton internal variance derived from the model ensemble

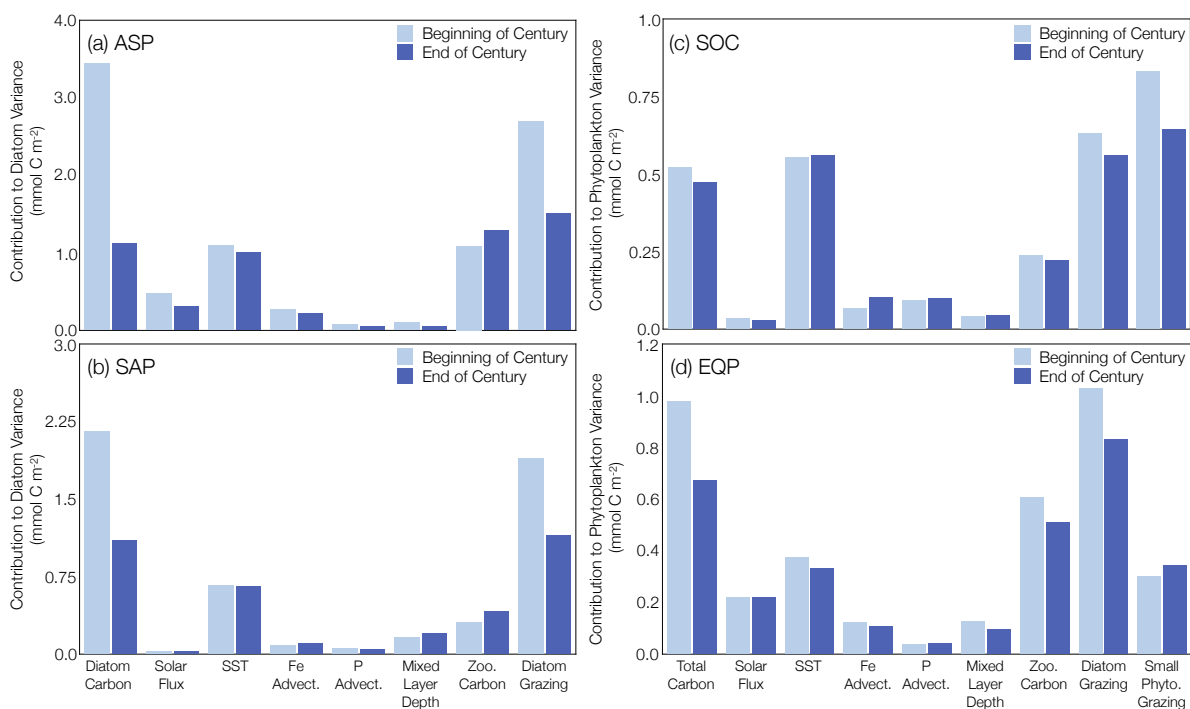


Figure 4.5: Reconstructed changes in the contribution of each driver variable to phytoplankton variance across the RCP8.5 forcing scenario (2006 to 2100) with the beginning of the century shown in light blue and the end of the century shown in dark blue. Marine ecological regions are defined in Tagliabue et al. [2021]. Regions were selected which aligned with the highest fisheries catch in the (a) Atlantic and (b) Pacific basins and the biogeochemically important (c) Southern Ocean and (d) Equatorial Pacific regions. The dominant phytoplankton functional type is considered in each region. In regions with a mixed ecological assemblage, total phytoplankton carbon is considered.

ble should be interpreted as an underestimate when considering changes in phytoplankton internal variance driven by anthropogenic warming. This caveat is particularly important to consider when interpreting projections from offline fisheries models in the context of fisheries adaptation and planning. Additionally, our statistical approach has inherent limitations, especially in the context of attributing drivers in an inherently coupled system such as an ESM (e.g. reconstructing relationships between terms with nonlinear, dependent relationships). However, the statistical method can be used as an effective tool to provide a first-order approximation of drivers of phytoplankton variance across the century.

While many studies attribute bottom-up controls to changing phytoplankton with anthro-

pogenic warming [Steinacher et al., 2010, Bopp et al., 2013, Lotze et al., 2019, Tittensor et al., 2021], top-down controls may also play an important role, particularly in our understanding of changing phytoplankton variance. Studies of phytoplankton change with climatic warming have demonstrated that grazing pressure is a driver of biomass decline in low to intermediate latitude regions across a suite of model simulations with different marine ecosystem models [Laufkötter et al., 2015] and that top-down controls can affect regional changes in NPP and export production [Bopp et al., 2001]. While grazing pressure has been shown to increase in response to climate change, several ecosystem models have also identified zooplankton grazing as a dominant driver of phytoplankton assemblage succession during blooms [Hashioka et al., 2012, Prowe et al., 2012a]. Additionally, top-down controls have also been observed to affect the onset of the spring bloom [Behrenfeld, 2010, Behrenfeld et al., 2013] and to influence primary production in a trait-based ecosystem model [Prowe et al., 2012b].

The relative simplicity of the ocean biogeochemical ecosystem model in CESM1 (BEC) (e.g. representation of a single zooplankton functional type with multiple grazing rates) may limit a more detailed evaluation of changing grazing pressures with climate change. While the recent parameterization of the biogeochemical ecosystem model in CESM2 (MARBL) includes similar representation of three PFTs and a single adaptive ZFT [Long et al., 2021], more complex configurations of MARBL include explicit representation of additional PFTs such as coccolithophores [Krumhardt et al., 2019] and ZFTs. Using more complex ecosystem models, additional insights into drivers of variability may be gained using our statistical approach. Additionally, the use of an ecosystem model of higher complexity may provide more realistic projections of the marine ecosystem with climate change considering change in phytoplankton and zooplankton species diversity with anthropogenic warming [Benedetti et al., 2021]. However, our regional analyses suggest that zooplankton grazing pressure should be considered as an important driver of changes in phytoplankton biomass and its variance with anthropogenic warming.

The magnitude and direction of regional changes in phytoplankton internal variance are an essential constraint for near-term (subseasonal to decadal) predictions of the local marine ecosystem,

particularly in important fisheries regions such as the subpolar Atlantic (ASP) and the subpolar Pacific (SAP) ecological provinces which align with the most productive fisheries region by catch in the Atlantic and Pacific Basins, respectively [FAO, 2020]. Accurate near-term predictions require foreknowledge of both internal climate variability and external climate change signals. On sub-seasonal to decadal timescales, the magnitude of internal climate variability is often stronger than forced climate change signals [Meehl et al., 2009, 2014]. In this context, a decline in phytoplankton internal variance with anthropogenic climate change may improve the accuracy of near-term predictions of phytoplankton biomass, producing more reliable forecasts of fisheries productivity. Future work can utilize these constraints on phytoplankton variance, particularly on regional scales, to inform climate mitigation and adaptation efforts.

Chapter 5

Summary and Conclusions

The abundance and distribution of phytoplankton in the global ocean is controlled by both internal climate variability and external anthropogenic forcing. While the ocean biosphere may be responding to anthropogenic climate change, the relatively short length of the observational record challenges our ability to disentangle fluctuations in internal climate variability from externally forced anthropogenic trends. In contrast, large ensembles of ESMs can be used to confidently isolate the response due to internal climate variability and external forcing, but may not skillfully represent observed spatial patterns in marine phytoplankton. In Chapter 2, the construction of an observationally constrained synthetic ensemble of surface ocean chlorophyll concentrations reveals the important role of internal variability in remotely sensed records of the ocean biosphere across the global ocean. This result cautions against interpreting long-term trends across the observational record as externally forced signals of anthropogenic climate change. The validation of this statistical methodology in the context of an ESM ensemble is presented in Chapter 3. The statistical methodology successfully reproduces variability in surface ocean chlorophyll concentrations simulated by the CESM1-LE. A wider range of possible trends in chlorophyll due to the sampling of internal variability are identified in subpolar regions than in subtropical regions, providing context for the regional interpretation of trends in the ocean biosphere. In Chapter 4, internal variability in global phytoplankton biomass is observed to decline with anthropogenic warming across a suite of ESM ensembles, with regional heterogeneity. Statistical analysis of a single model ensemble reveals zooplankton grazing as an important contributor to changes in phytoplankton variance in biogeo-

chemically and ecologically relevant regions, highlighting the importance of top-down controls in a warming climate. The results of this dissertation are timely in the contemporary scientific literature for several reasons.

While there is a mechanistic understanding of how anthropogenic climate change may affect the ocean biosphere over time, there is debate about whether these changes are already detectable from remotely sensed observations. Some studies suggest that the influence of anthropogenic warming on the ocean biosphere can be detected over an observational period as short as a decade [Behrenfeld et al., 2007, Castillo et al., 2019, Gregg and Rousseaux, 2019]. However, other studies suggest that a continuous observational record of between 20 and 60 years is required to detect a statistically significant trend in remote sensing datasets of chlorophyll concentration [Beaulieu et al., 2013, Henson, 2014, Gregg and Rousseaux, 2014, Henson et al., 2016, Krumhardt et al., 2017]. The research in this dissertation contributes to this debate by contextualizing trends in the ocean biosphere over the observational record in the presence of internal climate variability. While there are limitations in applying the statistical methodology of the observationally constrained synthetic ensemble over short time periods, it cautions against the interpretation of trends as externally forced across the majority of the global ocean. Additionally, the synthetic ensemble provides context for the likelihood of trends being externally forced across different regions of the global ocean, with a wider range of possible chlorophyll trends in subpolar regions than in subtropical regions. The results of the synthetic ensemble emphasize the importance of continued collection of ocean biosphere observations to provide more robust assessments of externally forced climate change impacts on marine phytoplankton.

The recent development of large ensembles of ESMs allow us to distinguish internal climate variability from external anthropogenic forcing among a variety of ocean biogeochemical variables [Rodgers et al., 2015, Long et al., 2016, McKinley et al., 2016, Lovenduski et al., 2016, Frölicher et al., 2016, Brady et al., 2019, Schlunegger et al., 2019]. While observational records of the ocean biosphere have historically been used to initialize, validate, and compare ESMs, a synthetic ensemble can be used to evaluate simulated phytoplankton variance. In Chapter 4, we compare the

range of phytoplankton variance in observed surface ocean chlorophyll to the range of phytoplankton variance simulated by the CESM1-LE. While the CESM1-LE underestimates the observed range of phytoplankton variance, the statistical method allows for the integration of observations and ESM ensembles in the context of internal variability. This is an important addition to the literature, as future work can utilize this statistical methodology to compare ranges of observed internal variability with ranges of simulated internal variability across a variety of Earth system variables. Indeed, new papers are emerging in the literature that aim to use this statistical approach for other important variables [Deser et al., 2020]. Additionally, the synthetic ensemble methodology can complement the use of observations in comparing the ability of multiple ESMs ensembles to simulate observed ranges internal variability, as is done in Chapter 4.

While internal variability in the coupled atmosphere-ocean climate system is often assumed to be constant with anthropogenic warming, there is growing recognition in the literature that internal variability may change as the climate warms [Resplandy et al., 2015, Thompson et al., 2015, Landschützer et al., 2018, Kwiatkowski and Orr, 2018, Rodgers et al., 2021]. This development is of particular importance in refining future projections under climate change scenarios. As the base of the marine food web, constraining change in phytoplankton variance is essential in reducing uncertainty in marine ecosystem projections. The research in this dissertation contributes to this gap of knowledge by quantifying how simulated variance in phytoplankton biomass changes with anthropogenic warming. Globally, we identify a decline in phytoplankton biomass with climate change in the CESM1-LE and across a suite of CMIP5 models, with heterogeneous regional trends. We observe large declines in phytoplankton variance with climate change in important fisheries regions in the CESM1-LE. Clarifying how variance in phytoplankton biomass may be changing over long time scales with climate change is important for fisheries management, especially at regional scales. Near-term predictions of phytoplankton biomass may also benefit from knowledge of the projected magnitude of internal variability, as the chaotic nature of internal variability hampers near-term predictions [Meehl et al., 2009, 2014].

Many studies attribute bottom-up controls, such as changes in nutrient flux, temperature,

and light availability, to changing phytoplankton growth in a warming climate [Steinacher et al., 2010, Bopp et al., 2013, Lotze et al., 2019, Tittensor et al., 2021]. However, top-down controls, such as zooplankton grazing, have also been shown to play a role [Bopp et al., 2001, Laufkötter et al., 2015, Prowe et al., 2012a,b, Hashioka et al., 2012]. In Chapter 4, we demonstrate through statistical analysis the importance of grazing (top-down) controls on phytoplankton variance with climatic warming. In contrast, bottom-up controls exert a minor influence on phytoplankton variance. This is an important contribution to the literature, as existing analyses have focused on attributing drivers to changes in the bottom-up controls such as nutrient flux and light availability. These results contribute additional information in the context of this ongoing debate of dominant drivers of marine phytoplankton in a warming climate. Additionally, future improvements in the complexity of biogeochemical ecosystem models may allow more detailed evaluation of changing grazing pressures with climate change. For example, more complex configurations of the ecosystem model MARBL [Long et al., 2021] include explicit representation of additional PFTs such as coccolithophores [Krumhardt et al., 2019] and multiple ZFTs. Potentially, these more complex ecosystem models will provide a more realistic representation of complex marine ecosystems.

Phytoplankton and zooplankton biodiversity is projected to change with anthropogenic warming, with a global increase in phytoplankton species richness and a slight decline in zooplankton species richness [Benedetti et al., 2021]. As species migrate poleward due to warming ocean temperatures, it will be essential to monitor changes in both ecosystem composition and location. The upcoming NASA’s Plankton Aerosol Cloud ocean Ecosystem (PACE) mission is positioned to provide this information with the first global measurements of phytoplankton functional type. The ability to identify phytoplankton community composition remotely will improve our understanding of Earth’s changing marine ecosystems and assist in the management of fisheries resources.

Bibliography

- V. Arora, J. Scinocca, G. Boer, J. Christian, K. Denman, G. Flato, V. Kharin, W. Lee, and W. Merryfield. Carbon emission limits required to satisfy future representative concentration pathways of greenhouse gases. Geophysical Research Letters, 38, 03 2011. doi: 10.1029/2010GL046270.
- C. Beaulieu, S. A. Henson, J. L. Sarmiento, J. P. Dunne, S. C. Doney, R. R. Rykaczewski, and L. Bopp. Factors challenging our ability to detect long-term trends in ocean chlorophyll. Biogeosciences, 10:2711–2724, 2013. doi: 10.5194/bg-10-2711-2013.
- M. Behrenfeld. Abandoning sverdrup’s critical depth hypothesis on phytoplankton blooms. Ecology, 91:977–89, 04 2010. doi: 10.1890/09-1207.1.
- M. Behrenfeld, J. Randerson, C. McClain, G. Feldman, S. Los, C. Tucker, P. Falkowski, C. Field, R. Frouin, W. Esaias, D. Kolber, and N. Pollack. Biospheric primary production during an ENSO transition. Science, 291:2594–7, 04 2001. doi: 10.1126/science.1055071.
- M. Behrenfeld, R. O’Malley, D. Siegel, C. McClain, J. Sarmiento, G. Feldman, A. Milligan, P. Falkowski, R. Letelier, and E. Boss. Climate-driven trends in contemporary ocean productivity. Nature, 444:752–5, 01 2007. doi: 10.1038/nature05317.
- M. Behrenfeld, S. Doney, I. Lima, E. Boss, and D. Siegel. Annual cycles of ecological disturbance and recovery underlying the subarctic atlantic spring plankton bloom: Phytoplankton blooms. Global Biogeochemical Cycles, 27, 06 2013. doi: 10.1002/gbc.20050.
- M. Behrenfeld, R. O’Malley, E. Boss, T. Westberry, J. Graff, K. Halsey, A. Milligan, D. Siegel, and M. Brown. Reevaluating ocean warming impacts on global phytoplankton. Nature Climate Change, Advanced Online Access, 10 2016.
- M. Bellacicco, J. Pitarch, E. Organelli, V. Martinez-Vicente, G. Volpe, and S. Marullo. Improving the retrieval of carbon-based phytoplankton biomass from satellite ocean colour observations. Remote Sensing, 12:3640, 11 2020. doi: 10.3390/rs12213640.
- S. Bimal and A. Anil. Picophytoplankton *synechococcus* as food for nauplii of amphibalanus amphitrite and *artemia salina*. Hydrobiologia, 835, 06 2019. doi: 10.1007/s10750-019-3923-x.
- F. Benedetti, M. Vogt, U. Hofmann Elizondo, D. Righetti, N. Zimmermann, and N. Gruber. Major restructuring of marine plankton assemblages under global warming. Nature Communications, 12, 09 2021. doi: 10.1038/s41467-021-25385-x.

- L. Bengtsson and K. Hodges. Can an ensemble climate simulation be used to separate climate change signals from internal unforced variability? *Climate Dynamics*, 52:3553–3573, 2019. doi: 10.1007/s00382-018-4343-8.
- N. Bindoff, W. Cheung, J. Kairo, J. Aristegui, V. Guinder, R. Hallberg, N. Hilmi, N. Jiao, M. Karim, L. Levin, S. O’Donoghue, S. Purca, B. Rinkevich, T. Suga, A. Tagliabue, P. Williamson, S. Acar, J. J. Alava, E. Allison, and C. Whalen. *Changing Ocean, Marine Ecosystems, and Dependent Communities (09 SROCC Ch05 FINAL-1)*, pages 447–588. 01 2019.
- J. Blanchard, S. Jennings, R. Holmes, J. Harle, G. Merino, I. Allen, J. Holt, N. Dulvy, and M. Barange. Potential consequences of climate change on primary production and fish production in large marine ecosystems. *Philosophical Transactions of the Royal Society B*, 367: 2979–2989, 11 2012. doi: 10.1098/rstb.2012.0231.
- J. Blanchard, R. Watson, E. Fulton, R. Cottrell, K. Nash, A. Bryndum-Buchholz, M. Büchner, D. Carozza, W. Cheung, J. Elliott, L. Davidson, N. Dulvy, J. Dunne, T. Eddy, E. Galbraith, H. Lotze, O. Maury, C. Müller, D. Tittensor, and S. Jennings. Linked sustainability challenges and trade-offs among fisheries, aquaculture and agriculture. *Nature*, 1, 08 2017. doi: 10.1038/s41559-017-0258-8.
- L. Bopp, P. Monfray, O. Aumont, J.-L. Dufresne, H. Treut, G. Madec, L. Terray, and J. Orr. Potential impact of climate change on marine export production. *Global Biogeochemical Cycles*, 15:81–100, 03 2001. doi: 10.1029/1999GB001256.
- L. Bopp, L. Resplandy, J. Orr, S. Doney, J. Dunne, M. Gehlen, P. Halloran, C. Heinze, T. Ilyina, R. Séférian, J. Tjiputra, and M. Vichi. Multiple stressors of ocean ecosystems in the 21st century: Projections with CMIP5 models. *Biogeosciences*, 10:6225–6245, 2013. doi: 10.5194/bg-10-6225-2013.
- L. Bopp, O. Aumont, L. Kwiatkowski, C. Clerc, L. Dupont, C. Ethé, R. Séférian, and A. Tagliabue. Diazotrophy as a key driver of the response of marine net primary productivity to climate change. *Biogeosciences*, 12 2021. doi: 10.5194/bg-2021-320.
- D. Boyce, M. Lewis, and B. Worm. Global phytoplankton decline over the past century. *Nature*, 466:591–6, 07 2010. doi: 10.1038/nature09268.
- R. X. Brady, N. S. Lovenduski, M. A. Alexander, M. Jacox, and N. Gruber. On the role of climate modes in modulating the air–sea CO₂ fluxes in eastern boundary upwelling systems. *Biogeosciences*, 16(2):329–346, 2019. doi: 10.5194/bg-16-329-2019.
- K. Brander. Impacts of climate change on fisheries. *Journal of Marine Systems*, 79:389–402, 02 2010. doi: 10.1016/j.jmarsys.2008.12.015.
- B. Brewin, S. Sathyendranath, T. Platt, H. Bouman, S. Ciavatta, G. Dall’Olmo, J. Dingle, S. Groom, B. Jönsson, T. Kostadinov, G. Kulk, M. Laine, V. Martinez-Vicente, S. Psarra, D. Raitsos, K. Richardson, M.-H. Rio, C. Rousseaux, J. Salisbury, and P. Walker. Sensing the ocean biological carbon pump from space: A review of capabilities, concepts, research gaps and future developments. *Earth-Science Reviews*, 217:103604, 03 2021. doi: 10.1016/j.earscirev.2021.103604.

- A. Cabre, I. Marinov, and S. Leung. Consistent global responses of marine ecosystems to future climate change across the ipcc ar5 earth system models. Climate Dynamics, 45:1–28, 10 2014. doi: 10.1007/s00382-014-2374-3.
- W. Cai, S. Borlace, M. Lengaigne, P. Rensch, M. Collins, G. Vecchi, A. Timmermann, A. Santoso, M. McPhaden, L. Wu, M. England, G. Wang, E. Guilyardi, and F.-F. Jin. Increasing frequency of extreme El Niño Events due to greenhouse warming. Nature Climate Change, 4:111–116, 01 2014. doi: 10.1038/nclimate2100.
- W. Cai, G. Wang, A. Santoso, M. McPhaden, L. Wu, F.-F. Jin, A. Timmermann, M. Collins, G. Vecchi, M. Lengaigne, M. England, D. Dommenges, K. Takahashi, and E. Guilyardi. Increased frequency of extreme La Niña Events under greenhouse warming. Nature Climate Change, 5: 132–137, 2015. doi: 10.1038/nclimate2492.
- W. Cai, B. Ng, G. Wang, A. Santoso, L. Wu, and K. Yang. Increased enso sea surface temperature variability under four ipcc emission scenarios. Nature Climate Change, 01 2022. doi: 10.1038/s41558-022-01282-z.
- C. Castillo, S. Signorini, E. Karakoylu, and S. Rivero-Calle. Is the southern ocean getting greener? Geophysical Research Letters, 46, 06 2019. doi: 10.1029/2019GL083163.
- E. Chassot, S. Bonhommeau, N. Dulvy, F. Mélin, R. Watson, and O. le pape. Global marine primary production constrains fisheries catches. Ecology Letters, 13:495 – 505, 03 2010. doi: 10.1111/j.1461-0248.2010.01443.x.
- F. P. Chavez, P. G. Strutton, and M. J. McPhaden. Biological-physical coupling in the Central Equatorial Pacific during the onset of the 1997-98 El Niño. Geophysical Research Letters, 25: 3543–3546, 1998.
- W. Cheung, V. Lam, J. Sarmiento, K. Kearney, R. Watson, and D. Pauly. Projecting global marine biodiversity impacts under climate change scenarios. Fish and Fisheries, 10:235 – 251, 09 2009. doi: 10.1111/j.1467-2979.2008.00315.x.
- W. Cheung, V. Lam, J. Sarmiento, K. Kearney, R. Watson, D. Zeller, and D. Pauly. Large-scale redistribution of maximum fisheries catch potential in the global ocean under climate change. Global Change Biology, 16:24 – 35, 01 2010. doi: 10.1111/j.1365-2486.2009.01995.x.
- V. Christensen and C. Walters. Ecopath with ecosim: Methods, capabilities and limitations. Ecological Modelling, 172:109–139, 03 2004. doi: 10.1016/j.ecolmodel.2003.09.003.
- V. Christensen, M. Coll, J. Buszowski, W. Cheung, T. Frölicher, J. Steenbeek, C. Stock, R. Watson, and C. Walters. The global ocean is an ecosystem: Simulating marine life and fisheries. Global Ecology and Biogeography, 24, 02 2015. doi: 10.1111/geb.12281.
- J. Christian, V. Arora, G. Boer, C. Curry, K. Zahariev, K. Denman, G. Flato, W. Lee, W. Merryfield, N. Roulet, and J. Scinocca. The global carbon cycle in the canadian earth system model (canesm1): Preindustrial control simulation. Journal of Geophysical Research (Biogeosciences), 115, 09 2010. doi: 10.1029/2008JG000920.
- E. Coria-Monter, M. Gómez, D. Salas de Leon, and E. Durán-Campos. Impact of the "Godzilla El Niño" Event of 2015–2016 on sea-surface temperature and chlorophyll-a in the Southern Gulf of

- California, Mexico, as evidenced by satellite and in situ data. Pacific Science, 72:411–422, 2018. doi: 10.2984/72.4.2.
- A. Dai and C. Bloecker. Impacts of internal variability on temperature and precipitation trends in large ensemble simulations by two climate models. Climate Dynamics, 52, 01 2019. doi: 10.1007/s00382-018-4132-4.
- G. Danabasoglu, S. C. Bates, B. P. Briegleb, S. R. Jayne, M. Jochum, W. G. Large, S. Peacock, and S. G. Yeager. The CCSM4 ocean component. Journal of Climate, 25(5):1361–1389, 2012. doi: 10.1175/JCLI-D-11-00091.1.
- C. Deser, A. Phillips, V. Bourdette, and H. Teng. Uncertainty in climate change projections: The role of internal variability. Climate Dynamics, 38:527–546, 2010. doi: 10.1007/s00382-010-0977-x.
- C. Deser, R. Knutti, S. Solomon, and A. Phillips. Communication of the role of natural variability in future North American climate. Nature Climate Change, 2:775–779, 2012. doi: 10.1038/nclimate1562.
- C. Deser, F. Lehner, K. Rodgers, T. Ault, T. Delworth, P. DiNezio, A. Fiore, C. Frankignoul, J. Fyfe, D. Horton, J. Kay, R. Knutti, N. Lovenduski, J. Marotzke, K. McKinnon, S. Minobe, J. Randerson, J. Screen, I. Simpson, and M. Ting. Insights from Earth system model initial-condition large ensembles and future prospects. Nature Climate Change, 10:277–286, 2020. doi: 10.1038/s41558-020-0731-2.
- S. Doney, K. Lindsay, I. Fung, and J. John. Natural variability in a stable, 1000-yr global coupled climate–carbon cycle simulation. Journal of Climate, 19:3033–3054, 2006. doi: 10.1175/JCLI3783.1.
- S. C. Doney, I. Lima, J. K. Moore, K. Lindsay, M. J. Behrenfeld, T. K. Westberry, N. Mahowald, D. M. Glover, and T. Takahashi. Skill metrics for confronting global upper ocean ecosystem–biogeochemistry models against field and remote sensing data. 76(1):95–112, 2009. doi: <https://doi.org/10.1016/j.jmarsys.2008.05.015>.
- J. Dunne, J. John, A. Adcroft, S. Griffies, R. Hallberg, E. Shevliakova, S. Ronald, W. Cooke, K. Dunne, M. Harrison, J. Krasting, S. Malyshev, P. Milly, P. Phillips, L. Sentman, B. Samuels, M. Spelman, M. Winton, A. Wittenberg, and N. Zadeh. Gfdl’s esm2 global coupled climate–carbon earth system models. part i: Physical formulation and baseline simulation characteristics. Journal of Climate, 25:6646–6665, 10 2012. doi: 10.1175/JCLI-D-11-00560.1.
- J. Dunne, J. John, E. Shevliakova, S. Ronald, J. Krasting, S. Malyshev, P. Milly, L. Sentman, A. Adcroft, W. Cooke, K. Dunne, S. Griffies, R. Hallberg, M. Harrison, H. Levy, A. Wittenberg, P. Phillips, and N. Zadeh. Gfdl’s esm2 global coupled climate–carbon earth system models. part ii: Carbon system formulation and baseline simulation characteristics*. Journal of Climate, 26: 2247–2267, 04 2013. doi: 10.1175/JCLI-D-12-00150.1.
- G. Elsworth, N. Lovenduski, K. McKinnon, K. Krumhardt, and R. Brady. Finding the fingerprint of anthropogenic climate change in marine phytoplankton abundance. Current Climate Change Reports, 6, 2020. doi: 10.1007/s40641-020-00156-w.
- G. Elsworth, N. Lovenduski, and K. McKinnon. Alternate history: A synthetic ensemble of ocean chlorophyll concentrations. Global Biogeochemical Cycles, 35(9), 2021.

- S. R. Emerson and J. I. Hedges. Chemical Oceanography and the Marine Carbon Cycle. Cambridge University Press, Cambridge, United Kingdom, 2008.
- J. Evjemo, O. Vadstein, and Y. Olsen. Feeding and assimilation kinetics of *artemia franciscana* fed *isochrysis galbana* (clone t. iso). Marine Biology, 136:1099–1109, 07 2000. doi: 10.1007/s002270000306.
- P. Falkowski. Ocean science: The power of plankton. Nature, 483:S17–20, 03 2012. doi: 10.1038/483S17a.
- U. FAO. The state of world fisheries and aquaculture 2020, 2020.
- A. Fay and G. McKinley. Global open-ocean biomes: mean and temporal variability. Earth System Science Data, 6, 08 2014. doi: 10.5194/essd-6-273-2014.
- L. Feng and C. Hu. Cloud adjacency effects on top-of-atmosphere radiance and ocean color data products: A statistical assessment. Remote Sensing of Environment, 174:301–313, 03 2016. doi: 10.1016/j.rse.2015.12.020.
- P. Flanagan, O. Jensen, J. Morley, and M. Pinsky. Response of marine communities to local temperature changes. Ecography, 42, 10 2018. doi: 10.1111/ecog.03961.
- P. Friedlingstein, M. Jones, M. O’Sullivan, R. Andrew, J. Hauck, G. Peters, W. Peters, J. Pongratz, S. Sitch, C. Le Quéré, D. Bakker, J. Canadell, P. Ciais, R. Jackson, P. Athoni, L. Barbero, A. Bastos, V. Bastrikov, M. Becker, and S. Zaehle. Global carbon budget 2019. Earth System Science Data, 11:1783–1838, 2019. doi: 10.5194/essd-11-1783-2019.
- T. Frölicher, K. Rodgers, C. Stock, and W. Cheung. Sources of uncertainties in 21st century projections of potential ocean ecosystem stressors. Global Biogeochemical Cycles, 30:1224–1243, 2016. doi: 10.1002/2015GB005338.
- R. Geider, H. Macintyre, and T. Kana. A dynamic regulatory model of phytoplanktonic acclimation to light, nutrients, and temperature. Limnology and Oceanography, 43:679–694, 06 1998. doi: 10.4319/lo.1998.43.4.0679.
- M. Giorgetta, J. Jungclaus, C. Reick, S. Legutke, J. Bader, M. Böttinger, V. Brovkin, T. Crueger, M. Esch, K. Fieg, K. Gorges, V. Gayler, H. Haak, H.-D. Hollweg, T. Ilyina, S. Kinne, L. Kornbluh, D. Matei, T. Mauritsen, and B. Stevens. Climate and carbon cycle changes from 1850 to 2100 in mpi-esm simulations for the coupled model intercomparison project phase 5. Journal of Advances in Modeling Earth Systems, 5, 09 2013. doi: 10.1002/jame.20038.
- S. Giovannoni and K. Vergin. Giovannoni sj, vergin kl.. seasonality in ocean microbial communities. science 335: 671-676. Science, 335:671–6, 02 2012. doi: 10.1126/science.1198078.
- H. Gordon and A. Morel. Remote Assessment of Ocean Color for Interpretation of Satellite Visible Imagery, volume 4. 01 1983. doi: 10.1007/978-1-4684-6280-7.
- W. Gregg and M. E. Conkright. Decadal changes in global ocean chlorophyll. Geophysical Research Letters, 29:20–1–20–4, 2002. doi: 10.1029/2002GL014689.
- W. Gregg and C. Rousseaux. Decadal trends in global pelagic ocean chlorophyll: A new assessment integrating multiple satellites, in situ data, and models. Journal of Geophysical Research: Oceans, 119:5921–5933, 2014. doi: 10.1002/2014JC010158.

- W. Gregg and C. Rousseaux. Global ocean primary production trends in the modern ocean color satellite record (1998–2015). Environmental Research Letters, 14:124011, 11 2019. doi: 10.1088/1748-9326/ab4667.
- M. Hammond, C. Beaulieu, S. Sahu, and S. Henson. Assessing trends and uncertainties in satellite-era ocean chlorophyll using space-time modeling: Ocean chlorophyll trends and uncertainty. Global Biogeochemical Cycles, 06 2017. doi: 10.1002/2016GB005600.
- M. Hammond, C. Beaulieu, S. Henson, and S. Sahu. Regional surface chlorophyll trends and uncertainties in the global ocean. Nature Scientific Reports, 10:15273, 2020. doi: 10.1038/s41598-020-72073-9.
- T. Hashioka, M. Vogt, Y. Yamanaka, C. Le Quéré, E. Buitenhuis, M. Aita, S. Alvain, L. Bopp, T. Hirata, I. Lima, S. Sailley, and S. Doney. Phytoplankton competition during the spring bloom in four plankton functional type models. Biogeosciences Discussions, 9, 12 2012. doi: 10.5194/bgd-9-18083-2012.
- J. Hauck, C. Voelker, T. Wang, M. Hoppema, M. Losch, and D. Wolf-Gladrow. Seasonally different carbon flux changes in the Southern Ocean in response to the Southern Annular Mode. Global Biogeochemical Cycles, 27:1236–1245, 2013. doi: 10.1002/2013GB004600.
- E. Hawkins and R. Sutton. The potential to narrow uncertainty in regional climate predictions. Bulletin of the American Meteorological Society, 90:1095–1108, 2009.
- E. Hawkins and R. Sutton. The potential to narrow uncertainty in projections of regional precipitation change. Climate Dynamics, 37:407–418, 2011. doi: 10.1007/s00382-010-0810-6.
- S. Henson. Slow science: The value of long ocean biogeochemistry records. Philosophical transactions. Series A, Mathematical, physical, and engineering sciences, 372, 2014. doi: 10.1098/rsta.2013.0334.
- S. Henson, H. Cole, C. Beaulieu, and A. Yool. The impact of global warming on seasonality of ocean primary production. Biogeosciences Discussions, 10:1421–1450, 06 2013. doi: 10.5194/bgd-10-1421-2013.
- S. Henson, C. Beaulieu, and R. Lampitt. Observing climate change trends in ocean biogeochemistry: When and where. Global Change Biology, 22:1561–1571, 2016. doi: 10.1111/gcb.13152.
- S. A. Henson, J. L. Sarmiento, J. P. Dunne, L. Bopp, I. Lima, S. C. Doney, J. John, and C. Beaulieu. Detection of anthropogenic climate change in satellite records of ocean chlorophyll and productivity. Biogeosciences, 7(2):621–640, 2010.
- C. Hu, Z. Lee, and B. Franz. Chlorophyll *a* algorithms for oligotrophic oceans: A novel approach based on three-band reflectance difference. 117(C1), 2020/06/25 2012. doi: 10.1029/2011JC007395.
- J. W. Hurrell, M. M. Holland, P. R. Gent, S. Ghan, J. E. Kay, P. J. Kushner, J.-F. Lamarque, W. G. Large, D. Lawrence, K. Lindsay, W. H. Lipscomb, M. C. Long, N. Mahowald, D. R. Marsh, R. B. Neale, P. Rasch, S. Vavrus, M. Vertenstein, D. Bader, W. D. Collins, J. J. Hack, J. Kiehl, and S. Marshall. The Community Earth System Model: A framework for collaborative research. Bulletin of the American Meteorological Society, 94(9):1339–1360, 2013. doi: 10.1175/BAMS-D-12-00121.1.

- T. Ilyina, K. Six, J. Segschneider, E. Maier-Reimer, H. Li, and I. Núñez-Riboni. Global ocean biogeochemistry model hamocc: Model architecture and performance as component of the mpi-earth system model in different cmip5 experimental realizations. Journal of Advances in Modeling Earth Systems, 5, 06 2013. doi: 10.1029/2012MS000178.
- A. Irwin and M. Oliver. Are ocean deserts getting larger? Geophysical Research Letters, 36: L18609, 09 2009. doi: 10.1029/2009GL039883.
- S. Jennings and K. Collingridge. Predicting consumer biomass, size-structure, production, catch potential, responses to fishing and associated uncertainties in the world’s marine ecosystems. PLoS ONE, 10, 07 2015. doi: 10.1371/journal.pone.0133794.
- D. Karl and R. Lukas. The Hawaii Ocean Time-series (HOT) program: Background, rational and field implementation. Deep Sea Research Part II: Topical Studies in Oceanography, 43:129–156, 1996.
- J. E. Kay, C. Deser, A. Phillips, A. Mai, C. Hannay, G. Strand, J. M. Arblaster, S. C. Bates, G. Danabasoglu, J. Edwards, M. Holland, P. Kushner, J.-F. Lamarque, D. Lawrence, K. Lindsay, A. Middleton, E. Munoz, R. Neale, K. Oleson, L. Polvani, and M. Vertenstein. The Community Earth System Model (CESM) Large Ensemble project: A community resource for studying climate change in the presence of internal climate variability. Bulletin of the American Meteorological Society, 96(8):1333–1349, 2015. doi: 10.1175/BAMS-D-13-00255.1.
- T. Kostadinov, S. Milutinovic, I. Marinov, and A. Cabre. Carbon-based phytoplankton size classes retrieved via ocean color estimates of the particle size distribution. Ocean Science (OS), 12: 561–575, 04 2016. doi: 10.5194/os-12-561-2016.
- K. Krumhardt, N. Lovenduski, M. Long, and K. Lindsay. Avoidable impacts of ocean warming on marine primary production: Insights from the CESM ensembles. Global Biogeochemical Cycles, 31:114–133, 2017. doi: 10.1002/2016GB005528.
- K. Krumhardt, N. Lovenduski, M. Long, M. Levy, K. Lindsay, J. Moore, and C. Nissen. Coccolithophore growth and calcification in an acidified ocean: Insights from community earth system model simulations. Journal of Advances in Modeling Earth Systems, 11, 05 2019. doi: 10.1029/2018MS001483.
- D. Kumar and A. Ganguly. Intercomparison of model response and internal variability across climate model ensembles. Climate Dynamics, 51:207–219, 07 2018. doi: 10.1007/s00382-017-3914-4.
- L. Kwiatkowski and J. Orr. Diverging seasonal extremes for ocean acidification during the twenty-first century. Nature Climate Change, 8:141–146, 02 2018. doi: 10.1038/s41558-017-0054-0.
- L. Kwiatkowski, L. Bopp, O. Aumont, P. Ciais, P. Cox, C. Laufkötter, Y. Li, and R. Sférian. Emergent constraints on projections of declining primary production in the tropical oceans. Nature Climate Change, 7, 04 2017. doi: 10.1038/nclimate3265.
- L. Kwiatkowski, O. Torres, L. Bopp, O. Aumont, M. Chamberlain, J. Christian, J. Dunne, M. Gehlen, T. Ilyina, J. John, A. Lenton, H. Li, N. Lovenduski, J. Orr, J. Palmiéri, Y. Santana-Falcón, J. Schwinger, R. Sférian, C. Stock, and T. Ziehn. Twenty-first century ocean warming, acidification, deoxygenation, and upper-ocean nutrient and primary production decline from CMIP6 model projections. Biogeosciences, 17:3439–3470, 2020. doi: 10.5194/bg-17-3439-2020.

- C. M. Lalli and T. R. Parsons. Biological oceanography: An introduction. Elsevier Butterworth-Heinemann, Burlington, MA, USA, 2nd edition, 1997.
- J. Lamarque, T. Bond, V. Eyring, C. Granier, A. Heil, Z. Klimont, D. Lee, C. Lioussé, A. Mieville, B. Owen, M. Schultz, D. Shindell, S. Smith, E. Stehfest, J. Aardenne, O. Cooper, M. Kainuma, N. Mahowald, J. McConnell, and D. Vuuren. Historical (1850-2000) gridded anthropogenic and biomass burning emissions of reactive gases and aerosols: methodology and application. Atmospheric Chemistry and Physics, 10:7017–7039, 2010. doi: 10.5194/acpd-10-4963-2010.
- P. Landschützer, N. Gruber, D. Bakker, I. Stemmler, and K. Six. Strengthening seasonal marine CO₂ variations due to increasing atmospheric CO₂. Nature Climate Change, 8:146–150, 02 2018. doi: 10.1038/s41558-017-0057-x.
- C. Laufkötter, M. Vogt, N. Gruber, M. Aita-Noguchi, O. Aumont, L. Bopp, E. Buitenhuis, S. Doney, J. Dunne, T. Hashioka, J. Hauck, T. Hirata, J. John, C. Le Quéré, I. Lima, H. Nakano, R. Séférian, I. Totterdell, M. Vichi, and C. Voelker. Drivers and uncertainties of future global marine primary production in marine ecosystem models. Biogeosciences Discussions, 12:3731–3824, 02 2015. doi: 10.5194/bgd-12-3731-2015.
- C. Le Quéré, J. Orr, P. Monfray, O. Aumont, and G. Madec. Interannual variability of the oceanic sink of CO₂ from 1979 through 1997. Global Biogeochemical Cycles, 14:1247–1266, 2000. doi: 10.1029/1999GB900049.
- P. Lehodey, R. Murtugudde, and I. Senina. Bridging the gap from ocean models to population dynamics of large marine predators: A model of mid-trophic functional groups. Progress In Oceanography, 84:69–84, 02 2010. doi: 10.1016/j.pocean.2009.09.008.
- A. Lenton and R. Matear. Role of the Southern Annular Mode (sam) in Southern Ocean CO₂ uptake. Global Biogeochem. Cycles, 21, 2007. doi: 10.1029/2006GB002714.
- S. Leung, A. Cabre, and I. Marinov. A latitudinally banded phytoplankton response to 21st century climate change in the southern ocean across the cmip5 model suite. Biogeosciences, 12:5715–5734, 10 2015. doi: 10.5194/bg-12-5715-2015.
- S. Levitus, J. Antonov, T. Boyer, R. Locarnini, H. Garcia, and A. Mishonov. Global ocean heat content 1955–2008 in light of recently revealed instrumentation problems. Geophysical Research Letters, 36, 04 2009. doi: 10.1029/2008GL037155.
- J. Link and A. Marshak. Characterizing and comparing marine fisheries ecosystems in the united states: determinants of success in moving toward ecosystem-based fisheries management. Reviews in Fish Biology and Fisheries, 29, 03 2019. doi: 10.1007/s11160-018-9544-z.
- M. Long, J. Moore, K. Lindsay, M. Levy, S. Doney, J. Luo, K. Krumhardt, R. Letscher, M. Grover, and Z. Sylvester. Simulations with the marine biogeochemistry library (marbl). Journal of Advances in Modeling Earth Systems, 06 2021. doi: 10.1002/essoar.10507358.1.
- M. C. Long, K. Lindsay, S. Peacock, J. K. Moore, and S. C. Doney. Twentieth-Century Oceanic Carbon Uptake and Storage in CESM1(BGC). 26(18):6775–6800, 2013/10/11 2013. doi: 10.1175/JCLI-D-12-00184.1.

- M. C. Long, C. Deutsch, and T. Ito. Finding forced trends in oceanic oxygen. 30(2):381–397, 2016. ISSN 1944-9224. doi: 10.1002/2015GB005310. URL <http://dx.doi.org/10.1002/2015GB005310>. 2015GB005310.
- A. Longhurst. Ecological Geography of the Sea. Academic Press, 2007. doi: 10.1016/B978-012455521-1/50002-4.
- H. Lotze, D. Tittensor, A. Bryndum-Buchholz, T. Eddy, W. Cheung, E. Galbraith, M. Barange, N. Barrier, D. Bianchi, J. Blanchard, L. Bopp, M. Büchner, C. Bulman, D. Carozza, V. Christensen, M. Coll, J. Dunne, E. Fulton, S. Jennings, and B. Worm. Global ensemble projections reveal trophic amplification of ocean biomass declines with climate change. Proceedings of the National Academy of Sciences, 10, 06 2019. doi: 10.1073/pnas.1900194116.
- N. S. Lovenduski and N. Gruber. Impact of the Southern Annular Mode on Southern Ocean circulation and biology. Geophysical Research Letters, 32(11), 2005. doi: 10.1029/2005GL022727.
- N. S. Lovenduski, G. A. McKinley, A. R. Fay, K. Lindsay, and M. C. Long. Partitioning uncertainty in ocean carbon uptake projections: Internal variability, emission scenario, and model structure. 30(9):1276–1287, 2016. ISSN 1944-9224. doi: 10.1002/2016GB005426.
- M. Lozier, A. Dave, J. Palter, L. Gerber, and R. Barber. On the relationship between stratification and primary productivity in the north atlantic. Geophysical Research Letters, 38, 09 2011. doi: 10.1029/2011GL049414.
- S. Manabe and S. Ronald. Century-scale effects of increased atmospheric co2 on the ocean-atmosphere system. Nature, 364:215–218, 07 1993. doi: 10.1038/364215a0.
- I. Marinov, S. C. Doney, and I. D. Lima. Response of ocean phytoplankton community structure to climate change over the 21st century: partitioning the effects of nutrients, temperature and light. Biogeosciences, 7(12):3941–3959, 2010. doi: 10.5194/bg-7-3941-2010.
- I. Marinov, S. Doney, I. Lima, K. Lindsay, J. Moore, and N. Mahowald. North-south asymmetry in the modeled phytoplankton community response to climate change over the 21st century: Phytoplankton response to climate. Global Biogeochemical Cycles, 27, 12 2013. doi: 10.1002/2013GB004599.
- S. Maritorena, D. Siegel, and A. Peterson. Optimization of a semianalytical ocean color model for global-scale application. Applied optics, 41:2705–14, 06 2002. doi: 10.1364/AO.41.002705.
- A. Marshak and J. Link. Primary production ultimately limits fisheries economic performance. Scientific Reports, 11:12154, 06 2021. doi: 10.1038/s41598-021-91599-0.
- V. Martinez-Vicente, H. Evers-King, S. Roy, T. Kostadinov, G. Tarran, J. Graff, B. Brewin, G. Dall’Olmo, T. Jackson, A. Hickman, R. Röttgers, H. Krasemann, E. Maranon, T. Platt, and S. Sathyendranath. Intercomparison of ocean color algorithms for picophytoplankton carbon in the ocean. Frontiers in Marine Science, 4, 12 2017. doi: 10.3389/fmars.2017.00378.
- O. Maury. An overview of apecosm, a spatialized mass balanced “apex predators ecosystem model” to study physiologically structured tuna population dynamics in their ecosystem. Progress In Oceanography, 84:113–117, 02 2010. doi: 10.1016/j.pocean.2009.09.013.

- G. McKinley, A. Ritzer, and N. Lovenduski. Mechanisms of northern North Atlantic biomass variability. Biogeosciences, 15:6049–6066, 2018. doi: 10.5194/bg-15-6049-2018.
- G. A. McKinley, D. J. Pilcher, A. R. Fay, K. Lindsay, M. C. Long, and N. S. Lovenduski. Timescales for detection of trends in the ocean carbon sink. Nature, 530(7591):469–472, 2016.
- G. A. McKinley, A. R. Fay, N. S. Lovenduski, and D. J. Pilcher. Natural variability and anthropogenic trends in the ocean carbon sink. Annual Review of Marine Science, 9(1):125–150, 2017. doi: 10.1146/annurev-marine-010816-060529.
- K. McKinnon and C. Deser. Internal variability and regional climate trends in an observational large ensemble. Journal of Climate, 31:6783–6802, 2018. doi: 10.1175/JCLI-D-17-0901.1.
- K. McKinnon, A. Poppick, E. Dunn-Sigouin, and C. Deser. An "observational large ensemble" to compare observed and modeled temperature trend uncertainty due to internal variability. Journal of Climate, 30:7585–7598, 2017. doi: 10.1175/JCLI-D-16-0905.1.
- G. Meehl, L. Goddard, J. Murphy, S. Ronald, G. Boer, G. Danabasoglu, K. Dixon, M. Giorgetta, A. Greene, E. Hawkins, G. Hegerl, D. Karoly, N. Keenlyside, M. Kimoto, B. Kirtman, A. Navarra, R. Pulwarty, D. Smith, D. Stammer, and T. Stockdale. Decadal prediction. can it be skillful? Bulletin of the American Meteorological Society, 10 2009.
- G. Meehl, A. Hu, J. Arblaster, J. Fasullo, and K. Trenberth. Externally forced and internally generated decadal climate variability associated with the interdecadal pacific oscillation. Journal of Climate, 26:7298–7310, 09 2013. doi: 10.1175/JCLI-D-12-00548.1.
- G. Meehl, L. Goddard, G. Boer, R. Burgman, G. Branstator, C. Cassou, S. Corti, G. Danabasoglu, F. Doblas-Reyes, E. Hawkins, A. Karspeck, M. Kimoto, A. Kumar, D. Matei, J. Mignot, R. Msadek, H. Pohlmann, M. Rienecker, T. Rosati, and S. Yeager. Decadal climate prediction: An update from the trenches. Bulletin of the American Meteorological Society, 95:243–267, 02 2014. doi: 10.1175/BAMS-D-12-00241.1.
- M. Meinshausen, S. Smith, K. Calvin, J. Daniel, M. Kainuma, J.-F. Lamarque, K. Matsumoto, S. Montzka, S. Raper, K. Riahi, A. Thomson, G. J. M. Velders, and D. Vuuren. The rcp greenhouse gas concentrations and their extensions from 1765 to 2300. Climatic Change, 109: 213–241, 11 2011. doi: 10.1007/s10584-011-0156-z.
- G. Meister, B. Franz, E. Kwiatkowska, and C. McClain. Corrections to the calibration of modis aqua ocean color bands derived from seawifs data. IEEE T. Geoscience and Remote Sensing, 50: 310–319, 01 2012. doi: 10.1109/TGRS.2011.2160552.
- K. Mills, A. Pershing, C. Brown, Y. Chen, F.-S. Chiang, D. Holland, S. Lehuta, J. Nye, J. Sun, A. Thomas, and R. Wahle. Fisheries management in a changing climate: Lessons from the 2012 ocean heat wave in the northwest atlantic. Oceanography, 26, 06 2013. doi: 10.5670/oceanog.2013.27.
- C. Moore, J. Morley, B. Morrison, M. Kolian, E. Horsch, T. Frolicher, M. Pinsky, and R. Griffis. Estimating the economic impacts of climate change on 16 major u.s. fisheries. Climate Change Economics, 11 2021. doi: 10.1142/S2010007821500020.
- J. Moore and O. Braucher. Sedimentary and mineral dust sources of dissolved iron to the world ocean. Biogeosciences, 5, 2008. doi: 10.5194/bg-4-1279-2007.

- J. Moore, K. Lindsay, S. Doney, M. Long, and K. Misumi. Marine ecosystem dynamics and biogeochemical cycling in the community earth system model [cesm1(bgc)]: Comparison of the 1990s with the 2090s under the rcp4.5 and rcp8.5 scenarios. Journal of Climate, 26:9291–9312, 12 2013. doi: 10.1175/JCLI-D-12-00566.1.
- J. K. Moore, S. C. Doney, D. M. Glover, and I. Y. Fung. Iron cycling and nutrient-limitation patterns in surface waters of the World Ocean. 49(1-3):463 – 507, 2002. ISSN 0967-0645. doi: DOI:10.1016/S0967-0645(01)00109-6. The US JGOFS Synthesis and Modeling Project: Phase 1.
- K. Moore, S. Doney, and K. Lindsay. Upper ocean ecosystem dynamics and iron cycling in a global three-dimensional model. Global Biogeochemical Cycles, 18, 2004. doi: 10.1029/2004GB002220.
- A. Morozov. Emergence of holling type iii zooplankton functional response: Bringing together field evidence and mathematical modelling. Journal of theoretical biology, 265:45–54, 07 2010. doi: 10.1016/j.jtbi.2010.04.016.
- R. Neville and J. Gower. Passive remote sensing of phytoplankton via chlorophyll a fluorescence. Journal of Geophysical Research, 92(24):3487–3493, 1977.
- M. Osman, S. Das, L. Trusel, M. Evans, H. Fischer, M. Grieman, S. Kipfstuhl, J. McConnell, and E. Saltzman. Industrial-era decline in subarctic atlantic productivity. Nature, 569:1–5, 05 2019. doi: 10.1038/s41586-019-1181-8.
- D. Pauly and V. Christensen. Pauly, d. christensen, v. primary production required to sustain global fisheries. nature 374, 255-257. Nature, 374, 03 1995. doi: 10.1038/374255a0.
- A. Perry, P. Low, J. Ellis, and J. Reynolds. Climate change and distribution shifts in marine fishes. Science, 308:1912–1915, 07 2005. doi: 10.1126/science.1111322.
- A. Phillips, C. Deser, and J. Fasullo. Evaluating modes of variability in climate models. EOS, 95, 2014. doi: 10.1002/2014EO490002.
- J. J. Polovina, E. A. Howell, and M. Abecassis. Ocean’s least productive waters are expanding. 35 (3), 2019/05/15 2008. doi: 10.1029/2007GL031745.
- H.-O. Pörtner, D. M. Karl, P. W. Boyd, W. W. L. Cheung, S. E. Lluch-Cota, Y. Nojiri, D. N. Schmidt, and P. O. Zavialov. Ocean systems. In C. B. Field, V. R. Barros, D. J. Dokken, K. J. Mach, M. D. Mastrandrea, T. E. Bilir, M. Chatterjee, K. L. Ebi, Y. O. Estrada, R. C. Genova, B. Girma, E. S. Kissel, A. N. Levy, S. MacCracken, P. R. Mastrandrea, and L. L. White, editors, Climate Change 2014: Impacts, Adaptation, and Vulnerability. Part A: Global and Sectoral Aspects. Contribution of Working Group II to the Fifth Assessment Report of the Intergovernmental Panel on Climate Change, pages 411–484. Cambridge University Press, United Kingdom and New York, NY, USA, 2014.
- A. F. Prowe, M. Pahlow, S. Dutkiewicz, M. Follows, and A. Oschlies. Top-down control of marine phytoplankton diversity in a global ecosystem model. Progress In Oceanography, 101, 01 2012a. doi: 10.1016/j.pocean.2011.11.016.
- A. F. Prowe, M. Pahlow, and A. Oschlies. Controls on the diversity–productivity relationship in a marine ecosystem model. Ecological Modelling, 225:167–176, 01 2012b. doi: 10.1016/j.ecolmodel.2011.11.018.

- M.-H. Radenac, F. Leger, A. Singh, and T. Delcroix. Sea surface chlorophyll signature in the tropical pacific during Eastern and Central Pacific ENSO events. Journal of Geophysical Research: Oceans, 117, 2012. doi: 10.1029/2011JC007841.
- L. Resplandy, R. Séférian, and L. Bopp. Natural variability of CO₂ and O₂ fluxes: What can we learn from centuries-long climate models simulations? Journal of Geophysical Research: Oceans, 120:384–404, 2015. doi: 10.1002/2014JC010463.
- M. Rhein, S. Rintoul, S. Aoki, E. Campos, D. Chambers, R. Feely, S. Gulev, G. Johnson, S. Josey, A. Kostianoy, C. Mauritzen, D. Roemmich, and L. Talley. Observations: Ocean. 01 2013.
- K. Rodgers, J. Lin, and T. Frölicher. Emergence of multiple ocean ecosystem drivers in a large ensemble suite with an Earth system model. Biogeosciences Discussions, 11:18189–18227, 2015. doi: 10.5194/bgd-11-18189-2014.
- K. Rodgers, S.-S. Lee, N. Rosenbloom, A. Timmermann, G. Danabasoglu, C. Deser, J. Edwards, J.-E. Kim, I. Simpson, K. Stein, M. Stuecker, R. Yamaguchi, T. Bódai, E.-S. Chung, L. Huang, W. Kim, J.-F. Lamarque, D. Lombardozzi, W. Wieder, and S. Yeager. Ubiquity of human-induced changes in climate variability. Earth System Dynamics, 07 2021. doi: 10.5194/esd-2021-50.
- S. Roy, S. Sathyendranath, and T. Platt. Size-partitioned phytoplankton carbon and carbon-to-chlorophyll ratio from ocean colour by an absorption-based bio-optical algorithm. Remote Sensing of Environment, 194:177–189, 06 2017. doi: 10.1016/j.rse.2017.02.015.
- V. Saba, M. Friedrichs, M.-E. Carr, D. Antoine, R. Armstrong, I. Asanuma, O. Aumont, N. Bates, M. Behrenfeld, V. Bennington, L. Bopp, J. Bruggeman, E. Buitenhuis, M. Church, A. Ciotti, S. Doney, M. Dowell, J. Dunne, S. Dutkiewicz, and A. Yool. Challenges of modeling depth-integrated marine primary productivity over multiple decades: A case study at bats and hot. Global Biogeochemical Cycles, 24, 09 2010. doi: 10.1029/2009GB003655.
- V. Saba, M. Friedrichs, D. Antoine, R. Armstrong, I. Asanuma, M. Behrenfeld, A. Ciotti, M. Dowell, H. N, K. Hyde, J. Ishizaka, T. Kameda, J. Marra, M. F, M. A, R. J, S. M, W. Smith, and T. Westberry. An evaluation of ocean color model estimates of marine primary productivity in coastal and pelagic regions across the globe. Biogeosciences, 8, 02 2011. doi: 10.5194/bg-8-489-2011.
- B. Santer, C. Mears, C. Doutriaux, P. Caldwell, P. Gleckler, T. Wigley, S. Solomon, N. Gillett, D. Ivanova, T. Karl, J. Lanzante, G. Meehl, P. Stott, K. Taylor, P. Thorne, M. Wehner, and F. Wentz. Separating signal and noise in atmospheric temperature changes: The importance of timescale. Journal of Geophysical Research (Atmospheres), 116, 11 2011. doi: 10.1029/2011JD016263.
- J. L. Sarmiento and N. Gruber. Ocean Biogeochemical Dynamics. Princeton University Press, Princeton, NJ, USA, 2006.
- S. Sathyendranath, T. Platt, Z. Kovac, J. Dingle, T. Jackson, B. Brewin, P. Franks, E. Maranon, G. Kulk, and H. Bouman. Reconciling models of primary production and photoacclimation. Applied Optics, 59, 02 2020. doi: 10.1364/AO.386252.
- S. Schlunegger, K. Rodgers, J. Sarmiento, T. Frölicher, J. Dunne, M. Ishii, and R. Slater. Emergence of anthropogenic signals in the ocean carbon cycle. Nature Climate Change, 9:719–726, 2019. doi: 10.1038/s41558-019-0553-2.

- A. Schmittner. Decline of the marine ecosystem caused by a reduction in the atlantic overturning circulation. Nature, 434:628–33, 04 2005. doi: 10.1038/nature03476.
- A. Schmittner, A. Oschlies, H. D. Matthews, and E. Galbraith. Correction to “future changes in climate, ocean circulation, ecosystems, and biogeochemical cycling simulated for a business-as-usual co 2 emission scenario until year 4000 ad”. Global Biogeochemical Cycles, 23, 03 2008. doi: 10.1029/2007GB002953.
- D. Schneider and C. Deser. Tropically driven and externally forced patterns of antarctic sea ice change: reconciling observed and modeled trends. Climate Dynamics, 50, 06 2018. doi: 10.1007/s00382-017-3893-5.
- T. Schreiber and A. Schmitz. Improved surrogate data for non-linearity tests. Physical Review Letters, 77:635–638, 09 1996. doi: 10.1103/PhysRevLett.77.635.
- T. Schreiber and A. Schmitz. Surrogate time series. Physica D: Nonlinear Phenomena, 142:346–382, 08 2000. doi: 10.1016/S0167-2789(00)00043-9.
- R. S  ferian, L. Bopp, M. Gehlen, D. Swingedouw, J. Mignot, E. Guilyardi, and S. Jerome. Multiyear predictability of tropical marine productivity. Proceedings of the National Academy of Sciences, 111, 07 2014. doi: 10.1073/pnas.1315855111.
- D. Siegel, M. Behrenfeld, S. Maritorea, C. McClain, D. Antoine, S. Bailey, P. Bontempi, E. Boss, H. Dierssen, S. Doney, R. Jr, R. Evans, G. Feldman, E. Fields, B. Franz, N. Kuring, C. Mengelt, N. Nelson, F. Patt, and J. Yoder. Regional to global assessments of phytoplankton dynamics from the SeaWiFS mission. Remote Sensing of Environment, 135:77–91, 2013. doi: 10.1016/j.rse.2013.03.025.
- D. Sigman and M. Hain. The biological productivity of the ocean. Nature Education, 3:1–16, 01 2012.
- M. Staudinger, K. Mills, K. Stamieszkin, N. Record, C. Hudak, A. Allyn, T. Diamond, K. Friedland, W. Golet, M. Henderson, C. Hernandez, T. Huntington, R. Ji, C. Johnson, D. Johnson, A. Jordaan, J. Kocik, Y. Li, M. Liebman, and K. Yakola. It’s about time: A synthesis of changing phenology in the gulf of maine ecosystem. Fisheries Oceanography, 28, 04 2019. doi: 10.1111/fog.12429.
- M. Steinacher, F. Joos, T. Fr  licher, L. Bopp, P. Cadule, V. Cocco, S. Doney, M. Gehlen, K. Lindsay, J. Moore, B. Schneider, and J. Segsneider. Projected 21st century decrease in marine productivity: A multi-model analysis. Biogeosciences, 7:979–1005, 03 2010. doi: 10.5194/bg-7-979-2010.
- C. Stock, J. John, R. Rykaczewski, R. Asch, W. Cheung, J. Dunne, K. Friedland, V. Lam, J. Sarmiento, and R. Watson. Reconciling fisheries catch and ocean productivity. Proceedings of the National Academy of Sciences, 114, 01 2017. doi: 10.1073/pnas.1610238114.
- T. Stocker and A. Schmittner. Influence of co2 emission rates on the stability of the thermohaline circulation. Nature, 388:862–865, 08 1997. doi: 10.1038/42224.
- W. Sunda. Trace metal interactions with marine phytoplankton. Biological Oceanography, 6: 411–442, 10 2013. doi: 10.1080/01965581.1988.10749543.

- A. Tagliabue, L. Kwiatkowski, L. Bopp, M. Butenschön, W. Cheung, M. Lengaigne, and J. Vialard. Persistent uncertainties in ocean net primary production climate change projections at regional scales raise challenges for assessing impacts on ecosystem services. *Frontiers in Climate*, 3:738224, 11 2021. doi: 10.3389/fclim.2021.738224.
- K. Taylor, S. Ronald, and G. Meehl. An overview of cmip5 and the experiment design. *Bulletin of the American Meteorological Society*, 93:485–498, 11 2011. doi: 10.1175/BAMS-D-11-00094.1.
- J. Theiler, S. Eubank, A. Longtin, B. Galdrikian, and J. Farmer. Testing for nonlinearity in time series: The method of surrogate data. *Physica D: Nonlinear Phenomena*, 58:77–94, 09 1992. doi: 10.1016/0167-2789(92)90102-S.
- A. C. Thomas, P. Brickley, and R. Weatherbee. Interannual variability in chlorophyll concentrations in the Humboldt and California Current Systems. *Progress in Oceanography*, 83(1):386–392, 2009. doi: 10.1016/j.pocean.2009.07.020.
- D. Thompson, E. Barnes, C. Deser, W. Foust, and A. Phillips. Quantifying the role of internal climate variability in future climate trends. *Journal of Climate*, 28, 2015. doi: 10.1175/JCLI-D-14-00830.1.
- G. C. Tiao, G. C. Reinsel, D. Xu, J. H. Pedrick, X. Zhu, A. J. Miller, J. J. DeLuisi, C. L. Mateer, and D. J. Wuebbles. Effects of autocorrelation and temporal sampling schemes on estimates of trend and spatial correlation. 95(D12):20507–20517, 1990. ISSN 2156-2202. doi: 10.1029/JD095iD12p20507.
- A. Timmermann, J. Oberhuber, A. Bacher, M. Esch, M. Latif, and E. Roeckner. Increased El Niño frequency in a climate model forced by future greenhouse warming. *Nature*, 398(6729):694–697, 1999. doi: 10.1038/19505.
- D. Tittensor, T. Eddy, H. Lotze, E. Galbraith, W. Cheung, M. Barange, J. Blanchard, L. Bopp, A. Bryndum-Buchholz, M. Büchner, C. Bulman, D. Carozza, V. Christensen, M. Coll, J. Dunne, J. Fernandes, E. Fulton, A. Hobday, V. Huber, and N. Walker. A protocol for the intercomparison of marine fishery and ecosystem models: Fish-mip v1.0. *Geoscientific Model Development*, 11: 1421–1442, 04 2018. doi: 10.5194/gmd-11-1421-2018.
- D. Tittensor, J. Blanchard, E. Fulton, W. Cheung, C. Novaglio, C. Harrison, R. Heneghan, N. Barrier, D. Bianchi, L. Bopp, A. Bryndum-Buchholz, G. Britten, M. Büchner, V. Christensen, M. Coll, J. Dunne, T. Eddy, J. Everett, J. Fernandes, and C. Stock. Next-generation ensemble projections reveal higher climate risks for marine ecosystems. *Nature Climate Change*, 11 2021. doi: 10.1038/s41558-021-01173-9.
- M. Travers-Trolet, Y.-J. Shin, S. Jennings, E. Machu, J. Huggett, J. Field, and P. Cury. Two-way coupling versus one-way forcing of plankton and fish models to predict ecosystem changes in the benguela. *Ecological Modelling*, 220:3089–3099, 11 2009. doi: 10.1016/j.ecolmodel.2009.08.016.
- L. Tupas, F. Santiago-Mandujano, D. Hebe, C. Nosse, L. Fujieki, E. Firing, R. Lukas, and D. Karl. Hawaii Ocean Time-series data report 8: 1996. 1997.
- M. Vichi, I. Allen, S. Masina, and N. Hardman-Mountford. The emergence of ocean biogeochemical provinces: A quantitative assessment and a diagnostic for model evaluation. *Global Biogeochemical Cycles*, 25, 06 2011. doi: 10.1029/2010GB003867.

- S. Wang and J. Moore. Variability of primary production and air-sea CO₂ flux in the Southern Ocean. Global Biogeochemical Cycles, 26, 2012. doi: 10.1029/2010GB003981.
- E. C. Weatherhead, G. C. Reinsel, G. C. Tiao, X.-L. Meng, D. Choi, W.-K. Cheang, T. Keller, J. DeLuisi, D. J. Wuebbles, J. B. Kerr, A. J. Miller, S. J. Oltmans, and J. E. Frederick. Factors affecting the detection of trends: Statistical considerations and applications to environmental data. 103(D14):17149–17161, 1998. ISSN 2156-2202. doi: 10.1029/98JD00995.
- T. Wernberg, S. Bennett, R. Babcock, T. de Bettignies, K. Cure, M. Depczynski, F. Dufois, J. Fromont, C. Fulton, R. Hovey, E. Harvey, T. Holmes, G. Kendrick, B. Radford, J. Santana-Garcon, B. Saunders, D. Smale, M. Thomsen, C. Tuckett, and S. Wilson. Climate-driven regime shift of a temperate marine ecosystem. Science, 353:169–172, 07 2016. doi: 10.1126/science.aad8745.
- D. Wilks. Resampling hypothesis tests for autocorrelated fields. J. Climate, 10(1):65–82, 1997.
- J. Yoder and M. Kennelly. Seasonal and ENSO variability in global ocean phytoplankton chlorophyll derived from 4 years of SeaWiFS measurements. Global Biogeochemical Cycles, 17, 2003. doi: 10.1029/2002GB001942.
- L. Zhai, T. Platt, C. Tang, S. Sathyendranath, and A. Walne. The response of phytoplankton to climate variability associated with the North Atlantic Oscillation. Deep Sea Research Part II: Topical Studies in Oceanography, 93:159 – 168, 2013. doi: 10.1016/j.dsr2.2013.04.009.

Appendix A

Supplementary Material for Chapter 3

This supplemental information contains regression coefficients between the climate modes ENSO and PDO and global chlorophyll concentrations from the MODIS ocean color dataset. Figure S1 displays the spatially varying regression coefficients of the two climate modes and chlorophyll concentration estimated via linear regression.

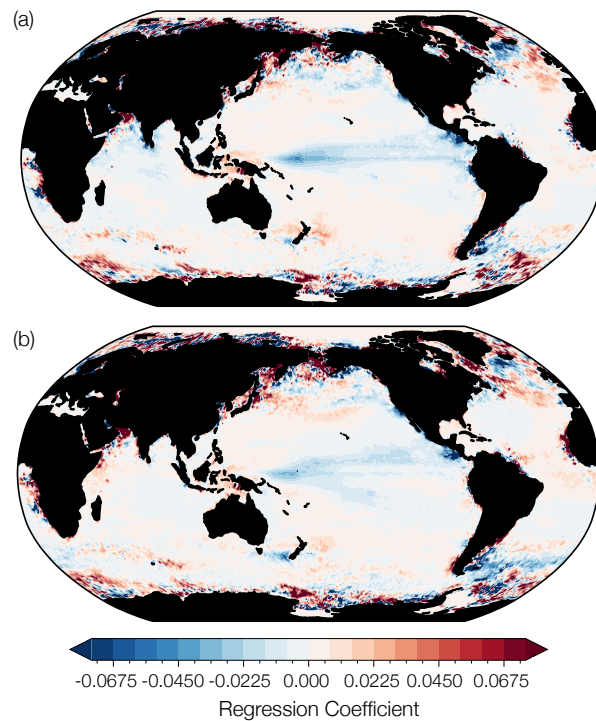


Figure A.1: The sensitivity of chlorophyll concentration derived from the MODIS ocean color record to (a) ENSO and (b) PDO. Regression coefficients are estimated using linear regression.

Appendix B

Supplementary Material for Chapter 4

In our discussion of zooplankton grazing as a driver of changing phytoplankton variance with anthropogenic warming, we consider the parameterization of zooplankton grazing in the CESM1-LE. The biogeochemical ecosystem model simulates a single generic zooplankton functional type (ZFT) with different grazing rates and half saturation constants prescribed for different PFTs (e.g. slower zooplankton grazing rates for larger phytoplankton). Grazing rate for the single ZFT is computed using a Holling Type III (sigmoidal) relationship:

$$G = g_{max} \cdot T_{lim} \cdot Z \cdot \frac{P^2}{P^2 + K^2} \quad (\text{B.1})$$

where g_{max} is the maximum grazing rate, T_{lim} is the temperature limitation (Q10) function, Z is the zooplankton concentration, P is the phytoplankton concentration, and K is the half-saturation constant for grazing. Zooplankton loss scales with temperature and a linear mortality term which represents zooplankton losses from predation.

Figure B.1 illustrates changes in grazing rate as a function of diatom concentration using this parameterization. To approximate the effects of climatic warming, we plot the relationship for across a series of increasing temperatures: (blue) 5°C, (orange) 10°C, and (green) 15°C. The maximum grazing rate increases with warming temperatures. Changes in diatom concentration in mmol m^{-3} between the beginning and end of the century are denoted by dark and light orange circles, respectively.

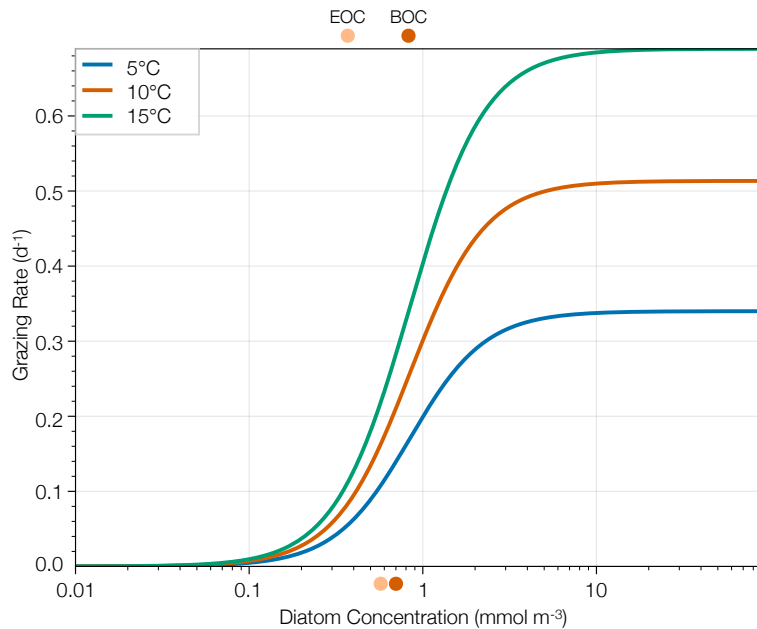


Figure B.1: Holling Type III (sigmoidal) functional parameterization of zooplankton grazing rate in the biogeochemical ecosystem model of the CESM1-LE across a range of temperatures. Changes in diatom concentration between the beginning and end of the century are shown in the dark and light orange circles, respectively, with the changes in the ASP region shown above and changes in the SAP region shown below.

To provide context for the CESM1-LE results, we examine changes in chlorophyll variance from a subset of the Coupled Model Intercomparison Project 5 (CMIP5) models [Taylor et al., 2011]: the GFDL-ESM2M from the Geophysical Fluid Dynamics Laboratory (GFDL; [Dunne et al., 2012, 2013], the CanESM2 from the Canadian Centre for Climate Modelling and Analysis [Christian et al., 2010, Arora et al., 2011], and the MPI-ESM-LR from the Max Planck Institute (MPI; [Giorgetta et al., 2013, Ilyina et al., 2013], consisting of 30, 50, and 100 ensemble members, respectively. Similarly to the CESM1-LE, historical forcing was applied through 2005, followed by RCP8.5 forcing through 2100.

We compare the variance in chlorophyll observed among the large ensembles to a synthetic ensemble generated from observational chlorophyll concentrations over the MODIS remote sensing record [Elsworth et al., 2020, 2021]. A synthetic ensemble is a novel technique that allows the observational record to be statistically emulated to create multiple possible evolutions of the observed

record, each with a unique sampling of internal climate variability [McKinnon et al., 2017, McKinnon and Deser, 2018]. We use the synthetic ensemble of chlorophyll concentration to compare the variability observed in the real world to the variability simulated across a suite of ESM ensembles.

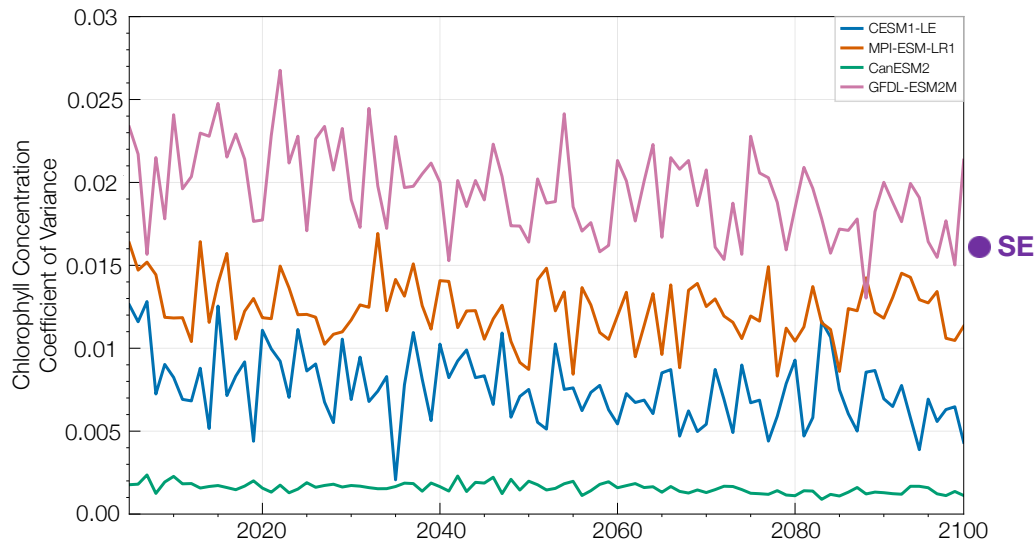


Figure B.2: Coefficient of variance (internal standard deviation divided by ensemble mean) in annual mean global surface ocean chlorophyll concentration from 2006 to 2100 across a suite of CMIP5 model ensembles: (blue) CESM1-LE (orange) MPI-ESM-LR1, (green) CanESM2, and (pink) GFDL-ESM2M. The average coefficient of variance of the synthetic ensemble created using the MODIS surface ocean chlorophyll record is shown in the purple dot on the vertical axis [Elsworth et al., 2020, 2021].

To provide context for Figure 4.3, we include the spatial distribution of total phytoplankton carbon concentration (Figure B.3a) and standard deviation in phytoplankton carbon concentration (Figure B.3b) simulated by the CESM1-LE across the RCP8.5 forcing scenario (2006 to 2100). Total phytoplankton carbon concentration is relatively high in the subpolar Atlantic and Pacific, the Southern Ocean, and the Eastern Equatorial Upwelling Zone and relatively low in the subtropical gyre regions (Figure B.3a). Regions of relatively high phytoplankton carbon concentrations correspond to regions of high variance (Figure B.3b).

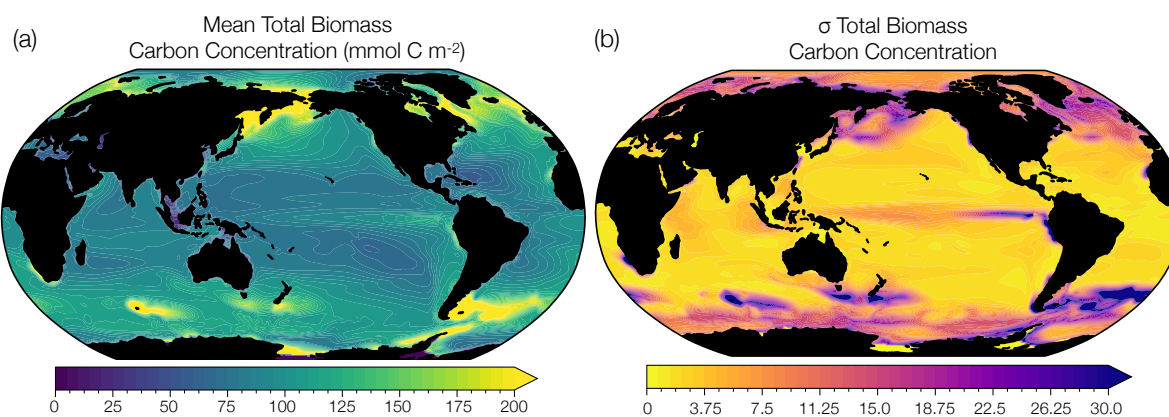


Figure B.3: (a) Total phytoplankton carbon concentration simulated by the CESM1-LE in mmol C m^{-2} averaged across the RCP8.5 forcing scenario (2006 to 2100). (b) Standard deviation in total phytoplankton carbon concentration averaged over the same period.